Institut für Erd- und Umweltwissenschaften
Mathematisch-Naturwissenschaftliche Fakultät
der Universität Potsdam

Formation and evolution of channel steps and their role for sediment dynamics in a steep mountain stream

Kumulative Dissertation

zur Erlangung des akademischen Grades
Doktor der Naturwissenschaften (Dr. rer. nat.)
in der Wissenschaftsdisziplin Geomorphologie

Eingereicht an der Mathematisch-Naturwissenschaftlichen
Fakultät der Universität Potsdam

Antonius Golly

Potsdam, den 22.11.2017

Disputation am 24.05.2018

Hauptbetreuer
Prof. Dr. Niels Hovius (Gfz Potsdam)

1. Gutachter
Prof Dr. Francesco Comiti (Universität Bozen)

2. Gutachter
Dr. Jens Turowski (Gfz Potsdam)

Published online at the
Institutional Repository of the University of Potsdam:
URN urn:nbn:de:kobv:517-opus4-411728
http://nbn-resolving.de/urn:nbn:de:kobv:517-opus4-411728

To Christian Brieler

Summary

Steep mountain channels are an important component of the fluvial system. On geological timescales, they shape mountain belts and counteract tectonic uplift by erosion. Their channels are strongly coupled to hillslopes and they are often the main source of sediment transported downstream to low-gradient rivers and to alluvial fans, where commonly settlements in mountainous areas are located. Hence, mountain streams are the cause for one of the main natural hazards in these regions. Due to climate change and a pronounced populating of mountainous regions the attention given to this threat is even growing. Although quantitative studies on sediment transport have significantly advanced our knowledge on measuring and calibration techniques we still lack studies of the processes within mountain catchments. Studies examining the mechanisms of energy and mass exchange on small temporal and spatial scales in steep streams remain sparse in comparison to low-gradient alluvial channels.

In the beginning of this doctoral project, a vast amount of experience and knowledge of a steep stream in the Swiss Prealps had to be consolidated in order to shape the principal aim of this research effort. It became obvious, that observations from within the catchment are underrepresented in comparison to experiments performed at the catchment's outlet measuring fluxes and the effects of the transported material. To counteract this imbalance, an examination of mass fluxes within the catchment on the process scale was intended. Hence, this thesis is heavily based on direct field observations, which are generally rare in these environments in quantity and quality. The first objective was to investigate the coupling of the channel with surrounding hillslopes, the major sources of sediment. This research, which involved the monitoring of the channel and adjacent hillslopes, revealed that alluvial channel steps play a key role in coupling of channel and hillslopes. The observations showed that hillslope stability is strongly associated with the step presence and an understanding of step morphology and stability is therefore crucial in understanding sediment mobilization. This finding refined the way we think about the sediment dynamics in steep channels and motivated continued research of the step dynamics. However, soon it became obvious that the technological basis for developing field tests and analyzing the high resolution geometry measured in the field was not available. Moreover, for many geometrical quantities in mountain channels definitions and a clear scientific standard was not available. For example, these streams are characterized

by a high spatial variability of the channel banks, preventing straightforward calculations of the channel width without a defined reference. Thus, the second and inevitable part of this thesis became the development and evaluation of scientific tools in order to investigate the geometrical content of the study reach thoroughly. The developed framework allowed the derivation of various metrics of step and channel geometry which facilitated research on the a large data set of observations of channel steps. In the third part, innovative, physically-based metrics have been developed and compared to current knowledge on step formation, suggested in the literature. With this analyses it could be demonstrated that the formation of channel steps follow a wide range of hydraulic controls. Due to the wide range of tested parameters channel steps observed in a natural stream were attributed to different mechanisms of step formation, including those based on jamming and those based on key-stones. This study extended our knowledge on step formation in a steep stream and harmonized different, often time seen as competing, processes of step formation. This study was based on observations collected at one point in time. In the fourth part of this project, the findings of the snap-shot observations were extended in the temporal dimension and the derived concepts have been utilized to investigate reach-scale step patterns in response to large, exceptional flood events. The preliminary results of this work based on the long-term analyses of 7 years of long profile surveys showed that the previously observed channel-hillslope mechanism is the responsible for the short-term response of step formation.

The findings of the long-term analyses of step patterns drew a bow to the initial observations of a channel-hillslope system which allowed to join the dots in the dynamics of steep stream. Thus, in this thesis a broad approach has been chosen to gain insights into the complex system of steep mountain rivers. The effort includes in situ field observations (article I), the development of quantitative scientific tools (article II), the reach-scale analyses of step-pool morphology (article III) and its temporal evolution (article IV). With this work our view on the processes within the catchment has been advanced towards a better mechanistic understanding of these fluvial system relevant to improve applied scientific work.

Table of Contents

List of Figures

List of Tables

1 General Introduction

This doctoral thesis is about the study of a steep mountain channel. Steep mountain channels have by definition gradients greater than 3% and are present on all five continents. Despite the areal prevalence of mountain channels, of which steep channels represent a considerable fraction, they have drawn broader research interest only since a few decades (Wohl, 2000). At the beginning of the scientific study of mountainous regions and their landforms biological patterns and the zonation of species were the focus of interest (von Humboldt, 1852). This research put mountain ecosystems among the most unique and fragile ecosystems on the planet (Jeník, 1997). Today, about one third of the worldwide environmentally protected areas are in mountains (Ives et al., 1997). With an expanding populating of mountainous regions, the need to understand physical processes became more important, e.g. to minimize hazards due to floods or debris flows in densely populated areas, like the Swiss Alps. Since then, the role of rivers as the main sources of sediments received growing attention (Horton, 1945; Rapp, 1960). New technologies, as remote sensing or radiometric dating techniques, led to new applications of the study of

Fig. 1: The Erlenbach in Switzerland, a mountain channel with large roughness elements in the channel bed. In this section boulders with a diameter of 1.6 m are present.

geomorphic processes and landscape evolution in mountains (Young and Twidale, 1993). Nowadays, the study of mountain streams incorporates a wide set of questions but they remain less understood in comparison to low-land alluvial channels. There are two main reasons for the increasing scientific interest in steep mountain channels. Mountain regions are progressively populated and residential buildings and facilities are getting closer to such channels, and hence become regularly prone to the negative effects of extreme events (Ives and Messerli, 1989). Moreover, due to climatic change extreme events might be more frequent and more intense (Raymond Pralong et al., 2015), increasing the severity of hazards. Thus, the increased research interest is justified and studies on the dynamics of mountain channels timely and important.

In this thesis, fundamental concepts of the system of mountain channels are studied. Detailed field observations are used to identify principal process links and to investigate and test morphological models proposed in the literature. After a general motivation why we care about the exciting threshold systems of mountain channels (section 1.1), a detailed introduction into the objectives of this thesis is presented (section 1.2).

1.1 Mountain channels

In steep terrain, steep mountain channels are dominant in drainage area and channel length. For example in Switzerland, 74% percent of the total stream length is represented by mountain channels with a gradient above 3% (Fig. 2) (Nitsche et al., 2012b). An increasing number of people live in the vicinity of such catchments and thus the research of risks and impacts emanating from these landforms is a pressing issue. Moreover are these headwater catchments studied all over the world to understand the interplay of climate, tectonics and erosion. It follows an introduction regarding these aspects.

1.1.1 The role of mountain channels for landscape evolution

Steep headwater catchments are the main source of sediment transported to alluvial channels (Schumm, 1977; Buffington and Montgomery, 2013). The general concept of sediment flux from headwater sources to depositional zones, also referred to as the sediment cascade (Burt and Allison, 2009), ascribes mountain channels a special role for the evolution of the landscape: mountain channels are crucial for the formation, expansion and alteration of drainage networks, the adjustment of river channel shape and slope, and the routing of sediment (Howard, 1994; Whipple and Tucker, 1999; Stark and Stark, 2001;

Whipple, 2004). Base level changes of mountain channels are propagated to the upstream river network (Schumm, 1993), setting the base level for hillslopes. This transient

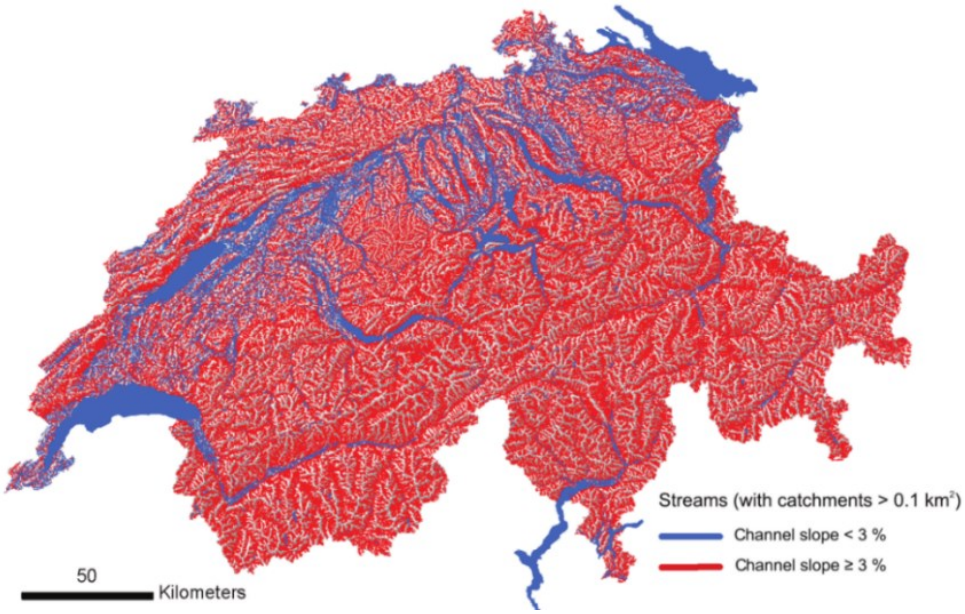

Fig. 2: Map of Switzerland with red areas indicating catchments with channels that have a slope of ≥ 3° (Source data: DTM-AV © 2012 swisstopo).

migration of knickpoints can locally destabilize adjacent hillslopes through steepening, undercutting or debuttressing (Harvey, 2002; Azanon et al., 2005). Thus, channel-hillslope coupling is pronounced in mountain channels and represents a key control on the generation of sediment from a catchment (Howard, 1994; Hovius and Stark, 2006; Grimaud et al., 2016). The processes of mass movement include a large range of temporal and spatial scales. On the smallest scales, high-frequency (e.g. daily) processes occur, such as suspended load. On the largest scales, high-magnitude events occur, such as debris flows during exceptional floods (Bartnik et al., 1992; Turowski et al., 2010). The resulting mass export is responsible for eroding mountains and building relief on geologic timescales, counteracting tectonic uplift and therefore sets the height and relief of mountain belts (Willett and Brandon, 2002). Moreover, the transported sediment has secondary effects. For example, through the transported sediment fluvial bedrock erosion is facilitated by the 'tools-effect' (Beer and Turowski, 2015), which actively controls the steady-state slope of bedrock channels (Sklar and Dietrich, 2006), and may determine the temporal evolution, life span and final topography of mountain belts (Egholm et al., 2013). In addition, the mobilized sediment frequently accounts for damage on property and infrastructure.

1.1.2 Hazardous potential of steep streams

Sediment from steep headwater catchments is released to valley floors during extreme events (Rickenmann and Jakob, 2015). In these valley floors the settlements are commonly located and severe damage and fatality can occur as a result of sediment transport (Marston, 2008; Totschnig et al., 2011). The worldwide costs of damages due to sediment transport amounted to USD 389 billion in the year 2011 (Munich Re, 2012). In Switzerland, one third to one half of the total costs of natural hazards are directly or indirectly related to fluvial sediment transport, amounting to on average CHF 110 million per year (Hilker et al., 2009; Badoux et al., 2014). The spatial distribution of these damages correlates generally with a regional measure of channel steepness (Fig. 3), highlighting the important role of steep channels as a hazard source. However, the damage itself commonly occurs in the valley bottoms where facilities and buildings are concentrated (Badoux et al., 2014). In addition to financial loss due to floods and sediment transport (e.g. debris flows) from mountain rivers, fatalities occur. Between 1946 and 2015 in Switzerland more than 1000 fatalities occurred due to natural hazards, of which 198 were a consequence of floods and landslides, including debris flows (Badoux et al., 2016).

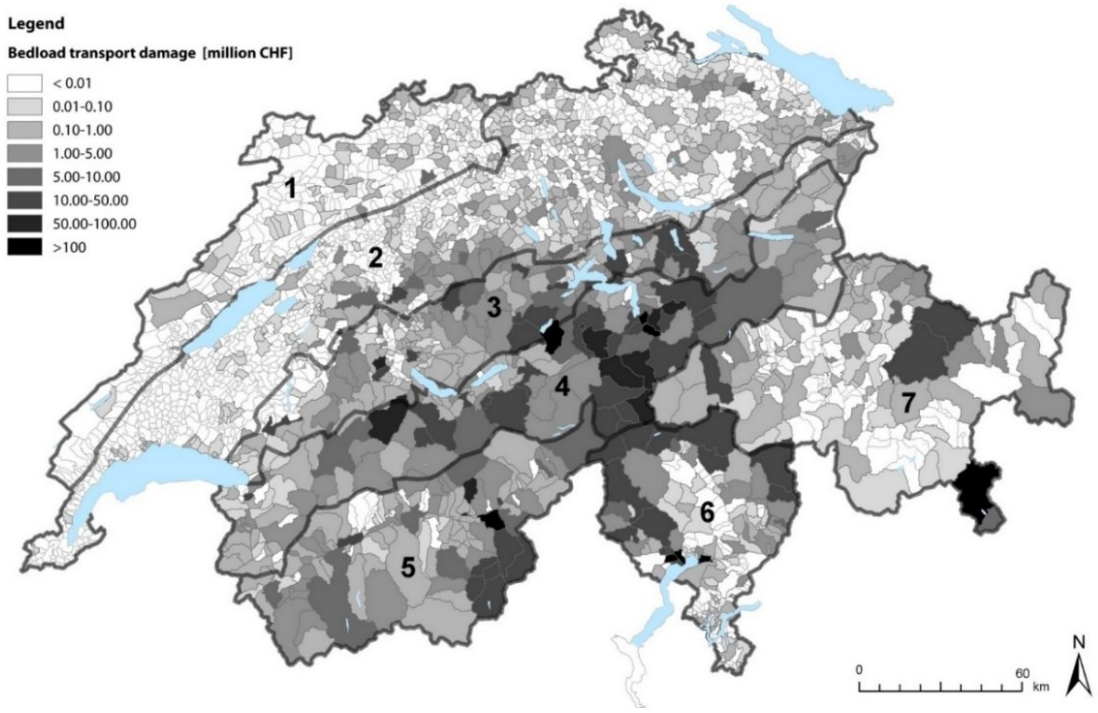

Fig. 3: Spatial distribution of damage costs caused by bed load transport, differentiated by affected communities (from Badoux et al., 2014).

Fig. 4: Three extreme events in Switzerland during which bedload from mountain catchments caused major damage. a) After a severe rainstorm in October 2000 the Baltschieder torrent deposited nearly 120.000 m^3 of sediment in the village causing CHF 50 Mio. of damage (Jäggi et al., 2004; Turowski et al., 2008), b) in August 2005 the Chärstelenbach torrent massively shifted its channel bed during an extreme event depositing a lot of sediment in the village (Bezzola and Hegg, 2007, 2008). c) In October 2011 sediment masses were deposited on the alluvial fan in the Lötschental valley.

1.2 Research gaps and objectives

This dissertation aims to improve our understanding of the principal mechanisms acting in the system of a steep mountain channel. Given the economic and social relevance of mountain catchments, this thesis consolidates insights of the processes acting within the catchment on small spatial and temporal scales. The individual contributions of this cumulative dissertation are designed to address fundamental research question that support applied research efforts with conceptual improvements. The following considerations will build the foundation for the articles (chapters 2 to 5) that this thesis yielded and the research questions addressed in the individual articles are formulated (green shaded boxes). In addition to the scientific work performed in the articles of this cumulative dissertation, broader research questions are formulated (blue shaded questions). The propositions of these questions go beyond the individual topics and represent a synthesis of the isolated contributions, which constitutes the main task of a doctoral thesis.

In the general morphological concept of the fluvial system the routing of sediment occurs from headwaters to alluvial plains and the bulk of this sediment is transported as bedload. Thus, bedload transport is a key process in mountain catchments and has been measured for decades in mountain rivers all over the world and through multiple approaches (Bänziger and Burch, 1990; Taniguchi and Itakura, 1992; Sear et al., 2001; Ergenzinger and De Jong, 2003; Mao et al., 2006; Bunte, 2010; Rickenmann et al., 2014), including indirect and direct measurements. For direct measurements sediment is trapped in mobile or stationary baskets or other reservoirs to then later (in rare cases also immediately) measure the weight or volume of the sediment. Indirect methods make use of the energetic or acoustic signal emitted by the transported sediment. The latter techniques require a calibration of the signals to yield proper estimates of sediment volumes.

To mitigate risks and hazards resulting from sediment transport, quantitative predictions are required. With recent technological development the sediment that is coming out of the catchment can be measured more precisely than just a few years ago (Habersack, 2001; Gray et al., 2010, 2017; Wyss et al., 2016c). However, there are still numerous challenges in modelling bedload transport, with reasons on different levels. Most directly, the calibration of indirect measurements of bedload transport signals to absolute volumes is difficult (Rickenmann and McArdell, 2007; Wyss et al., 2016a). A more conceptual issue

is that sediment transport exhibits considerable fluctuations, even under hydraulically steady conditions (Hoey, 1992; Turowski, 2010). For these fluctuations, multiple factors are relevant. On the one hand, sediment availability is often subject to large variability in mountain rivers (Lenzi et al., 2004; Recking, 2012). On the other hand, given sediment-rich conditions, sediment transport is commonly overpredicted due to the under-estimated effects of the macro-roughness elements (Rickenmann, 2001; Almedeij and Diplas, 2003; Barry et al., 2004; Nitsche et al., 2011; Schneider, 2014).

In the next paragraphs these issues of sediment supply (1.2.1) and the role of macro-roughness (1.2.3) in steep mountain streams are reviewed and the research questions, as addressed by this thesis, are formulated. Beyond that, the technical and methodological basis required to perform high-resolution analyses on the catchment scale, is presented (1.2.2). By the following considerations the focus of this thesis is narrowed from the broader motivation given in section 1.1 towards catchment and process scale research questions. The order in which the questions are derived reflects the order in which the work was performed. However, the chronological order of the work is not arbitrary but are the consequence of the natural process of comprehension. The logical link the articles exhibit are discussed in section 6.

1.2.1 Channel-hillslope coupling in steep streams

Forecasts of sediment transport remain challenging as transport rates exhibit fluctuations even for identical hydraulic conditions. For example, in natural channels hysteresis effects during events of bedload transport are observed (Turowski et al., 2009; Mao et al., 2014) and for many steep streams the discharge at the start of bedload transport varies over an order of magnitude (Fig. 5, Turowski et al., 2011). Furthermore, the correlation of water discharge at the start of bedload transport of an event to the discharge at end of transport of the previous event is strong for pro-glacial streams (Fig. 5a-c) but not in unglaciated streams (Fig. 5d). It is hypothesized that the good correlation of the pro-glacial stream is related to the characteristics of their flood regime, which are mainly melt-water-driven floods with short time-lags (Turowski et al., 2011). Another hypothesized cause are local changes of sediment availability resulting from a pronounced channel-hillslope coupling, which has been reported for the Erlenbach (Schuerch et al., 2006).

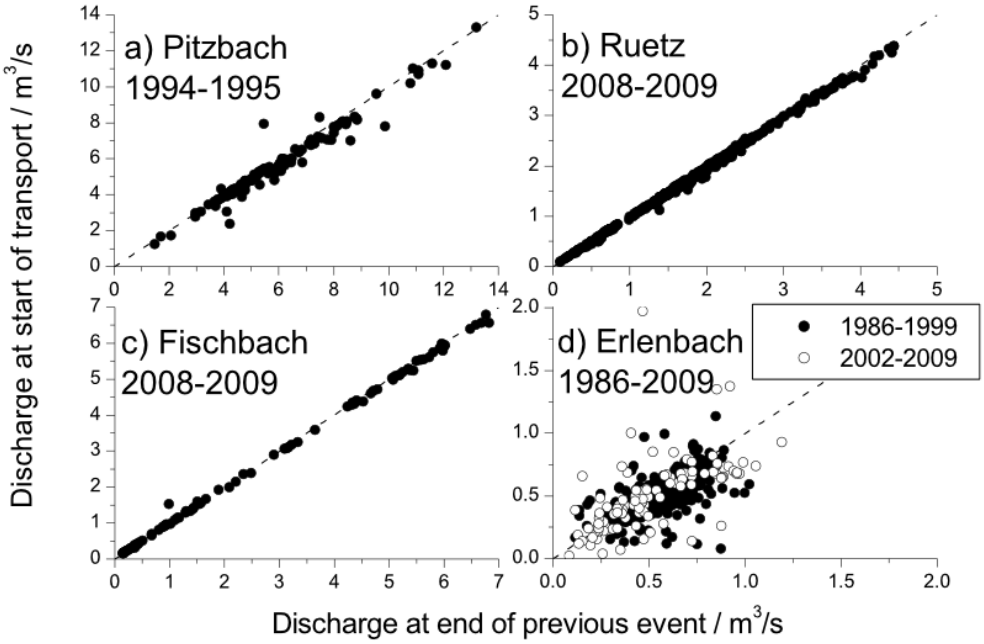

Fig. 5: The discharge at the start of bedload transport (x-axes) varies over an order of magnitude for four streams. The correlation of water discharge at the start of bedload transport of an event to the discharge at end of transport of the previous event is strong for pro-glacial streams (a to c) but not in the Erlenbach. Figure from Turowski et al. 2011.

This indicates that we have not fully understood the processes that occur within the catchment. In order to understand and model sediment transport, first and foremost the sediment sources need to be identified: sediment could be generated by the vertical incision of the stream, or alternatively, could be recruited from the hillslopes adjacent to the channel. In the latter case, the erosional processes could be dominated by lateral (bank) erosion or a different mechanism. Second, the processes in the coupling of sediment sources and transport zones need to be investigated. These processes are responsible for releasing sediment into the fluvial system, affecting the moment a channel turns from supply-limited to transport-limited conditions. Furthermore, the coupling mechanisms determine the timing of the input relative to the flood hydrograph, e.g. correlation of sediment and water discharge peaks (Turowski et al., 2013a). This, in turn, affects magnitudes of the sediment export out of the catchment measured downstream. Thus, a comprehensive understanding of the sediment dynamics of mountain streams must be based on process understanding.

The research questions regarding the coupling of sediment sources and transport zones are formulated as follows:

Q 1: Which processes are responsible for activating the sediment sources and mobilizing sediment?

Q 2: Are the processes of sediment generation threshold processes or continuous?

Q 3: If they are threshold processes, what floods are required to trigger them?

These questions are addressed in article I given in section 2 and further discussed in general conclusion in section 6.1.

1.2.2 Methods and tools for analyses of high-resolution geometrical data

The heterogeneous nature of steep mountain streams requires special attention to the tools and methods used to analyze their geometrical content. In comparison to low-gradient channels, in mountain rivers a number of exceptions exist which complicate straight-forward calculations. For example, the simple problem of the calculation of the channel gradient is straightforwardly answered for a homogenous river: it is the difference in elevation of two points A and B divided by their horizontal distance, while that distance can often be approximated manually. In contrast, the banks of mountain rivers are rarely straight, but show a high small-scale variability. Thus, even simple geometric features, such as channel length or slope, require precise definition as there are profoundly different interpretations of these metrics in mountain channels. For example, headwater channels rarely have bankfull flow and most of the time base flow conditions. The length of the channel can be either interpreted as the (artificial) line that lies in the center between the channel banks – the channel centerline – representing flood water flow paths, or as the path of the thalweg, which represents the water flow path during base flow conditions. Both yield individual channel lengths and hence individual local and average gradients (Fig. 6). In addition, the local channel width is required to quantitatively analyze the morphology of mountain channels. Thus, in order to analyze the geometrical content of these environments scientifically a framework is required that generates reproducible results with an established standard.

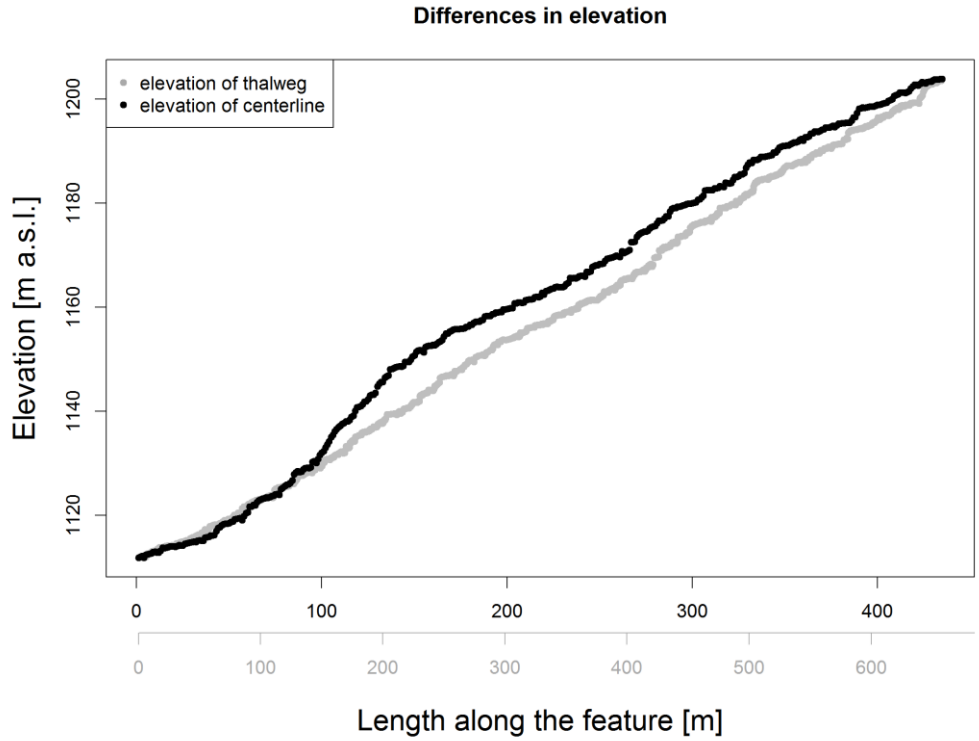

Fig. 6: Two channel long profiles of the same channel reach based on two different methods. The gray line represents the elevation profile of the thalweg (water flow during base flow conditions), resulting in a 640 m long profile. The black line represents the elevation profile of the channel centerline, an artificial line in the middle of the channel banks. The length of that profile is with 420 m considerably shorter. The two profiles show differences in the local channel gradient, which is quite consistent for the thalweg (gray line) but shows locally steep and flat sections for the centerline (black line). This demonstrates the importance of precisely defined and documented methods for the geometrical analyses of these channels.

The research question regarding quantitative tools for geomorphological research are formulated as follows:

Q 4: Can we develop a scientific standard by defining principal channel metrics in an objective and reproducible manner?

Q 5: Can we resolve the local channel width and slope as well as their local change in downstream direction with the necessary detail required for scientific research?

Q 6: Can we provide a structured framework for the analyses of channel geometry and secondary geomorphological features?

These questions are addressed in the article II given in section 3 and further discussed in general conclusion in section 6.2.

1.2.3 Step-pool systems

Sediment transport in steep mountain channels is commonly overpredicted by traditional models, typically due to sediment supply limitations and the effects of macro-roughness, while for the latter multiple cause-effect relations are debated. Proposed effects of macro-roughness include a decrease of flow velocities (Bathurst, 1985, 2002; Katul et al., 2002; Rickenmann and Recking, 2011) and an increase in the threshold of motion (Lamb et al., 2008) or a combination of both (Schneider et al., 2015). A third, hardly investigated effect is the drag by the roughness elements exerted on the mobile sediment, decreasing the transport efficiency. In summary, although the over prediction of sediment transport rates is caused by the inobservance of large macro-roughness elements in these channels (Rickenmann, 2001; Almedeij and Diplas, 2003; Barry et al., 2004; Nitsche et al., 2011; Schneider, 2014) no study provided an analytical and integral method for describing sediment transport in steep streams.

Typical macro-roughness elements in boulder-bed channels are depositional steps formed from the sediment routed through the channel (Montgomery and Buffington, 1997) and these steps dissipate the flow energy (Chin, 2003). Thus, channel morphology, the local flow hydraulics and the sediment transport are directly tied (Fig. 30). In order to understand the sediment transport within the channel, it is crucial to understand the development of this bed form, i.e. the processes of step formation. Several, often contradicting, theories of step formation exist in the literature but we lack detailed tests of these theories with high-resolution field observations of channel steps.

The research question regarding the dynamics of step-pool systems are formulated as follows:

Q 7: What are the characteristic morphological step metrics (step parameters) that are indicative for the various step forming theories?

Q 8: How do those theorized parameters compare with a set of natural channel steps observed in the field?

Q 9: Of the models of step formation suggested in the literature, which one or which ones apply in natural stream?

These questions are addressed in the article III given in section 4 and further discussed in general conclusion in section 6.3.

Detailed knowledge of the processes that lead to step formation are also key for investigating the temporal progression of step-pool systems. Especially for the organization or re-organization of the channel bed after large, exceptional flood events observations are scarce. Given a sufficiently long geometrical record of channel long profiles the temporal dimension of step formation could be investigated with a focus on the following research questions:

Q 10: How do patterns of channel steps evolve after exceptional floods that mobilize most of the channel steps?

Q 11: Do entropy concepts previously suggested prevail in natural steep streams?

Q 12: What step forming mechanisms dominate in which phase of the recovery after exceptional floods?

These questions are addressed in the article IV given in section 5 and further discussed in general conclusion in section 6.3.

1.2.4 Linking research questions

Integrating the research of the individual articles, this dissertation synthesizes the findings of the articles to answer questions of a broader perspective. Addressing the initially given issues, the questions are formulated as follows. The text belongs always to the question above it.

Q 13: What are the implications of the characteristics of channel-hillslope coupling processes on the sediment dynamics?

This broad question reviews what can be learned from a knowledge of the processes of channel-hillslope coupling with regard to sediment supply, initiation of motion and the timing of magnitudes of bedload transport rates. This aspect is discussed in paragraph 6.4.

Q 14: Does the development of technical tools advance the way we design studies of the morphometry in steep mountain streams?

The development of a technological basis was an extensive part of this work. But was it a crucial one? In this question, discussed in paragraph 6.5, the significance of such developments for how research is planned and conducted is explored.

Q 15: How do temporal and spatial variations of the channel width fit in the context of channel-hillslope coupling mechanisms and the evolution of step-pool systems?

Combining the findings of the study on channel-hillslope coupling and on the controlling factors of step formation, channel width variations constitute a link. Whether that link can be functional or collateral is discussed in paragraph 6.6.

Q 16: How can the temporal progression of different step types be explained by the previous findings of this work?

The observations of the temporal evolution of channel steps can be linked to the study on channel-hillslope coupling. An approach to combine these findings is attempted paragraph 6.7.

1.3 Field site Erlenbach

This thesis focuses on observations collected in the Erlenbach, a steep mountain channel in Switzerland. In the following paragraphs the catchment with the relevant metrics is introduced, and a brief overview of the long tradition of mountain channel research in this catchment is given. Finally, the long hydrological record of the Erlenbach is presented, which should be considered for the long-term morphodynamics of a stream.

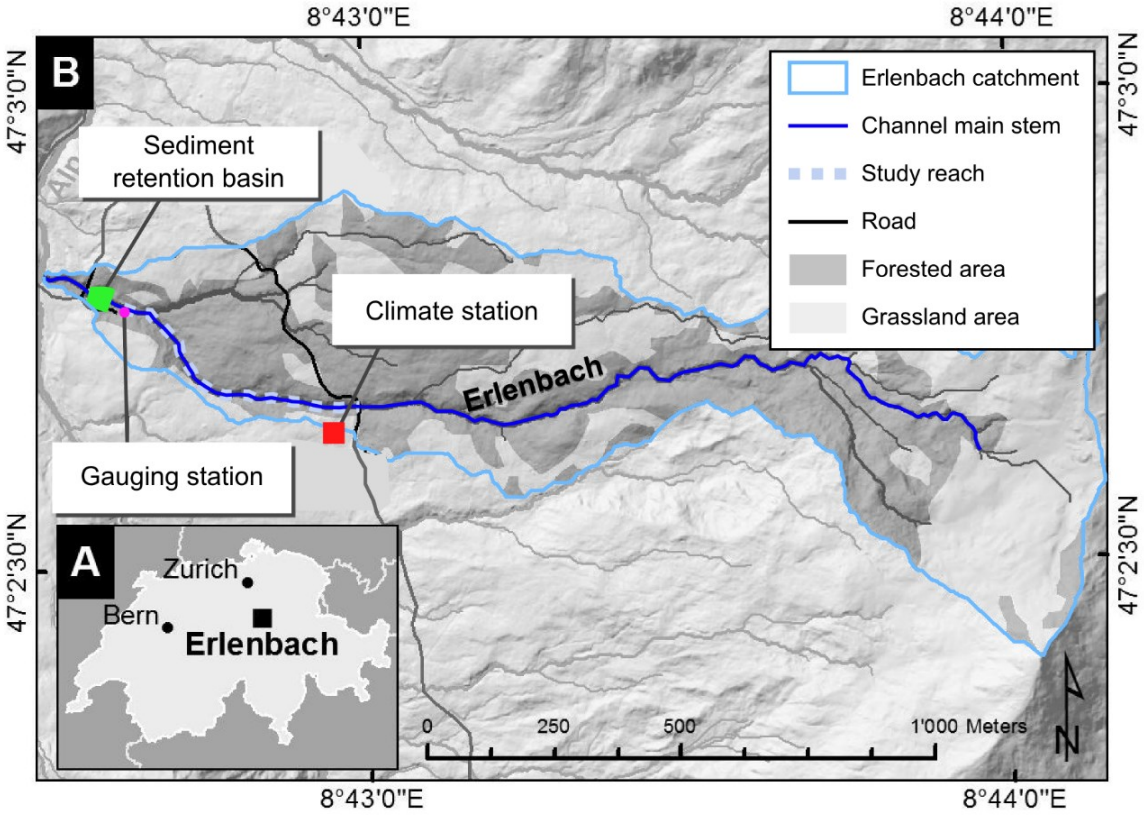

Fig. 7: Map of the Erlenbach catchment. After Turowski et al., 2016 (edited).

1.3.1 Location, geology and climate

The Erlenbach stream is located in Switzerland, 50 km south of Zurich, in the Alptal valley (Fig. 7). The catchment's outlet is located near the village Brunni at an elevation of 1110 m. a.s.l. The Erlenbach drains into the Alp river, which itself drains into the Sihl that confluence in Zurich with the Limmat. The catchment of the Erlenbach is characterized by a relatively small drainage area of 0.74 km² (Rickenmann and McArdell, 2007) reaching up to 1655 m a.s.l. at the drainage divide and is mainly forested. The main stem of the stream network is approximately 2 km long while the study reach referred to throughout

this thesis is an approximately 550 m long channel section upstream of a water gauge (Fig. 7). Despite the small catchment area, the Erlenbach is very active in terms of bedload transport events. Bedload transport occurs on ~20 occasions per year (Rickenmann et al., 2012) exporting on average 455 m^3/a of sediment from the catchment. The stream in the study reach has an average gradient of 17% and features a predominantly gravel-boulder bed and step-pool/cascading bedforms (Molnar et al., 2010) typical for steep mountain streams. Despite the steep gradient, no debris flow occurred during the 30 years long observational period and sediment transport has been fluvial even at the highest discharges (Turowski et al., 2013a). The Erlenbach stream bed is covered by alluvium and bed rock is not apparent within the catchment. The bed surface is characterized by coarse grains, with a D_{50} (D_{90}) of 8 cm (40 cm, Fig. 8) and large boulders of up to several meters diameter are present (Fig. 1).

Erlenbach catchment metrics

Location (outlet)	47.045153°N, 8.708619°E
Elevation (min, max)	1110 m, 1655 m a.s.l.
Catchment area	0.74 km^2
Channel width (mean, [25th -, 75th - percentile])	3.59 m [2.59 m, 4.37 m]
Mean annual precipitation	2300 mm/a
Mean number of rain days	161 d/a
Runoff coefficient	0.77
Mean annual discharge	1700 mm/a
Snow to rain ratio	30-40% / 60-70%
Mean annual sediment yield	455 m^3/a
Average erosion rate	0.64 mm/a
Mean annual flood discharge	2 m^3/s
Sediment retention basin size	2000 m^3

Table 1: Catchment and channel characteristics of the Erlenbach, the study area of this thesis.

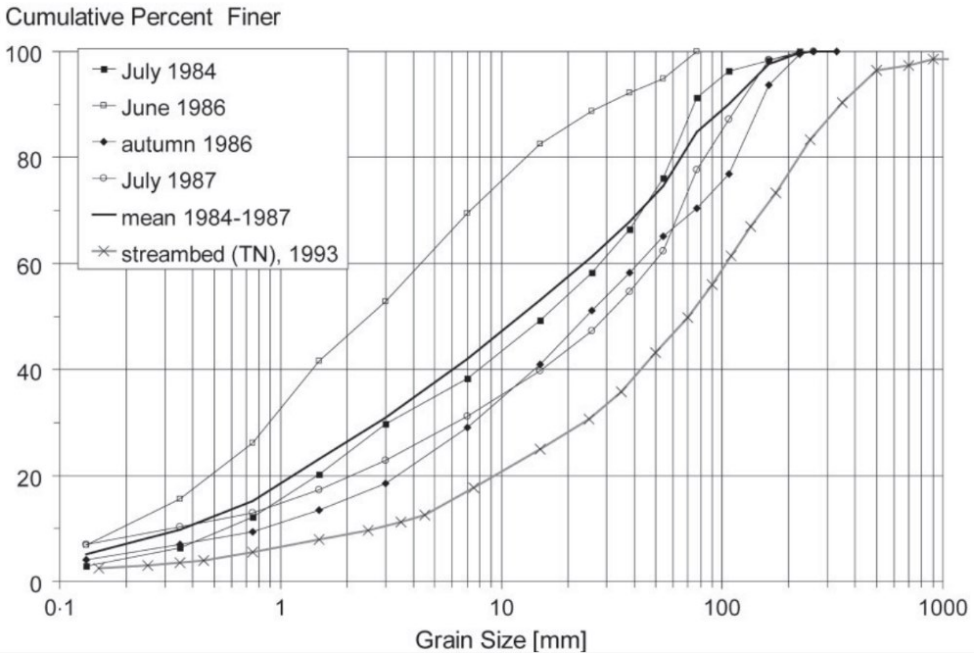

Fig. 8: Grain size distribution of the Erlenbach stream bed (line "streambed (TN), 1993) analyzed by the transect-by-number method. The other lines represent transported sediment material collected in the retention basin. From Rickenmann and McArdell (2007).

The Alptal is part of the Prealps of central Switzerland and due to the medium elevation glaciers are not present. The region is geologically classified as a Flysch zone, which mainly consists of conglomerates, arenites, pelites and fine-grained limestone (Winkler et al., 1985). The Erlenbach catchment is dominated by mudstones that are easily erodible even in clear water flow (Turowski et al., 2013a). This substrate is overlain by a thin cover of glacial till, which has been partly reworked by the stream (Winkler et al., 1985). As a consequence of the weak substrate, creeping and sliding hillslopes are frequent along most of the channel length (Schuerch et al., 2006). Furthermore, the clayey material is responsible for the high runoff coefficient of 0.77 (Turowski et al., 2009), leading to a mean annual water runoff of 1770 mm of the 2300 mm mean annual precipitation. Around 30-40% of that precipitation falls as snow between November and April, causing continuous elevated runoff during the snow-melt season (Rickenmann and McArdell, 2007). Although snow-melt discharge contributes significantly to the mean annual water runoff, it plays a minor role for the total sediment export from the catchment, which is mainly caused by short-duration, high-intensity rainfalls during the summer month (Rickenmann and McArdell, 2007).

1.3.2 Research activities and instrumentation

Scientific research in the Erlenbach catchment has a long history (Table 2), mainly carried out by the WSL (Swiss Federal Research Institute for Forest, Snow and Landscape, Birmensdorf, Switzerland). The site offers several benefits, as a good geographical (close to Zurich) and local (catchment features a maintained road) accessibility. Furthermore, flood and sediment transport events are frequent and thereby promote field studies. The focus of the early research was the study of the hydrologic effect of forests on floods in mountainous catchments (Hegg et al., 2006), following the negative effects of deforestation on hazard potentials that became obvious in the middle of the 19th century (Landolt, 1869). To achieve this objective from 1967 onwards 11 catchments in the Alptal valley had been equipped with hydrological sensors (Burch, 1994). In 1982 a new gauging station was built at the outlet of the Erlenbach in combination with a retention basin, trapping all transported clastic and organic sediment load from the catchment. With this retention basin long-term sediment transport volumes could be measured. For continuous measurements of bedload hydrophone-based sensors have been installed in 1986 (Bänziger and Burch, 1990), which later were replaced by geophone sensors, giving valuable insights into the runoff-bedload relation in mountain rivers (Hegg and Rickenmann, 1998; Rickenmann and McArdell, 2007; Turowski et al., 2009; Rickenmann et al., 2012). For an improved calibration of these indirect measurements to absolute transport rates, automatic basket samples have been installed in 2009 (Rickenmann et al., 2012).

The measurements of sediment transport on a high temporal resolution have not only been used to quantify absolute volumes, but also to study the initiation of motion (Turowski et al., 2011), finding a correlation between the discharge at the start of bedload transport to the discharge at the end of bedload transport of a previous event (Fig. 5). However, that correlation is not strong for the Erlenbach compared to other, pro-glacial streams (paragraph 1.2.1). Particles seem to get more mobile between events, as the discharge at the end of transport is higher than at the start (Turowski et al., 2011). This might be due to pronounced channel-hillslope coupling involving slow-moving landslide complexes along the channel banks of the Erlenbach (Schuerch et al., 2006), which facilitate sediment delivery. Furthermore, in the Erlenbach an annual hysteresis of bedload transport has been observed, meaning that for a given water flow rate more

bedload is carried by in the beginning of the year than towards the end of the year (Masteller and Finnegan, 2016), which is typical for mountain channels (Reid et al., 1985; Moog and Whiting, 1998). The main reasons for that behavior might be the snow cover and snow melt period.

The precise knowledge of bedload transport rates in the Erlenbach has promoted studies of the tools effect, the effect of sediment transport on bedrock erosion (Beer et al., 2015). With highly accurate measurements of bedload erosion rates and sediment transport rates, predictions by erosion models were significantly advanced (Beer and Turowski, 2015).

Sediment transport measurements	(Rickenmann, 1997; Rickenmann and McArdell, 2007; Rickenmann *et al.*, 2012, 2014; Schneider *et al.*, 2014; Roth *et al.*, 2016, 2017, Wyss *et al.*, 2016b, 2016c)
Improvement of sediment transport equations considering macro-roughness based on field data	(Rickenmann, 2001; Nitsche *et al.*, 2011, 2012a; Yager *et al.*, 2012c; Schneider *et al.*, 2015)
Classification and interpretation of channel morphology	(Yager *et al.*, 2012a; Turowski *et al.*, 2013a)
Step-pool sequences	(Turowski *et al.*, 2009; Molnar *et al.*, 2010)
Start and end of bedload transport, initiation of motion	(Turowski *et al.*, 2011)
Bedrock erosion and the relevance of bedload transport for bedrock erosion	(Turowski *et al.*, 2013b, 2015; Beer and Turowski, 2015; Beer *et al.*, 2015)
Channel-hillslope coupling, slow-moving landslides	(Schuerch *et al.*, 2006; Molnar *et al.*, 2010; Jochner, 2013)
Transport of organic matter, woody debris, log jams	(Jochner *et al.*, 2013, 2015; Smith *et al.*, 2013; Turowski *et al.*, 2013c, 2016)

Table 2: A brief overview of research projects related to channel morphology, sediment transport and fluvial processes carried out in the Erlenbach.

1.3.3 Flood history

The long hydrological record of the Erlenbach preserved detailed knowledge on the flood history of the Erlenbach. Events with high sediment yield and long return times that have a large effect on channel morphology (exceptional events) have lasting effects on the morphodynamics of mountain channels. If geomorphologic states are analyzed, i.e. to assess transient or stable channel states, it is crucial to consider this history. In the Erlenbach, four exceptional events in 1984, 1995, 2007 and 2010 occurred since the installation of new gauging stations in 1982 (Table 3). They all occurred during summer as a result of convective storms which were characterized by short durations and high intensities (Table 3). In the Erlenbach, these exceptional events caused the majority of the sediment load of the entire measuring period (Fig. 9), as is typical for Switzerland (Badoux et al., 2014). In the 2007 event, boulders of up to 1.35 m diameter have been moved, which is twice the diameter of boulders that would have been predicted to move based on shear stress calculations (Turowski et al., 2009). However, these events do not only affect momentary sediment transport rates, but have also a lasting effect, as sediment transport rates are shown to be elevated after these events (Turowski et al., 2009). However, the long-term effects of exceptional events on the system of the mountain channels, for example on the morphodynamics on step-pool systems, are under debate (Molnar et al., 2010; Turowski et al., 2013a).

	1984	*1995*	*2007*	*2010*
Date	25 July	14 July	20 June	1 August
Peak discharge	12 m^3/s	9.8 m^3/s	14.6 m^3/s	10.9 m^3/s
Cumulative precipitation	106.7 mm	45.3 mm	55.2 mm	56.6 mm
Max. 10-min. precip. intensity	16.4 mm/10min	24.2 mm/10 min	24 mm/10 min	16.6 mm/10 min
Sediment yield	2230 m^3	890 m^3	1650 m^3	400 m^3
Estimated return interval	42 a	27 a	47 a	20 a

Table 3: Event metrics of the four exceptional flood events in the Erlenbach since the installation of hydraulic sensors in 1982. From Turowski et al. 2009 and Turowski et al. 2013.

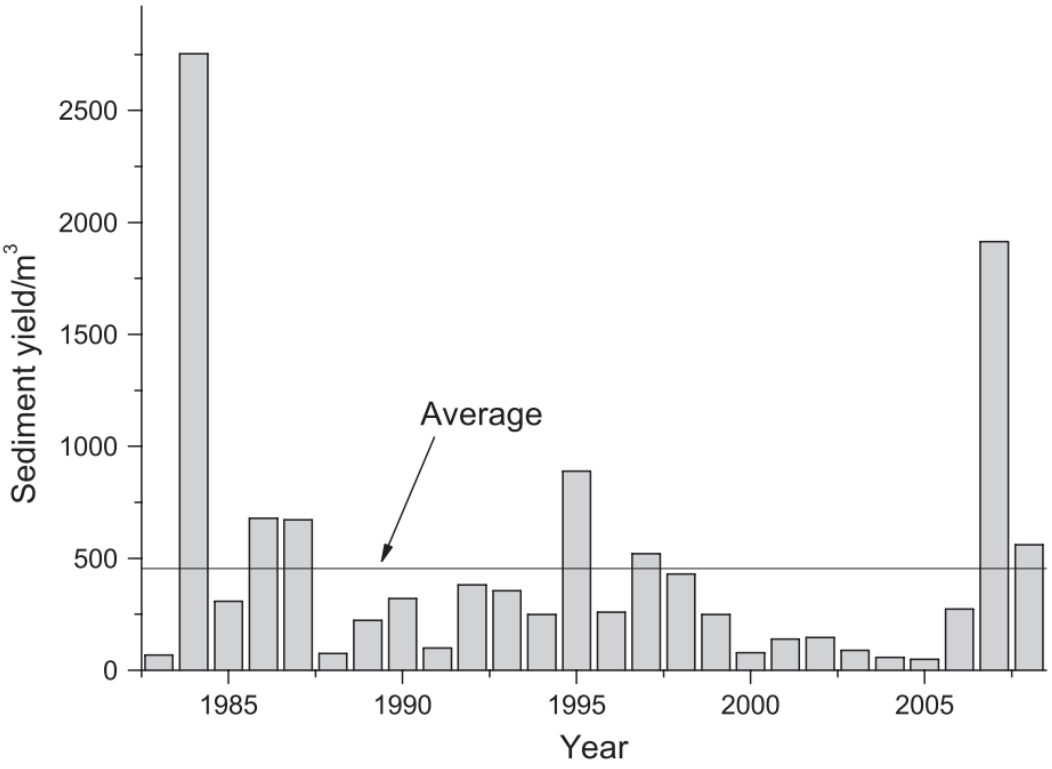

Fig. 9: Annual sediment load measured in the retention basin in the Erlenbach until 2008. Most of the years sediment yield is below the average, indicating that the majority of the total sediment export can be attributed to exceptional events with long return intervals. From Turowski et al., 2009.

1.4 General information on methods and technologies

During this work, intensive field work has been carried out in the Erlenbach. In the next paragraphs the methods and technologies used for this study are described in detail. Most of the research performed in the Erlenbach focuses on a 550 m reach upstream of the retention basin, which is approximately a quarter of the main stream length. Whenever study reach is mentioned, this 550 m reach of the Erlenbach is meant.

1.4.1 Total station surveys

A total station is an instrument to measure the angle and distance of objects relative to the total station. In order to make quantitative measurements, a setup of the station is required so that position and orientation of the station is known. For this reason, permanent reference points with known locations are installed at the retention basin of the Erlenbach. Once set up, measurements of channel geometry can be performed into the

catchment with a high accuracy of a few centimeters. Over the course of a survey, for example of the long profile, a series of single point measurements to movable objects are performed in the study reach. The objects detectable by the station need to have a high reflectance, thus, usually reflectors or round prisms are used for the single point measurements operated by field assistant.

Fig. 10: During a field survey of the long profile the total station (right) is setup with known coordinates and orientation. Then, single point measurements to a reflector held by an assistant in the channel bed are performed. A usual long profile survey of the 550 m study reach consists of ~1000 single point measurements surveyed over a period of three days.

The total station surveys in the study reach of the Erlenbach were performed between 2012 and 2017, and include a wide range of collected geometry and features, which are listed next. The thalweg – the water flow path during base flow conditions – is the main object of investigation and has been collected in all surveys (Table 4). The measuring protocol for this feature (Milzow et al., 2006) dictates to capture all changes of the vertical and planform profile of the thalweg. Thus, surveying from downstream to upstream, the start of a pool, the deepest point in the pool, the end of the pool and the step crest are

covered, even without doing an interpretation of what is potentially a step (Fig. 11). The horizontal spacing of the measurements can differ. For example, measurements of start of pool and deepest point in pool can have a distance of 80 cm, but the end of pool is usually in close distance to the step crest. The average horizontal spacing over the study reach is 65 cm, resulting in ~1000 single point measurements on the 550 m long channel reach. This shows an approximate increase in length of the water flow path at low flow conditions in comparison to high flow conditions of 15% (Fig. 6) due to meandering of the thalweg.

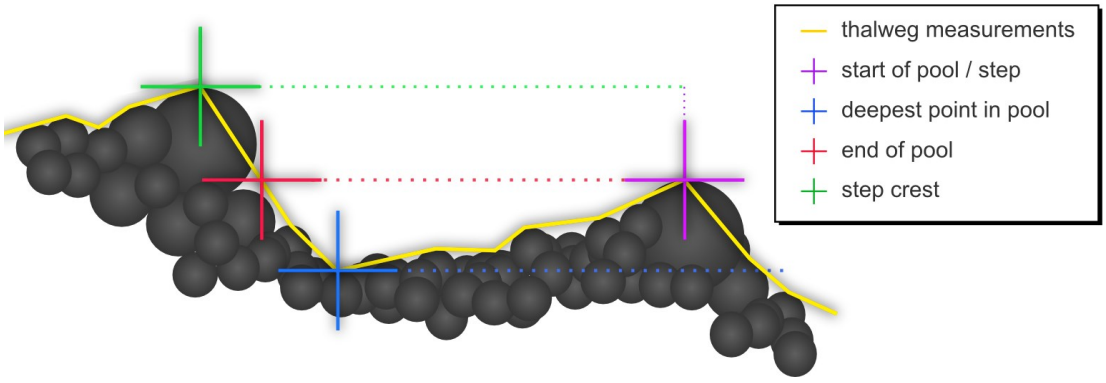

Fig. 11: Visualization of the protocol of the thalweg survey. Certain changes are captured by single point measurements: start of pool, deepest point in pool, end of pool and step crest. In the field, a classification of whether or not a step is present is not required, as these rules are objective.

The channel banks are defined as the margin of the active channel bed, determined by the transition from sediment cover to the vegetated riparian strip and have been surveyed with an average spacing of 2.1 m during all surveys since 2012. The spatial measurement interval was increased where rapid changes in the planform geometry of the channel bed occurred. A survey of 88 fixpoints markers were added to the survey in 2015 (Table 4). These markers were deployed along the channel bed in close distance to the channel with an average spacing of ~5m as aluminum poles with a head of reflective tape (Fig. 59c,d,e). They are assumed to have a fixed position over the course of a year but are re-surveyed in case they have moved by creeping of the adjacent hillslopes. The fixpoint markers are used to establish a spatial reference network in the study reach, and first and foremost used to reference the three-dimensional model of the study reach (section 1.4.2).

	2010		*2011*		*2012*		*2013*		*2014*		*2015*		*2016*	*2017*
Date	27 Apr	3 Sep	22 June	18 Nov	20 July	29 Oct	4 June	11 Sep	9 Apr	15 Nov	13 May	1 Oct	20 May	3 June
Thalweg survey	•[1)]	•	•	•	•	•	•	•	•	•	•	•	•	•
Channel bank survey	-	-[2)]	-	-	•	-	-	•	•	•	•	•	•	•
Fixpoint survey	-	-	-	-	-	-	-	-	-	-	•	-	•	•
Boulder survey	-	-	-	-	-	-	-	-	-	-	•	•	-	-
Used in this study	-	•	•	•	•	•	•	•	•	•	•	•	•	•
Performed by author	-	-	-	-	-	-	-	•	•	•	•	•	•	•

Table 4: List of total station surveys performed in the Erlenbach as used in this thesis. Further surveys have been performed in the 2004, 2007, 2009, but have not been included in this list as they these data were not used for analyses, which rely on the calculation of the channel width (see article III). 1) This thalweg survey followed a different protocol. Due to a resulting in courser spatial resolution this survey was not used in this study. 2) For surveys lacking channel bank surveys the calculation of the width is not possible. For these surveys the bank geometry of the temporally closest survey was taken.

1.4.2 Photogrammetric surveys with Agisoft PhotoScan

Photogrammetry for the scientific study of the Earth surface receives growing attention as recording devices and post-processing tools are getting economically and technically viable (e.g. Dietrich, 2014; Cook, 2017). For example, applications of photogrammetric methods in geomorphology have gathered wide acceptance (Westoby et al., 2012; Gómez-Gutiérrez et al., 2014; Micheletti et al., 2015; Eltner et al., 2017; Mosbrucker et al., 2017). A full three dimensional model of a mountain stream is currently not available, but such a model facilitates new and innovative research. For example, channel roughness could be assessed in an unprecedented accuracy, or consecutive surveys could gain insights into local erosion and deposition patterns in the stream bed. During this doctoral project the infrastructure and the equipment has been developed to generate a fully quantitative three-dimensional model based on the photogrammetric method (Fig. 13). The model has also been used in this dissertation as step properties have been extracted from the model (article III, section 4.2).

The principle of photogrammetry (or structure from motion) is to capture an object from multiple viewing angles and resolve its three-dimensional shape by analyzing the relative

distance of identical points in the imagery. Identical points alter their relative distance to each other due to the parallax effect. The reconstruction of the three-dimensional shape is nowadays done by user-friendly software tools, as for example Agisoft Photoscan (Agisoft, 2017), which was also used in this study. The model was created from a series of images collected in the Erlenbach with two digital cameras (Canon PowerShot D20) mounted to a 3 m portable pole (Fig. 59 f+g). Approximately 5000 images have been collected during two days of surveying, walking the stream bed of the study reach upstream. For a good model result, it is crucial to not miss patches of the stream bed and to capture every single point of the stream bed by multiple images. Good model results can be achieved with an effective image overlap of above 5, which is defined as the average number of images each point in the model covers. For our model, we reach values of above 9 (Fig. 12), indicating a high overlap of images. The study reach was divided into 15 separate channel stretches, to facilitate a more stable processing within the Agisoft software. For the first stretch, the ground resolution of the model is 1.42 mm/pixel and the total error (sum of x-,y-,z-error) of the fixpoints markers is 2.06 cm.

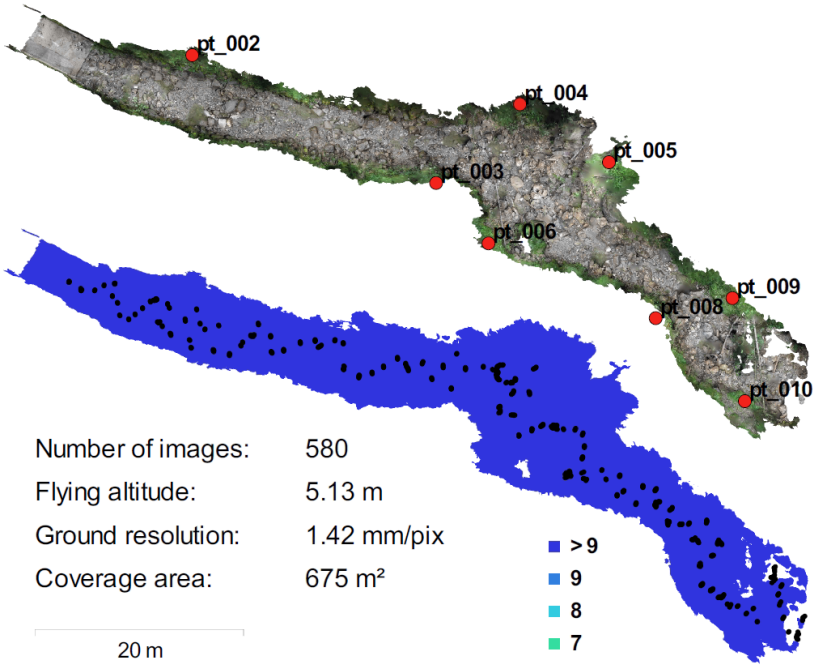

Fig. 12: The first stretch of the three-dimensional model of the Erlenbach stream, which represents ~8% of the Erlenbach channel length. In the lower map, black dots indicate the back-calculated camera positions during survey, showing a wide lateral coverage of the channel bank. This is necessary in order to reduce shadows in the resulting model. The blue color indicates an effective overlap of over 9, representing ideal conditions for a high-quality model.

Fig. 13: An example of the three-dimensional model of the Erlenbach. The image shows the meshed dense point cloud rendered with the texture from the images in Agisoft Photoscan. The pink points on the channel bed indicate the total station measurements of the thalweg (water flow path during base-flow conditions). The green markers indicate the position of alluvial channel steps identified with the automated algorithm by Zimmermann et al., 2008. A link to a video of the model can be found in Appendix A.

The resulting model of the Erlenbach shows a good agreement with the independently measured thalweg (Fig. 13) and is hence suitable to extract geometric metrics. A link to a video of the model can be found in the Appendix A.

1.4.3 Time lapse image analyses with SciLapse

Time lapse photography is a cost-effective and off-the-shelf solution to capture and quantify the progress of geomorphic processes, for example the quantification of erosional processes in fluvial geomorphology (e.g. Trimble, 1997; Cook et al., 2014; Nichols et al., 2016). During this doctoral project 10 automatic time lapse cameras have been deployed in the Erlenbach catchment to monitor different objects, as for example individual slow-moving landslides, log jams, steps or stream network confluences. The cameras were of the model Bushnell Nature View Cam HD that had a battery life of about four months taking a picture every 30 minutes. Time lapse camera images have been used for article I, studying the controls and feedbacks in the coupling of the Erlenbach stream and adjacent hillslopes. Quantitative data has been derived from the time lapse imagery using a

framework for the extraction of geometrical content (Fig. 14) specifically developed by the author. The software tool is capable of measuring polylines and polygon within the imagery that are manually drawn onto the images. The coordinates of the geometries along with the time-stamps of the particular image are stored within a database, which can be opened in R or other programming languages. Furthermore, the series of time lapse images can be coupled to other temporal data. For example, timeseries of precipitation or temperature can be loaded into the tool allowing a quick navigation to certain events, e.g. floods, or visual comparisons. The tool is developed as a web-based application and will soon be released under http://scilapse.org/ for public use.

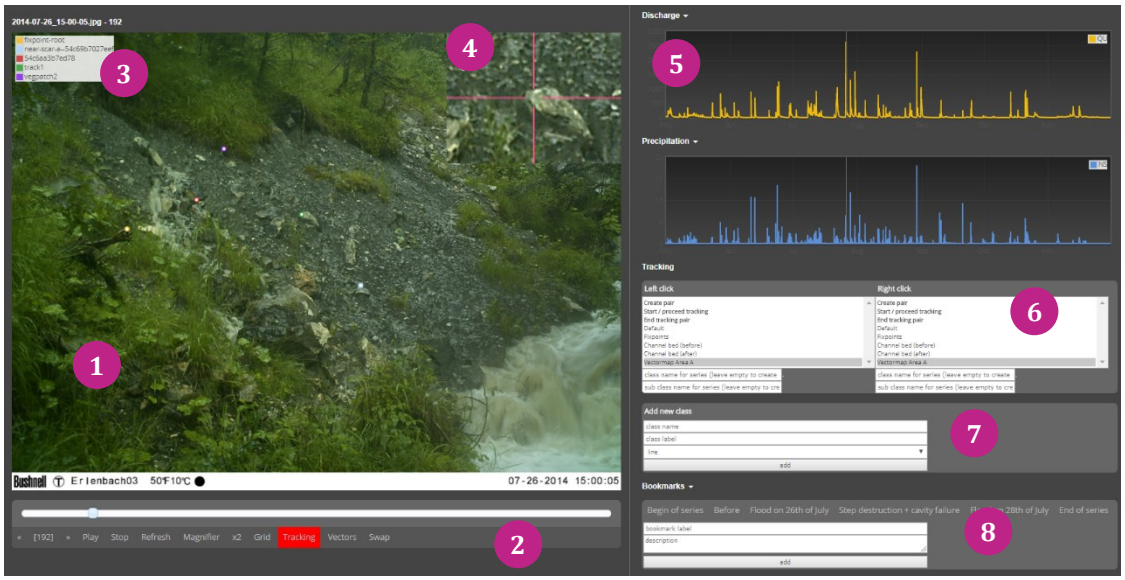

Fig. 14: The main view of SciLapse, a tool for the manual tracking of objects or extraction of geometrical data from time lapse images. The panels are 1: image viewer, behaves like a standard desktop application, 2: controls for the image panel (next/previous image, start slide show, magnifier), 3: legend of tracked objects, that are shown on top of the images, 4: magnifier the area around the cursor, 5: climate data or other time series, which are tied to the image viewer (e.g. clicks in the time series will show the corresponding images, and browsing through the images in panel 1 will update the cursor in the timeseries), 6: tracking panel for polylines and points, 7: adding new tracking features, 8: bookmark managing and browsing.

1.5 Overview of publications and the author's contribution

The bulk of the work of this dissertation has been performed by the author. However, this work would not have been possible without the guidance, assistance and support of many people which are acknowledged in section 7 individually. The scientific body of this cumulative dissertation are the articles I to IV presented in the following chapters 2 to 5. Of these articles, article I and II have been published, and article III is under review, all in international ISI-listed peer-reviewed journals. Article IV is at an early stage of development and gives first insights into preliminary results and interpretation rather than representing a ready-to-submit manuscript. Hereinafter, a list of the contributions and their status is given.

Article I: Golly, A., Turowski, J. M., Badoux, A., & Hovius, N. (2017). Controls and feedbacks in the coupling of mountain channels and hillslopes. Geology, 45(4), 307-310, doi: 10.1130/G38831.1

A.G. conducted the field experiments and performed the data analyses. A.G. and J.M.T. conceptualized the manuscript. A.B. and N.H. constantly improved the manuscript with comments and during discussions. A.B. gave logistical and financial support for field work.

The article has been published on 23 January 2017 in the journal GEOLOGY.

Article II: Golly, A., & Turowski, J. M. (2017). Deriving principal channel metrics from bank and long-profile geometry with the R package cmgo. Earth Surface Dynamics, 5(3), 557, doi: 10.5194/esurf-5-557-2017

A.G. designed the algorithms and developed the software and its implementation as an R-package. A.G. and J.M.T. equally contributed to structure the publication, which was written by A.G. with additional input by J.M.T.

The article has been published on 14 September 2017 in the journal Earth Surface Dynamics.

Article III: Golly, A., Turowski, J. M., Badoux, A., & Hovius, N. (2017). Testing models of step formation against observations of channel steps in a steep mountain stream *(under review)*.

A.G. performed the field surveys with assistance of many helpers and did the statistical data analyzes. A.G. and J.M.T. conceived the study developed field tests and data analysis strategy, and wrote the manuscript with input of A.B. and N.H. A.B. gave logistical and financial support for field work.

The article is under review as of 8 November 2017 in Earth Surface Processes and Landforms.

Article IV: Golly, A., Turowski, J. M., Badoux, A. The evolution of step-pool systems after an exceptional flood event (*draft*).

A.G. organized and managed the field surveys and the data analyzes. A.G. and J.M.T. conceived the study and outlined the draft manuscript. A.B. gave logistical and financial support for field work.

The manuscript is presented as a draft in this thesis and gives first insights into preliminary results and their interpretation.

2 Article I: Controls and feedbacks in the coupling of mountain channels and hillslopes

Authors: Antonius Golly [1] , Jens M. Turowski [1] , Alexandre Badoux [2] , and Niels Hovius [1,3]
Submitted to: Geology (GSA Publications)
Manuscript submitted: 16 September 2016
Manuscript accepted: 6 December 2016
Manuscript published: 23 January 2017

[1] German Research Centre for Geosciences (GFZ), Section 5.1 - Geomorphology, Telegrafenberg, 14473 Potsdam, Germany
[2] Swiss Federal Institute for Forest, Snow and Landscape Research WSL, Zürcherstrasse 111, 8903 Birmensdorf, Switzerland
[3] University of Potsdam, Institute of Earth and Environmental Science, Am Neuen Palais 10, 14469 Potsdam, Germany

Abstract

Mountain channels can be strongly coupled with adjacent hillslopes, exchanging both mass and energy. However, hypotheses of the underlying cause and effect relations are based on indirect field observations that do not resolve the mechanics of channel-hillslope coupling at the process scale. Here, we present direct observational data of a coupled channel-hillslope system in the Erlenbach, Switzerland. A slow-moving landslide flanking this alpine torrent failed after a flood had eroded an alluvial step in the channel at its base, representing evidence for an upsystem link in channel-hillslope coupling. Progressive accumulation of landslide debris in the channel eventually resulted in a renewed step, stabilizing the hillslope and restoring the channel long-profile in a downsystem link. The observations highlight that upsystem and downsystem coupling mechanisms are joined in a negative feedback cycle. In this cycle, debuttressing and re-buttressing due to channel bed erosion and alluviation are the dominant controls on hillslope stability. Based on an order of magnitude estimate it is plausible that the observed feedback mechanism is a relevant process in the production of coarse (>2mm) sediment in the Erlenbach on centennial scales.

2.1 Introduction

In mountain valleys, channels and hillslopes are in a permanent feedback relation (Montgomery and Buffington, 1997). Sediment input from hillslopes affects sediment availability (Hovius et al., 2000) and local flow hydraulics in the channel (downsystem coupling). Conversely, vertical and lateral erosion of the channel bed impacts the stability of adjacent hillslopes (upsystem coupling) (Harvey, 2002; Azanon et al., 2005). The characteristics of these coupling mechanisms determine the sediment dynamics of catchments on large scales. A precise identification of the processes and their dominant controls is therefore key to quantitative landscape evolution theories. However, direct field observations are scarce. In the Erlenbach, a steep mountain stream in the Swiss Pre-Alps, Molnar (2010) observed that active landslides are located in close proximity to steps in the channel long profile. This qualitative observation suggests a link but does not identify its direction: landslides may form channel steps or step migration may induce landsliding. In an experimental landscape with artificial base-level fall, Bigi et al. (2006) recorded a greater number of failing slopes downstream of sharp changes in the channel gradient, reflecting upsystem coupling. Yet, it remains unclear how this mechanism scales up to natural environments and conditions, for example for vegetated hillslopes under natural flood cycles. Wistuba et al. (2015) found evidence both for upsystem and downsystem coupling along a semi-alluvial channel, but their dendrochronological data could not resolve the triggers, dominant controls and timescale of the processes involved. And finally, on regional scales, increased hillslope erosion rates correlate spatially with local channel bed lowering (Gallen et al., 2011; Lévy et al., 2012; Roering et al., 2015; Bennett et al., 2016), but dominant controls and process scale mechanics have not been determined. Moreover, feedbacks between the mechanisms responsible for upsystem and downsystem coupling have not yet been demonstrated.

Here, we present direct observational data of a channel reach featuring an alluvial step and an adjacent hillslope with a suspended landslide in the Erlenbach catchment, Switzerland. Landslides in this catchment are deep-seated and slow moving, permitting documentation of the processes and feedbacks in the coupled channel-hillslope system with time-lapse photography. Our monitoring captured two rare flood events, which eroded the alluvial step, followed by the activation of landslide movement ultimately resulting in the formation of a new channel step and the end of landslide activity. Thus, the

data provide insight into an entire cycle of channel-hillslope interactions. Based on this, we propose a conceptual model of channel-hillslope coupling in steep streams and explore its implications for the sediment dynamics in headwater catchments.

2.2 Field Site and Methods

The Erlenbach, a small mountain torrent (catchment area of 0.74 km^2) in the Alptal valley of the Swiss Pre-alps (Fig. 15), is an extensively studied field site for sediment transport and sediment export is constantly monitored (e.g. Rickenmann et al., 2012). The channel has an average slope of 17% and an alternating step-pool/cascade morphology (Turowski et al., 2009). 92 steps with a mean height of 0.79 m were identified from a long-profile survey in April 2014. Stream discharge is measured at 10-min intervals at a stationary gauge at the catchment outlet and precipitation rates are measured at 10-min intervals at a climate station located within the catchment (Fig. 15) (Turowski et al., 2009). The mean annual precipitation is 2300 mm, 80% of which falls as summer rain, and the mean annual peak discharge is approximately 2 m^3/s. Bedload transport begins at a water discharge of around 0.5 m^3/s (Turowski et al., 2011) and is frequent with ~20 events per year, mainly driven by convective summer storms. The catchment is underlain by clay-rich flysch and glacial tills, hosting a large number of slow-moving landslides with exposed subsoils that occupy 35% of the channel banks (Schuerch et al., 2006).

In the Erlenbach, we monitored the evolution of a 20 m long channel reach about 150 m upstream of the gauge (Fig. 15) that initially featured a 0.5 m high alluvial step spanning the 1.6 m wide stream. The step was located at the downstream end of a suspended slow-moving landslide with a width of 16 m along the channel bank and a hillslope length of 12 m. We used stationary time-lapse cameras to monitor the channel and the suspended slow-moving landslide at 30-minute intervals during three periods: 12 to 16 April 2014, 11 July to 27 November 2014 and 2 August to 3 October 2015. Schuerch et al. (2006) identified that this landslide was embedded within a larger, dormant landslide complex (65 x 35 m). This larger complex was not monitored directly here, but from frequent field visits it is known that there has not been significant movement during the observational period. We measured the channel long-profile before and after the monitoring period and determined the migration of the step from the time-lapse images. Image interpretations were validated during three field visits over the monitoring period. The landslide exhibited episodic movement, which was measured in units of image pixels by manual

tracking of features at the landslide surface (e.g. a characteristic feature of a tree root or boulder) between the time-lapse images. The pixel coordinates, which were translated into a constant, independent reference frame, scale linearly to real-world coordinates since the viewing distance stayed constant throughout the monitoring period, and the camera lens does not exhibit distortion. The pixel length in the zone where movement was measured ranged from 1.5 to 1.65 mm.

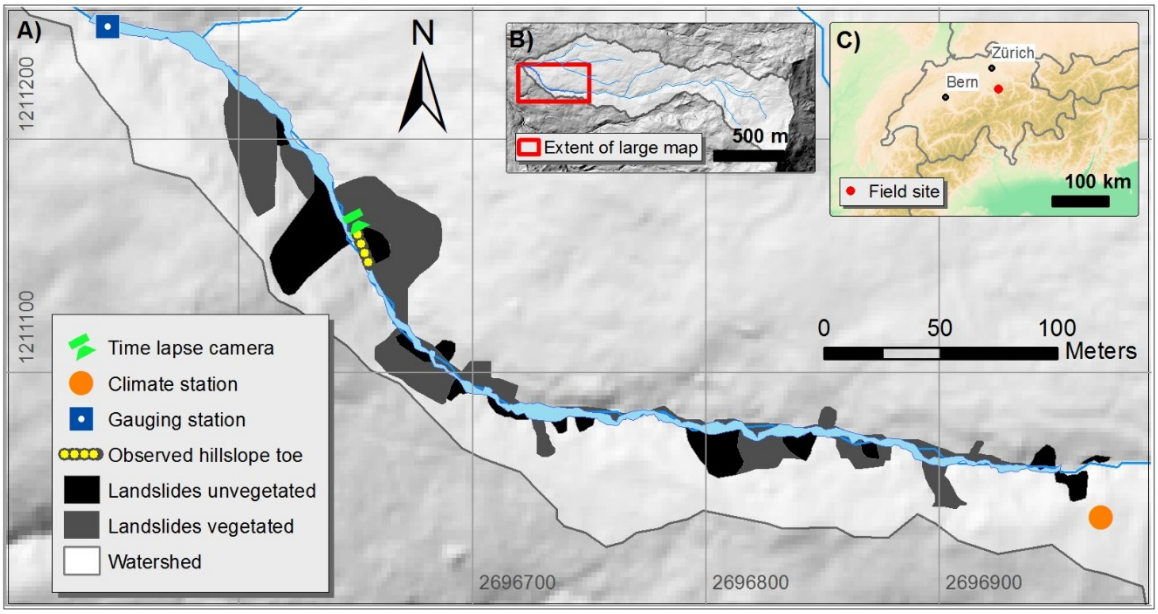

Fig. 15: Study site (A) with landslides mapped by Schuerch et al. (2006) and its location in the Erlenbach catchment (B). The time lapse camera (green symbol) points upstream to a channel-hillslope ensemble with the monitored landslide toe (yellow dotted line). Coordinates refer to the CH1903+ system. DHM source: dhm25 © 2016 swisstopo (5704 000 000).

2.3 Observations

Rainfall can drive channel and hillslope activity. Between 12 April and 27 November 2014, 129 rainfall events (rainfall episodes delimited by at least five hours without precipitation) occurred in the Erlenbach catchment, totaling 1998 mm precipitation. Hereinafter we give long-term average precipitation intensities in mm/d, event-averaged intensities in mm/h and maximum intensities in mm/10min to reflect the relevant time scale. Before 26 July 2014, no measurable surface displacement of the landslide occurred (Fig. 16), despite the incidence of 55 precipitation events totaling 1073 mm of rain (10.1 mm/d on average). The largest event during that time delivered 149 mm of rain within 4

days, ending on 11 July 2014. The highest event intensity occurred on 10 June 2014 with 3 mm/h over 7.7 hours, while the highest measured peak intensity was 13.4 mm/10-min on 23 June 2014. Bedload transport occurred during these three events and on five other occasions before 26 July 2014, during floods with peak discharges between 0.7 and 1.5 m^3/s. After these events, channel discharge returned to base flow (< 0.2 m^3/s) within a day, as is common for the Erlenbach.

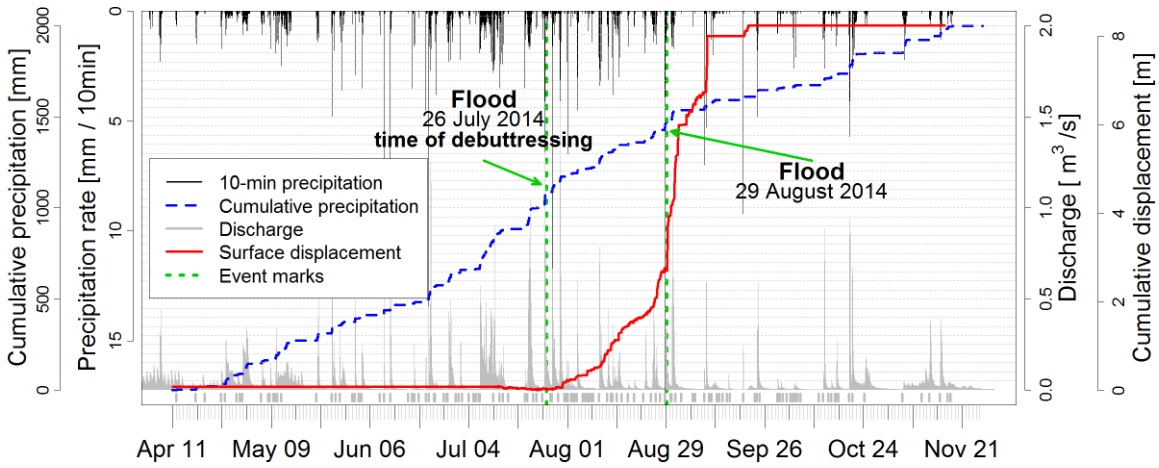

Fig. 16: Timeline of precipitation rates (black bars), cumulative precipitation (dashed blue line), discharge (gray graph) and hillslope surface displacement (red line) between April and November 2014 in the Erlenbach catchment. Vertical green lines indicate large flood events on 26 July and 29 August 2014.

A rainfall event starting on 26 July 2014 (86 mm of rain, max. intensity 6.4 mm/10min, averaged intensity 2.1 mm/h) caused a flood with a peak discharge of 3.9 m^3/s and a return time of ~5 years (Liechti, 2008). While earlier events had not noticeably modified the monitored reach, this larger flood resulted in a ~4 m upstream migration of the alluvial step at the downstream end of the landslide (Fig. 17, Movie in Appendix B). During the flood, a bank failure ensued between the initial and the new step position (Fig. 17B), which led to a doubling of the channel width. A deep-seated hillslope motion was not apparent during and shortly after this discharge event and base flow conditions were restored 20 hours after peak discharge. Then, 40 hours after peak discharge, the landslide entered a 45-day phase of continuous and integral motion (Fig. 16), during which intermittent precipitation averaged 10.8 mm/d. A second large flood on 29 August 2014 (peak discharge 4.8 m^3/s, return time ~7 years) removed more sediment from the channel bed, causing the step to migrate a further 4 m upstream (Fig. 17C and D). Subsequently,

hillslope surface displacement rates increased by 400%. This displacement caused the channel to narrow gradually until the original channel width was restored on 11 September 2014. During a subsequent rainstorm on 21 September hillslope displacement further narrowed the channel so that entrained boulders and large wood of the landslide built a new channel step at the landslide toe. This new step formed near the position of the original step and had a height of ~1 m. The total landslide displacement length amounts to 8 m over a width of 10 m. Large rainstorms occurred after this date, with the largest total precipitation 71.2 mm on 4 November 2014, and the highest rainfall intensity 5.8 mm/h over 8 hours and peak intensity 5.7 mm/10min on 20 October 2014. Over the remaining monitoring period, occasional hillslope movement occurred in patches 10 m upslope of the hillslope toe. However, further sediment supply to the channel was not observed.

Fig. 17: The phases of the feedback cycle captured by the time-lapse camera. A: the Erlenbach stream with an alluvial step at the downstream end of a suspended landslide, B: flood causes step destruction and an immediate bank failure, C: channel width increases due to step destruction, D: landslide enters a phase of integral motion as a response, E: final blockage of the channel with hillslope material forming a new step (initial step position indicated in red) leading to landslide stabilization. Note: the camera pan between D and E was considered for the calculation of the displacement rates. Large image versions can be found in the Appendix C, as well as in the movie in in Appendix B.

The larger vegetated landslide complex, within which the monitored landslide was located, did not exhibit significant motion over the observational period.

2.4 Discussion

In 2014, the monitored reach of the Erlenbach appears to have gone through a full channel-hillslope feedback cycle. To ascertain this, the dominant control on the hillslope's stability needs to be identified. Generally, hillslope stability is compromised by steepening, debuttressing of the landslide toe (Korup et al., 2010) or water infiltrating the ground, causing for example an increase of the pore water pressure within the landslide body (Van Asch et al., 1999). In our case, hillslope angle and substrate remained constant during the relevant period, leaving changes in the toe geometry and the soil moisture as possible major drivers. Rainstorms prior to the activation of landslide motion surpassed the triggering event on 26 July 2014 in terms of maximum intensity, event-averaged intensity, as well as total precipitation, and average daily rainfall was similar before and during the period of movement. Therefore, hydraulic controls are unlikely to have been the root cause of the observed landslide displacement. Instead, we identify debuttressing of the landslide front, due to erosion of the alluvial channel step, as the likely trigger. Landsliding accelerated after the channel step had migrated to the upstream end of the landslide front in late August 2014, suggesting that the degree of debuttressing has an influence on the rate of sliding. At the time hillslope displacement ceased, the hydrological and meteorological conditions had not changed significantly, but a channel step had reformed at the toe of the landslide. Therefore, we argue that in our study reach, hillslope stabilization was primarily due to re-buttressing of the landslide, closing the feedback loop in the Erlenbach channel-hillslope system. Notably, after activation, hillslope displacement rates never dropped to zero until 11 September 2014 (date of restoration of the original channel width), even during dry episodes, indicating that gravitational forces exert the dominant control after the activation of movement. However, the rate of the displacement seems to respond to precipitation.

The entire feedback cycle of the channel-hillslope system can be described with a six-step conceptual model (Fig. 18). In the *initial position* (1) before the flood of 26 July 2014, the hillslope was inactive and no hillslope-internal characteristic was able to cause displacement. The *trigger* (2), causing hillslope movement, was the debuttressing of the landslide due to the erosion of an alluvial channel step at the landslide toe. This solicited

an immediate bank failure in the landslide toe and after a *delay* (3) of 40 hours the onset of deep-seated movement of the entire landslide body. Sustained *landsliding* (4) delivered sediment to the channel and, as the advected boulders and wood accumulated, a new channel *step formed* (5) at the landslide toe. Ultimately, step formation caused the end of hillslope movement and the onset of a new phase of *slope stability* (6).

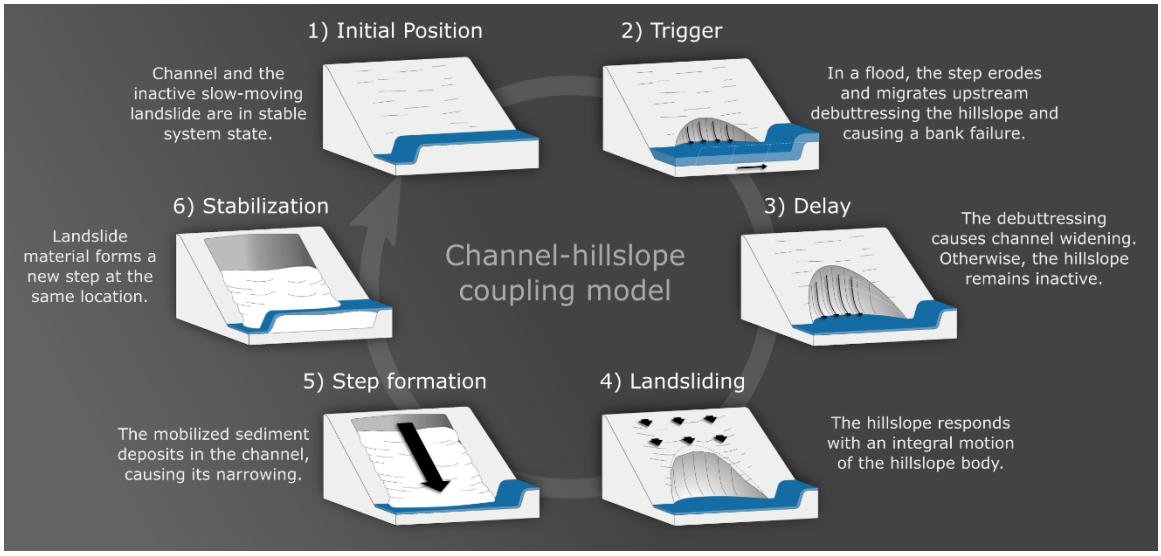

Fig. 18: The proposed conceptual model of channel-hillslope coupling based on the observations of the event cycle in the Erlenbach catchment. The cycle can be re-initiated – step 6) to 1) – once hillslope sediment is refilled, e.g. through sediment supply from further upslope.

Our monitoring data are direct observational evidence for general concepts in the coupling of channels and hillslopes as proposed by previous studies based on indirect, large-scale terrain analysis. First, our observations confirm that debuttressing by channel erosion can be a main cause of landslide activation in an upsystem link. This mechanism has also been invoked for the transient hillslope response to the upstream migration of knickpoints (Gallen et al., 2011; Mackey et al., 2014; Bennett et al., 2016) and, thus, appears to be applicable across channel and step scales. Second, we have documented the downsystem mechanism that counteracts channel incision and ultimately impedes hillslope erosion by accumulation of landslide debris in the channel. Importantly, we have observed that these two coupling mechanisms are directly linked in a negative feedback loop, in which the start and end state of a local channel long-profile are similar, despite the intervening reorganization of both channel and hillslope. Such a self-stabilizing feedback effect has

previously been suggested (Bennett et al., 2016; Shobe et al., 2016), but has not been observed directly.

Next, we explore whether the proposed channel-hillslope feedback cycle can be a relevant process for the production of coarse sediment (>2mm) in the Erlenbach. For that, we compare the recurrence interval of flood events known to break up a large fraction of the channel steps in the Erlenbach $RI_{trigger} \approx 20\ years$ (Turowski et al., 2009) to the back-calculated recurrence interval of the observed feedback cycle ($RI_{feedback}$). We derive $RI_{feedback}$ for the hypothetical case that the estimated sediment volume S_{LS} – generated during a feedback cycle activating all landslides in the catchment once – equals the total annual sediment flux S_{tot} (scenario A), and for the case that S_{LS} equals the annual coarse sediment flux S_{coarse} (scenario B). These scenarios reflect that over long time scales, hillslopes are the dominant source of sediment in the Erlenbach, since repeated long-profile surveys show neither significant aggradation nor erosion (Molnar et al., 2010). In scenario B it is assumed that other hillslope erosion processes, e.g. surface wash, convey only fine sediment into the channel. We approximate S_{LS} geometrically by $Width_{LS} * Length_{LS} * Depth_{LS}$. The landslide width $Width_{LS}$ is the total channel network length $L = 4644$ m times the measured fraction of landslides, $r_{LS} = 0.35$. Lacking better estimates, $Length_{LS}$ is taken from our point observation ($L_{LS} = 8\ m$). $Depth_{LS}$ is set at the average step height $\bar{h} = 0.79\ m$ multiplied by the cosine of the hillslope angle θ. Thus, the back-calculated recurrence interval of the feedback cycle $RI_{feedback}$ is given by

$$RI_{feedback} = \frac{S_{LS}}{S_{tot/coarse}} = \frac{L * r_{LS} * L_{LS} * \bar{h} * \cos(\theta)}{S_{tot/coarse}}$$

with $S_{LS} = \sim 7870\ m^3$, $S_{tot} = 1140\ m^3$ (Smith *et al.*, 2013) and $S_{coarse} = 380\ m^3$ (Rickenmann et al., 2012). Scenario A yields an $RI_{feedback}$ of ~7 years, which is at least three times smaller than $RI_{trigger}$. In this case, it is not plausible that landslides triggered by debuttressing capture the total long-term sediment export from the catchment exclusively. Scenario B yields an $RI_{feedback}$ of ~21 years which is in the same order of magnitude as $RI_{trigger}$. This case underlines that it is plausible that the observed feedback cycle can be relevant for the total coarse sediment flux in the Erlenbach. However, the calculation is subject to large uncertainties as we lack information on representative parameter values for the entire catchment. For example, the displacement length L_{LS} likely

depends on local landslide and channel dimensions and r_{LS} might not be constant throughout the catchment.

We hypothesize that the feedback mechanism can run through a number of cycles, given sediment supply from upslope (not observed during the monitoring period). The time T until upslope storage is exhausted is given by

$$T = \frac{L_h}{L_{LS}} * RI_{feedback}$$

where L_h is the total hillslope length to the catchment border (~120 m, taken from a DEM). This yields $T \approx 100\ years$, suggesting that the feedback mechanism at this location could be maintained on the centennial time scale before net base-level fall is required to sustain it.

2.5 Conclusion

Our field observations along a section of the Erlenbach stream demonstrate controls and feedbacks in the coupling of channels and hillslopes through the operation of upsystem and downsystem mechanisms. Hillslope motion and the release of sediment to the channel were first detected after the erosion of a small channel step debuttressing the hillslope toe. This upsystem link destabilized the coupled system and initiated a feedback cycle during which the hillslope responded in a downsystem link with sustained motion and sediment delivery to the channel. Eventually, the feedback loop closed when supplied sediment stabilized the hillslope by re-buttressing. This resulted in a net production of sediment propagating to the stream, emphasizing the relevance of the coupling mechanism for sediment availability on the catchment scale. The sequence underlines the importance of integrated channel-hillslope monitoring, as previous studies reporting landslide displacement rates in this catchment were limited to hillslope observations. The flood that triggered the event cycle had a recurrence interval of only ~5 years, making channel-hillslope coupling processes frequent and relevant for the sediment dynamics of steep streams since they are not limited to exceptional events as previously suggested. The time scales of the observed process links span from minutes of the triggering flood to months of inactivity, demonstrating the value of long-term high-resolution field observations for geomorphological studies.

2.6 Acknowledgements

We thank the reviewers Georgie Bennett, Martin Hurst and Lorenzo Marchi for constructive comments on the original manuscript, Joel Scheingross for encouragement and discussion, Kari Steiner for support with equipment and maintenance at the field site, Luzi Bernard for climate data and Tom Baumeister for creating the 3D sketch of the conceptual model. This research was funded by the GFZ, German Research Centre for Geosciences.

3 Article II: Deriving principle channel metrics from bank and long-profile geometry with the R-package cmgo

Authors: Antonius Golly [1] , Jens M. Turowski [1]
Submitted to: Earth surface dynamics (Copernicus Publications)
Manuscript submitted: 10 May 2017
Manuscript accepted: 21 Aug 2017
Manuscript published: 14 Sep 2017

[1] German Research Centre for Geosciences (GFZ), Section 5.1 - Geomorphology, Telegrafenberg, 14473 Potsdam, Germany

Abstract

Landscape patterns result from landscape forming processes. This link can be exploited in geomorphological research by reversely analyzing the geometrical content of landscapes to develop or confirm theories of the underlying processes. Since rivers represent a dominant control on landscape formation, there is a particular interest in examining channel metrics in a quantitative and objective manner. For example, river cross-section geometry is required to model local flow hydraulics which in turn determine erosion and thus channel dynamics. Similarly, channel geometry is crucial for engineering purposes, water resource management and ecological restauration efforts. These applications require a framework to capture and derive the data. In this paper we present an open-source software tool that performs the calculation of several channel metrics (length, slope, width, bank retreat, knickpoints, etc.) in an objective and reproducible way based on principle bank geometry that can be measured in the field or in a GIS. Furthermore, the software provides a framework to integrate spatial features, for example the abundance of species or the occurrence of knickpoints. The program is available https://github.com/AntoniusGolly/cmgo and is free to use, modify and redistribute under the terms of the GNU General Public License version 3 as published by the Free Software Foundation.

3.1 Introduction

Principle channel metrics, for example channel width or gradient, convey immanent information that can be exploited for geomorphological research (Wobus et al., 2006; Cook et al., 2014) or engineering purposes (Pizzuto, 2008). For example, a snap-shot of the current local channel geometry can provide an integrated picture of the processes leading to its formation, if examined in a statistically sound manner (Ferrer-Boix et al., 2016). Repeated surveys, as time-series of channel gradients, can reveal local erosional characteristics that sharpen our understanding of the underlying processes and facilitate, inspire, and motivate further research (Milzow et al., 2006). However, these geometrical measures are not directly available. Typically, the measurable metrics are limited to the position of features, such as the channel bed or water surface, or the water flow path or thalweg in two- or three-dimensional coordinates. The data can be either collected during field surveys with GPS or total stations or through remote sensing, with the need of post-processing for example in a GIS (geographical information system). To effectively generate channel metrics such as channel width, an objective and reproducible processing of the geometric data is required, especially when analyzing the evolution of channel metrics over time. For river scientists and engineers a convenient processing tool should incorporate a scale-free approach applicable to a broad spectrum of environments. It should be easy to access, use, and modify, and generate output data that can be integrated in further statistical analysis. Here, we present a new algorithm that meets these requirements and describe its implementation in the R package *cmgo* (https://github.com/AntoniusGolly/cmgo). The package derives a reference (centerline) of one or multiple given channel shapes and calculates channel length, local and average channel widths, local and average slopes, knickpoints based on a scale-free approach (Zimmermann et al., 2008), local and average bank retreats, and the distances from the centerline, as well as allows to project additional spatial metrics to the centerline.

3.2 Literature review

Computer-aided products for studying rivers have a long tradition, and solutions for standardized assessments include many disciplines, as for example for assessing the ecological status of rivers (Asterics, 2013) or for characterizing heterogeneous reservoirs (Lopez et al., 2009). There are also numerous efforts to derive principle channel metrics from remote or in-situ measurements of topography or directly of features such as channel

banks. Available products, which we review in detail (Table 5), are helpful for many scientific applications and are used by a large community. However, they often do not provide the degree of independency, transparency or functionality that is necessary to fit the versatile requirements of academic or applied research and thus the call for software solutions remains present (Amit, 2015). The currently available solutions can be separated into two groups: extensions for GIS applications and extensions for statistical programming languages. The first group incorporates programs that are published as extensions for the proprietary GIS software ArcMap (ESRI, 2017), which are generally not open source and are thus lacking accessibility and often transparency and modifiability. Furthermore, the individual solutions lack functionality. For example, the *River Width Calculator* (Mir et al., 2013) calculates the average width of a given river (single value), without providing spatially resolved information. The toolbox *Perpendicular Transects* (Ferreira, 2014) is capable of deriving channel transects locally, which are generally suitable for calculating the width. However, the required centerline to which the orthogonals are computed is not generated within the tool itself. Thus, the tool does not represent a full stack solution. Similarly, the *Channel Migration Toolbox* (Legg et al., 2014), *RivEX* (Hornby, 2017) and *HEC-GeoRAS* (Ackerman, 2011) require prerequisite products – a centerline – to compute transects and calculate the width. A centerline could be created with the toolbox *Polygon to Centerline* (Dilts, 2015), but manual post-processing is required to ensure that lines connect properly. Further, the details of the algorithm are poorly documented and intermediate results are not accessible, making it difficult to evaluate the data quality. Apart from this, all of these products are dependent on commercial software, are bound to a graphical user interface (not scriptable) and cannot be parametrized to a high degree.

The second group of solutions represent extensions for statistical scripting languages. The full stack solution *RivWidth* (Pavelsky and Smith, 2008) is written as a plugin for IDL, a data language with restricted usage. The program requires two binary raster masks, a channel mask and a river mask, which need to be generated in a pre-processing step, using for example a GIS. Bank geometry obtained from direct measurements, for example from GPS surveys, do not represent adequate input. As a result of the usage of pixel-based data – which in the first place does not properly represent the nature of the geometrical data – computational intensive transformations are necessary, resulting in long computation times (the authors describe up to an hour for their example). More importantly, the

centerline position depends on the resolution of the input rasters, and thus is scale-dependent. Good results can only be obtained when the pixel size is at least an order of magnitude smaller than the channel width. The MATLAB toolbox *RivMap* also works with raster data. It is well documented and has a scientific reference (Schwenk et al., 2017). However, intermediate results are not accessible. For example the transects used for generating the local width are not accessible. Thus, the tool lacks an important mechanism to validate its results. However, since *RivMap* represents the best documented and most versatile tool, we compare results from our package with this package in section 3.9.

To quantify channel bank retreat for repeated surveys, tools designed for other purposes could potentially be used. Examples are *DSAS* (Thieler et al., 2009) and *AMBUR* (Jackson, 2009), designed for analyzing migrating shorelines. These tools also require a baseline that is not derived by the program. *AMBUR*, scripted in the open-source environment R (Jackson, 2009) could be adapted to channels. However, we judge its approach to derive transects to be unreliable and unsuitable for rivers, as the transects do not cross the channel orthogonally, leading to implausible results especially in regions with large curvature. A further correction step is included to alleviate this problem, but the resulting distances of the baselines seem arbitrary. Thus, although the tool is among the best documented and accessible solutions currently available, its algorithm is not suitable for generating channel metrics in an objective manner. We conclude that none of the available approaches combines the criteria of being a tool for objectively deriving channel metrics, being easy and free to use and modify, and allowing a high degree of parametrization and fine-tuning.

3.3 Description of the algorithm

Our aim with this package was to develop a program that does not have the shortcomings of previous approaches and offers a transparent and objective algorithm. The algorithm (full list of steps in Table 6 and visualization in Fig. 19) has two main parts. First, a centerline of the channel – defined by the channel bank points – is derived and second, from this centerline the metrics – channel length, width and gradient (the latter only if elevation is provided) – are calculated. Furthermore, this reference centerline allows for projecting secondary metrics (as for example the occurrence of knickpoints) and performing temporal comparisons (more information on temporal analyses in section 3.6).

Name of the tool	Platform	Data format	Last updated	Free to use [1]	Free to modify [2]	Configurable	Full-stack solution [3]	Scientific reference	Note
cmgo (this paper)	R	Vector	July 2017	yes, yes	yes	yes	yes	yes [4]	
RiverWidth-Calculator	ArcMap	Raster	June 2013	no, yes	no	no	no	yes	• single, average value for a stream
Perpendicular Transects	ArcMap	Vector	Dec 2014	no, yes	yes	limited, no smoothing	no	no	• weak output on non-smooth centerlines
Channel Migration Toolbox	ArcMap	Vector	Oct 2014	no, yes	no	limited	no	yes	• fails silently
RivEX	ArcMap	Vector	Feb 2017	no, no	no	yes	no	no	• works only on demo data
HEC-GeoRAS	ArcMap	Raster	July 2017	no, yes	no	yes	no	no	• only verified until ArcMap 10.2
Polygon to Centerline	ArcMap	Vector	Nov 2016	no, yes	no	limited, no smoothing	no	no	• weak output for high-resolution bank geometry
Fluvial Corridor Toolbox	ArcMap	Vector	Jan 2016	no, yes	no	yes	no	yes	• cannot be applied on the raw data, requires pre-vectorization of channel features
Stream Restoration Toolbox	ArcMap	Vector	[5]	no, yes	no	very limited	no	no	• limited functionality • highly unstable
RivWidth	IDL	Raster	May 2013	no, yes	yes	[5]	[5]	yes	• limited access due to IDL license
DSAS	ArcMap	Vector	Dec 2012	no, yes	no	yes	no	yes	• primarily designed for coastlines
AMBUR	R	Vector	June 2014	yes, yes	yes	limited	no	yes	• no multi-temporal analyses allowed
RivMap	MATLAB	Raster	Apr 2017	no, yes	yes	yes	limited	yes	• primarily for large scale river systems • fails silent on errors

Table 5: overview of existing products, [1] the two values indicate free use of framework (first) and plugin (second value), [2] a product is considered free to modify if users can access and edit the source code and a license explicitly allows users to do so, [3] a product is considered a full-stack solution if it performs all steps from the bank geometry to the derived channel metrics, [4] this publication, [5] gray cells indicate that no information could be gathered.

Step	Description	Function
1.1	Generate polygon from bank points	CM.generatePolygon()
1.2	Interpolate polygon points	
2.1	Create Voronoi polygons and convert to paths	CM.calculateCenterline()
2.2	Filter out paths that do not lie within channel polygon entirely	
2.3	Filter out paths that are dead ends (have less than 2 connections)	
2.4	Sorting of the centerline segments to generate centerline	
2.5	Spatially smooth the centerline segments (mean filter)	
2.6	Measure the centerline's length and slope	
2.7	Project elevation to the centerline points (optional)	
3.1	Derive transects of the centerline	CM.processCenterline()
3.2	Calculate intersections of the centerline with the banks	
3.3	Project custom geospatial data onto centerline (optional)	
3.4	Calculate knickpoints based on scale-free approach (Zimmermann et al. 2008)	

Table 6: Full list of steps of the algorithm of the package *cmgo* and their functions. A visual illustration of these processing steps can be found in Fig. 19.

It follows a detailed description of all steps of the algorithm. In step 1.1, the algorithm creates a polygon feature from the bank points (Fig. 19b), where the points are linearly interpolated (step 1.2) to increase their spatial resolution. This is a crucial step for improving the shape of the resulting centerline – even for straight channel beds (Fig. 20). From the interpolated points, Voronoi polygons (also called Dirichlet or Thiessen polygons) are calculated (2.1, Fig. 19c). In general, Voronoi polygons are calculated around center points (here the bank points) and denote the areas within which all points are closest to that center point. Next, the polygons are disassembled into single line segments. The segments in the center of the channel polygon form the desired centerline (see Fig. 19c). The algorithm then filters for these segments by first removing all segments that do not lie entirely within the channel banks (step 2.2, Fig. 21b).

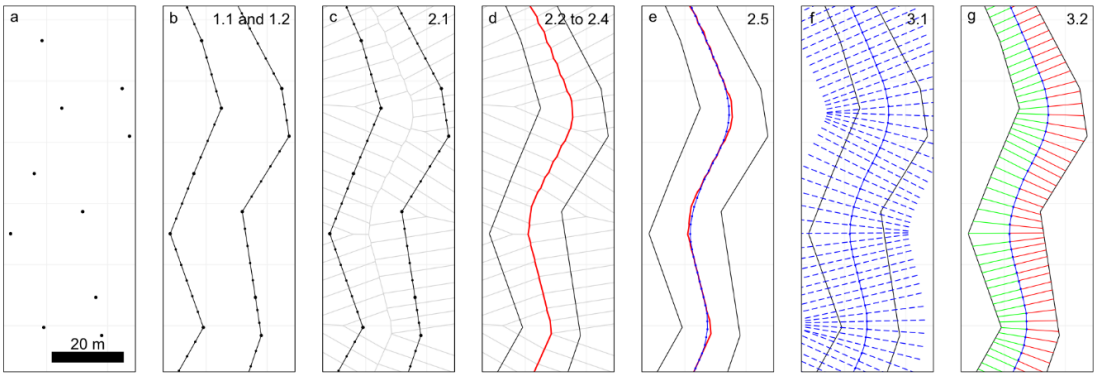

Fig. 19: Visualization of the work flow of the package, a) the channel bank points represent the data input, b) a polygon is generated where bank points are linearly interpolated, c-d) the centerline is calculated via Voronoi polygons, e) the centerline is spatially smoothed with a mean filter, f) transects are calculated, g) the channel width is derived from the transects.

In a second step, dead ends are removed (step 2.3, Fig. 21c). Dead ends are segments that branch from the centerline but are not part of it, which are identified by the number of connections of each segment. All segments, other than the first and the last, must have exactly two connections. The filtering ends successfully if no further dead ends can be found. In step 2.4, the centerline segments are chained to one consistent line, the "original" centerline. In the final step 2.5 of the centerline calculation, the generated line is spatially smoothed (Fig. 19e) with a mean filter with definable width (see section 3.4.2) to correct for sharp edges and to homogenize the resolution of the centerline points. This calculated centerline, the "smoothed" centerline, is the line feature representation of the channel – for example it represents its length, which is calculated in step 2.6. If elevation data is provided with the bank point information (input data) the program also projects the elevation to the centerline points and calculates the slope of the centerline in step 2.7. The program also allows projecting custom geospatial features to the centerline – such as the abundance of species or the occurrence of knickpoints (see section 3.4.2). Projecting means here that elevation information or other spatial variables are assigned to the closest centerline points.

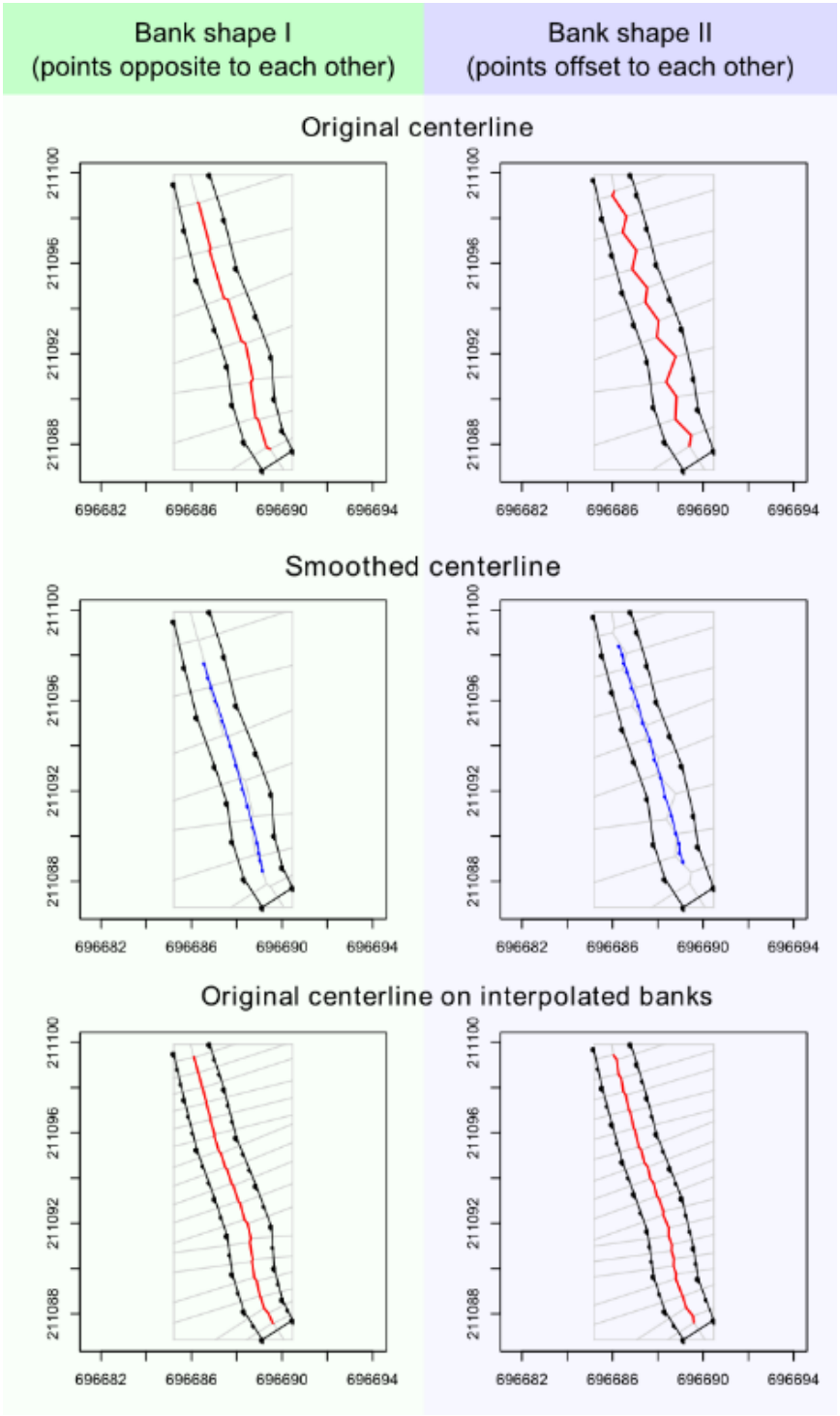

Fig. 20: Two digitizations (Bank shape I and II) of the same channel stretch. They differ only in the arrangement of bank points which are mainly opposite (Bank shape I, left column) or offset (Bank shape II, right column) to each other. One can see how the offset negatively influences the shape of the centerline (top row). The problem can be overcome by smoothing the centerline a-posteriori (middle row) or interpolating between the bank points a-priori (bottom row). A combination of both methods is recommended and set as the default in cmgo.

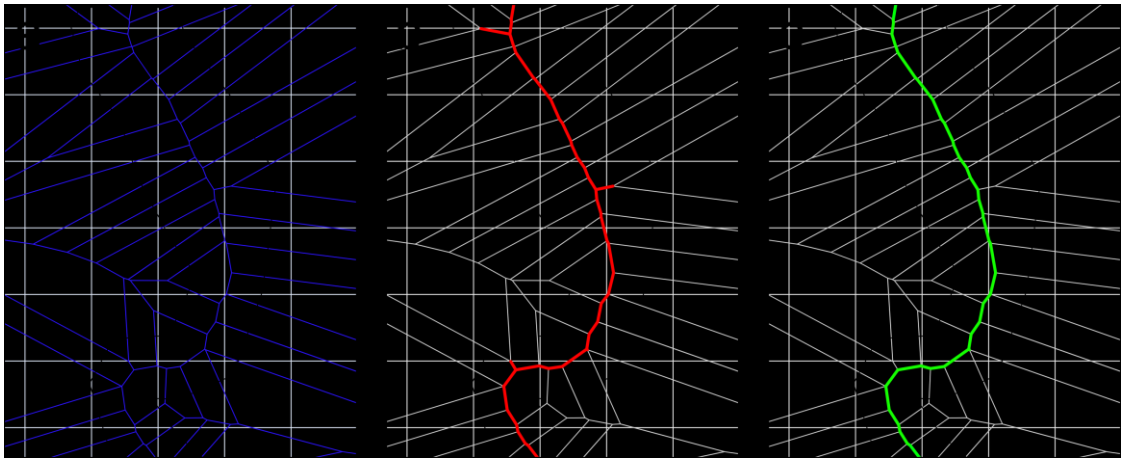

Fig. 21: The filtering of the centerline segments, a) original Voronoi segments, b) Voronoi segments filtered for segments that lie fully within the channel polygon, and c) filtered for dead ends.

To calculate the channel metrics based on the centerline, channel transects are derived (step 3.1). Transects are lines perpendicular to a group of centerline points. In step 3.2, the intersections of the transects with the banks are calculated (Fig. 19g). When transects cross the banks multiple times, the crossing point closest to the centerline is used. The distance in the x-y-plane between the intersections represent the channel width at this transect. In addition to the width, the distances from the centerline points to banks are stored separately for the left and the right bank.

3.4 Implementation and execution

The program is written as a package for the statistical programming language R (R Development Core Team, 2008). The program can be divided into three main parts which are worked through during a project: 1. initialization (loading data and parameters, section 3.4.1), 2. data processing (calculating centerline and channel metrics, section 3.4.2), and 3. review of results (plotting or writing results to file, section 3.5).

3.4.1 Initialization: input data and parameters

The package *cmgo* requires basic geometrical information of the points that determine a channel shape – the bank points (Fig. 19a) – while in addition to the coordinates, the side of the channel must be specified for each point. In principle, a text file with the three columns “x”, “y” and “side” represent the minimum input data required to run the program (Codebox 1). The coordinates “x” and “y” can be given in any number format representing

Cartesian coordinates, and the column “side” must contain strings (e.g. “left” and “right”) as it represents information to which of the banks the given point is associated. Throughout this paper we refer to left and right of the channel always in regard to these attributes. Thus, the user is generally free to choose which side to name “left”. However, we recommend to stick to the convention to name the banks looking in downstream direction. In addition, a fourth column “z” can be provided to specify the elevation of the points. This allows for example for the calculation of the channel gradient. Note, that the order of the bank points matter. By default it is expected that the provided list are all bank points in upstream direction. If one – this can be the case when exporting the channel bed from a polygon shape – or both banks are reversed, the parameters `bank.reverse.left` and/or `bank.reverse.right` should be set `TRUE`. The units of the provided coordinates can be specified in the parameter `input.units` and defaults to `m` (meters).

```
Name POINT_X POINT_Y
right 401601.0819 3106437.335
right 401586.5327 3106406.896
right 401568.3238 3106383.586
right 401558.4961 3106364.129
...
left 401621.4337 3106431.134
left 401602.9913 3106405.991
left 401574.6073 3106352.232
left 401582.2671 3106323.134
```

Codebox 1: Example of input data table with columns side and x,y-coordinates.

The data can be either collected during field surveys with GPS or total stations or through remote sensing techniques with further digitizing for example in a GIS. In the latter case the data needs to be exported accordingly. The input can be given in any ASCII table format. By default, the program expects a table with tab-delimited columns and one header line with the column names `POINT_X`, `POINT_Y` and `POINT_Z` (the coordinates of the bank points) where the z component is optional and `Name` (for the side). The tab delimiter and the expected column names can be changed in the parameters (see Appendix D for details). The input file(s) – for multiple files see also section 3.6 – have to be placed in the input directory specified by the parameter `input.dir` (defaults to "./input") and can have any file extension (.txt, .csv, etc.). The data reading function iterates over all files in that directory and creates a data set for each file.

All the data and parameters used during runtime are stored in one variable of type list (see R documentation): the global data object. Throughout the following examples this variable is named `cmgo.obj` and its structure is shown in Codebox 2. The global data object also contains the parameter list, a list of more than 50 parameters specifying the generation and plotting of the model results. The full list of parameters with explanations can be found in Appendix D.

```
cmgo.obj = list(
data = list(                # the data set(s), different surveys of the channel
    set1 = list(            # survey 1
      filename                      = "input.1.csv",      # corresponding filename
      channel                       = list(),       # input coordinates of banks
      polygon.bank.interpolate      = TRUE,
      polygon                       = list(),       # polygon object
      polygon.bank.interpolate.max.dist       = 6,
      cl                            = list(),       # centerlines (original and
smoothed)
      metrics                       = list()        # calculated metrics (width,
etc.)
    ),
    set2 = list()           # survey 2
    # ...
  ),
  par  = list()             # all model and plotting parameters
)
```

Codebox 2: structure of the global data object containing data and parameters.

To create this object, the function `CM.ini(cmgo.obj, par)` is used. Initially, the function builds a parameter object based on the second argument `par`. If the `par` argument is left empty, the default configuration is loaded. Alternatively, a parameter filename can be specified (see the R documentation of `CM.par()` for further information). Once the parameter object is built, the function fills the data object by the following rules (if one rule was successful, the routine stops and returns the global data object):

1. If `cmgo.obj$par$workspace.read` is `TRUE` (default) the function looks for an .RData workspace file named `cmgo.obj$par$workspace.filename` (defaults to "./user_workspace.RData"). Note: there will be no such workspace file once a new project is started, since it needs to be saved by the user with `CM.writeData()`. If such a workspace file exists the global data object is created from this source, otherwise the next source is tested.
2. If data input files are available in the directory `cmgo.obj$par$input.dir` (defaults to "./input") the function iterates over all files in this directory and creates the data

object from this source (see section "Input data" above for further information on the data format). In this case the program starts with the bank geometry data set(s) found in the file(s). Otherwise the next source is tested.

3. If the `cmgo.obj` argument is a string or `NULL`, the function will check for a demo data set with the same name or “demo” if `NULL`. Available demo data sets are "demo", "demo1", "demo2" and"demo3" (section 3.8).

`CM.ini()` returns the global data object which must be assigned to a variable, as for example `cmgo.obj = CM.ini()`. Once the object is created, the data processing can be started.

3.4.2 Controlling the data processing

The processing includes all steps from the input data (bank points) to the derivation of the channel metrics (Fig. 19). Next, we describe the parameters that are relevant during the processing described in section 3.3. When generating the channel polygon the original bank points are linearly interpolated (Fig. 19b). The interpolation is controlled through the parameters `cmgo.obj$par$bank.interpolate` and `cmgo.obj$par$bank.interpolate.max.dist`. The first is a Boolean (`TRUE`/`FALSE`) that enables or disables the interpolation (default `TRUE`). The second determines the maximum distance of the interpolated points. The unit is the same as of the input coordinates, which means, if input coordinates are given in meters, a value of 6 (default) means that the points have a maximum distance of 6 meters to each other. These parameters have to be determined by the user and are crucial for the centerline generation. Guidance of how to select and test these parameters can be found in section 3.7.

During the filtering of the centerline paths, there is a routine that checks for dead ends. This routine is arranged in a loop that stops when there are no further paths to remove. In cases, where the centerline paths exhibit gaps (see section 3.7), this loop would run indefinitely. To prevent this, there is a parameter `bank.filter2.max.it` (defaults to 12) that controls the maximum number of iterations used during the filtering.

In the final step of the centerline calculation, the generated line gets spatially smoothed with a mean filter (Fig. 19e) where the width of smoothing in numbers of points can be adjusted through the parameter `cmgo.obj$par$centerline.smoothing.width` (by default equals 7). Note, that the degree of smoothing has an effect on the centerline length (e.g. a

higher degree of smoothing shortens the centerline). Similar to the coast line paradox (Mandelbrot, 1967), the length of a channel depends on the scale of the observations. Technically, the length diverges to a maximum length at an infinitely high resolution of the bank points. However, practically there is an appropriate choice of a minimum feature size where more detail in the bank geometry only increases the computational costs without adding meaningful information. The user has to determine this scale individually and should be aware of this choice. To check the consequences of this choice, the decrease in length due to smoothing is saved as fraction value in the global data object under `cmgo.obj$data[[set]]$cl$length.factor`. A value of 0.95 means that the length of the smoothed centerline is 95% the length of the original centerline paths. For the further calculations of transects and channel metrics by default the smoothed version of the centerline is used.

The program will project automatically the elevation of the bank points to the centerline if elevation information is provided in the input files (z component of bank points, see section 3.4.1). Also additional custom geospatial features – if available to the user – can be projected to the centerline, such as the abundance of species or the occurrence of knickpoints. Additional features are required to be stored in the global data object as lists with x,y-coordinates (Codebox 3) to be automatically projected to the centerline. Projecting here means that features with x,y-coordinates are assigned to the closest centerline point. The distance and the index of the corresponding centerline point are stored within the global data object.

```
cmgo.obj$data[[set]]$features = list(
  custom_feature_1 = list(
    x = c(),
    y = c()
  ),
  knickpoints = list(
    x = c(),
    y = c()
  )
)
```

Codebox 3: The format of secondary spatial features to be projected to the centerline.

To calculate the channel metrics based on the centerline channel transects are derived. Transects are lines perpendicular to a group of n centerline points, where n – also called the transect span –is defined by the parameter `cmgo.obj$par$transects.span`. By default

this span equals three, which means for each group of three centerline points a line is created through the outer points of that group to which the perpendicular – the transect – is calculated (see Fig. 22b). The number of resulting transects equals the number of centerline points and for each centerline point the width `w` and further metrics are calculated (see Codebox 4). The distances of the centerline points to the banks is stored separately for the left and the right bank (`d.r`. and `d.l`), as well as a factor (`r.r` and `r.l`) representing the side of the bank with regard to the centerline. Normally, looking downstream the right bank is always right to the centerline (value of -1) and the left bank is always left to the centerline (value of +1). However, when using a reference centerline to compare different channel surveys, the centerline can be outside the channel banks for which the metrics are calculated. To resolve the real position of the banks for tracing their long-term evolution (e.g. bank erosion and aggradation) the factors of `r.r`. and `r.l` must be considered for further calculations (see also section 3.6.1). A sample result for a reach of a natural channel is provided in Fig. 23.

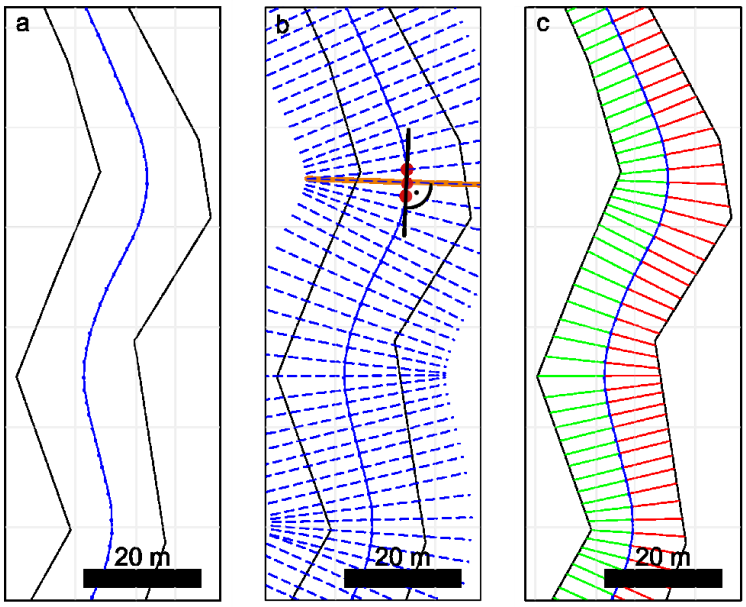

Fig. 22: a) the smoothed centerline, b) transects are calculated by taking a group of centerline points, creating a line through the outer points and calculate the perpendicular to that line, c) calculating the intersections of the transects with the channel banks.

```
$metrics$tr       # linear equations of the transects
$metrics$cp.r     # coordinates of crossing points transects / right bank
$metrics$cp.l     # coordinates of crossing points transects / left bank
$metrics$d.r      # distance of reference centerline point / right bank
$metrics$d.l      # distance of reference centerline point / left bank
$metrics$w        # channel width
$metrics$r.r      # direction value: -1 for right, +1 for left to the centerline
$metrics$r.l      # direction value: -1 for right, +1 for left to the centerline
$metrics$diff.r   # difference between right bank point of actual time series and
right bank
                  # point of reference series
$metrics$diff.l   # difference between left bank point of actual time series and
                  # left bank point of reference series
```

Codebox 4: the calculated metrics and their variable names (stored in the global data object under cmgo.obj$data[[set]]).

3.5 Review results: plotting and writing of the outputs

After the metrics are calculated and stored within the global data object, the results can be plotted or written to data files. The plotting functions include a map-like type plan view plot (`CM.plotPlanView()`), a plot of the spatial evolution of the channel width (`CM.plotWidth()`) and a plot of the spatial and temporal evolution of the bank shift (`CM.plotMetrics()`). All plotting functions require a data set to be specified that is plotted (by default "set1"). Additionally, all plotting functions offer ways to specify the plot extent to zoom to a portion of the stream for detailed analyses. In the plan view plot, multiple ways exist to define the plot region (also called extent), which is determined by a center coordinate (x,y-coordinate) and the range on the x and y axes (zoom length). The zoom length is given via the function parameter `zoom.length`, or – if left empty – is taken from the global parameter `cmgo.obj$par$plot.zoom.extent.length` (140 m by default). Multiple ways exist to determine the center coordinate: via pre-defined plot extent, via centerline point index, or directly by x,y-coordinates. Pre-defined plot extents allow for quickly accessing frequently considered reaches of the stream and are stored in the parameter list (see Codebox 5). The list contains named vectors, each with one x- and one y-coordinate. To apply a pre-defined extent the name of the vector has to be passed to the plot function as in `CM.plotPlanView(cmgo.obj, extent="extent_name")`. Another way of specifying the plot region is via a centerline point index, for example `CM.plotPlanView(cmgo.obj, cl=268)`. This method guarantees that the plot gets centered on the channel. To find out the index of a desired centerline point, centerline text labels can be enabled with `cmgo.obj$par$plot.planview.cl.tx = TRUE`. Finally, the plot center coordinate can be given

directly by specifying either an x- or y-coordinate or both. If either an x- or y-coordinate is provided, the plot centers at that coordinate and the corresponding coordinate will be determined automatically by checking where the centerline crosses this coordinate (if it crosses the coordinate multiple times, the minimum is taken). If both x- and y-coordinates are provided, the plot centers at these coordinates.

A plot of the width of the whole channel (default) or for a portion (via `cl` argument) can be created with `CM.plotWidth()`. Two data sets with the same reference centerline can also be compared. The `cl` argument accepts the range of centerline points to be plotted, if `NULL` (default) the full channel length is plotted. If a vector of two elements is provided (e.g. `c(200, 500)`), this cl range is plotted. If a string is provided (e.g. "cl1"), the range defined in `cmgo.obj$par$plot.cl.ranges$cl1` is plotted. Alternatively to the range of centerline indices, a range of centerline lengths can be provided with argument `d`. If a single value (e.g. `500`) is given 50 m around this distance is plotted. If a vector with two elements is given (e.g. `c(280, 620)`) this distance range is plotted.

The third plot function creates a plot of the bank shift (bank erosion and aggradation). This plot is only available when using multiple channel observations in the reference centerline mode (see section 3.6.1). The arguments of the function regarding the definition of the plot region is the same as of the function `CM.plotWidth()`.

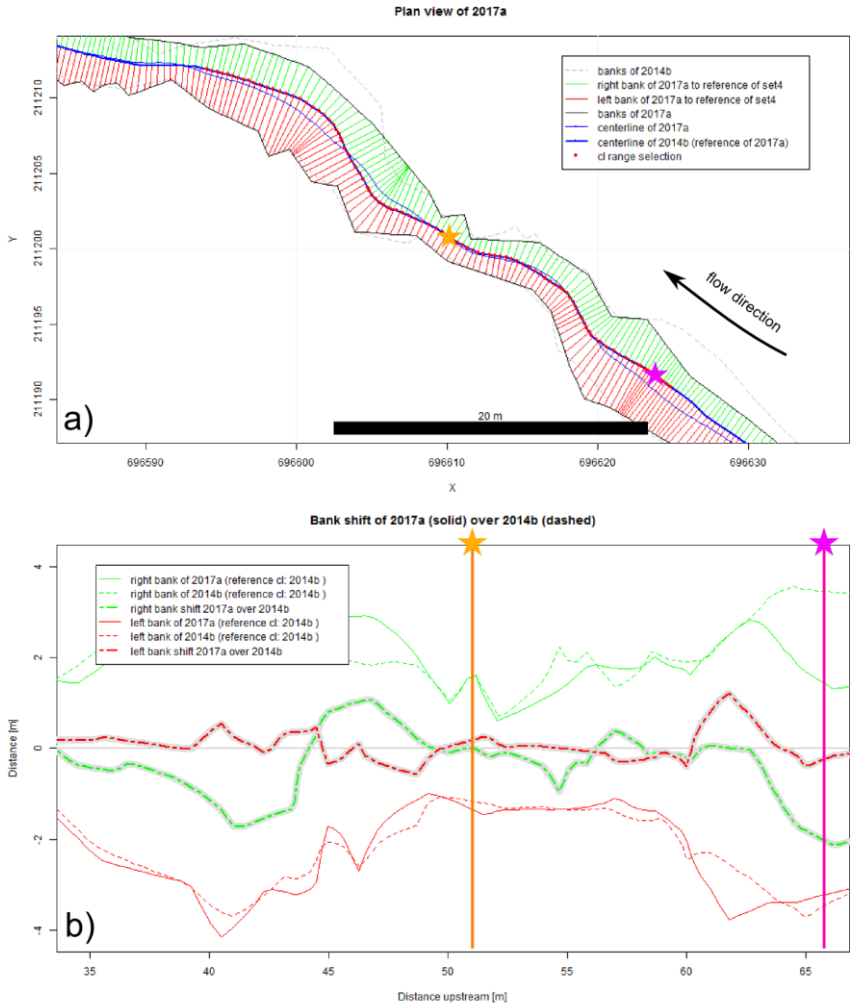

Fig. 23: a) plan view of a short channel reach showing two channel surveys, 2014a (dashed channel outline) and 2017a (solid channel outline. A centerline is calculated for both, but due to an enabled reference mode, the centerline of 2014a is used for both surveys. This allows for the calculation of bank shift in b). The two stars mark two random locations to compare the calculated metrics to each other.

```
plot.zoom.extents = list(       # presets (customizable list) of plot regions
  e1  = c(400480,  3103130),      # plot region definition e1 with x/y center
coordinate
  e2  = c(399445,  3096220),
  e3  = c(401623,  3105925),
  all = NULL
```

Codebox 5: definition of pre-defined plot extents that allow to quickly plot frequently used map regions. The names, here “e1”, “e2”, “e3”, contain a vector of two elements, the x and y-coordinates where the plot is centered at. To plot a pre-defined region call for example CM.plotPlanView(cmgo.obj, extent=”e2”).

In addition to the plotting, the results can be written to output files and to an R workspace file with the function `CM.writeData()`. The outputs written by the function depend on the settings in the parameter object. If `cmgo.obj$par$workspace.write = TRUE` (default is `FALSE`) a workspace file is written containing the global data object. The filename is defined in `cmgo.obj$par$workspace.filename`. Further, ASCII tables can be written containing the centerline geometry and the calculated metrics. If `cmgo.obj$par$output.write = TRUE` (default is `FALSE`) an output file for each data set is written to the output folder specified in `cmgo.obj$par$output.dir`. The file names are the same as the input filenames with the prefixes `cl_*` and `metrics_*`. All parameters regarding the output generation can be accessed with `?CM.par` executed in the R console or can be found in the Appendix D.

3.6 Temporal analysis of multiple surveys

The program can perform analyses on time series of channel shapes. To do this, multiple input files have to be stored in the input directory (see section 3.4.1). A data set for each file will be created in global data object, mapped to the sub lists “set1”, “set2”, etc. (see Codebox 1). The program automatically iterates over all data sets, processing each set separately. The order of the data sets is determined by the filenames. Thus, the files need to be named according to their temporal progression, e.g. “channel_survey_2017.csv", "channel_survey_2018.csv", etc. The mapping of the filenames to data sets is printed to the console and stored in each data set under `cmgo.obj$data[[set]]$filename`.

3.6.1 Reference centerline

The channel metrics are calculated based on the centerline, which exists for every river bed geometry. When there are multiple temporal surveys of a river geometry, a centerline for each data set exists. Multiple centerlines prevent a direct comparison of the channel metrics as they can be seen as individual channels. Thus, for temporal comparisons of the channel metrics, two modes exist. Metrics are either calculated for each channel geometry individually. In this mode, the channel metrics are the most accurate representation for that channel observation, for example channel width is most accurately measured, but do not allow for a direct comparison of consecutive surveys. In a second approach, a reference centerline for all metrics calculations can be determined. In this approach, all metrics for the various bank surveys are calculated based on the centerline of the data set defined in `cmgo.obj$par$centerline.reference` (default "set1"). This mode must be enabled manually (see Codebox 6) but should be used only if the bank surveys differ slightly. If there is

profound channel migration or a fundamental change in the bed geometry, the calculated channel metrics might not be representative (shown in Fig. 24). To compare channel geometries of which the individual centerlines are not nearly parallel we recommend to calculate the metrics based on individual centerlines and develop a proper spatial projection for temporal comparisons.

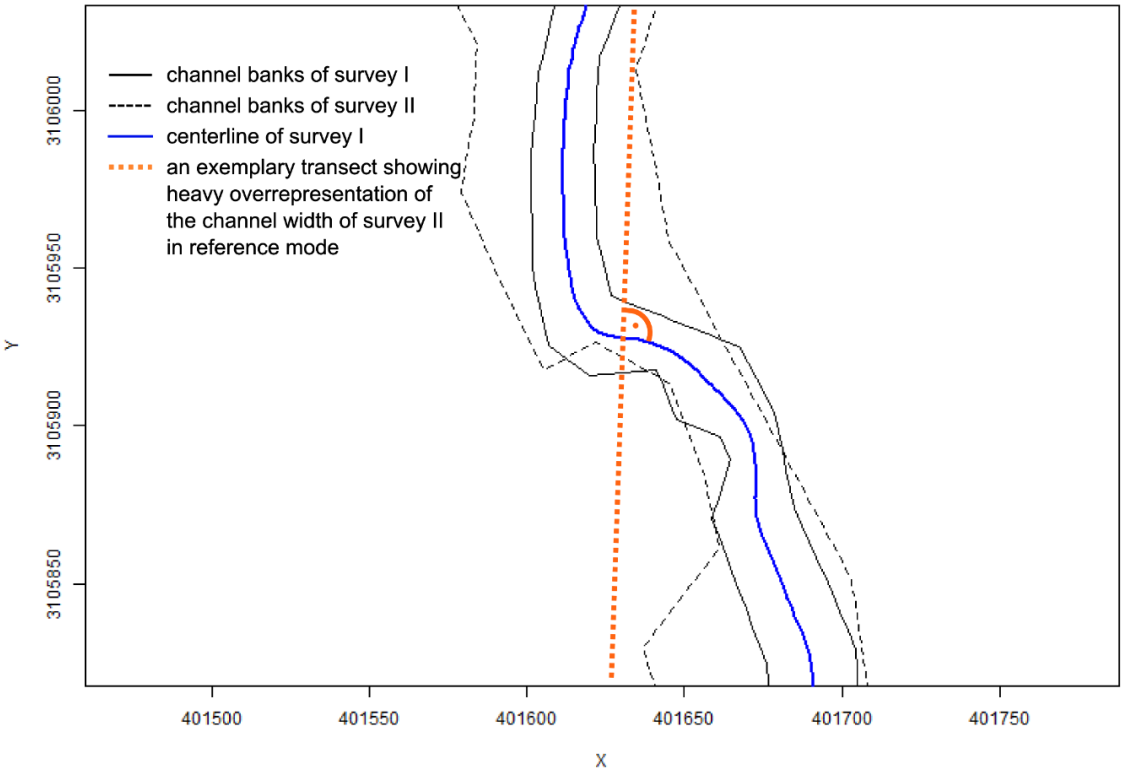

Fig. 24: Two consecutive channel geometries (surveys I and II) with a profound reorganization of the channel bed. In the reference mode a centerline of one survey is used to build transects. Here, using the centerline of the first survey (blue line) as a reference is not suitable to capture the channel width correctly for the second survey (dashed line) as the exemplary transect (dashed orange line) suggests.

3.7 Technical fails and how to prevent them

There are certain geometrical cases in which the algorithm can fail with the default parametrization. To prevent this, a customized parametrization of the model is required. The program prints notifications to the console during runtime if the generation of the centerline fails and offers solutions to overcome the issue. The main reason for failure occurs if the resolution of channel bank points (controlled via `cmgo.obj$par$bank.interpolate.max.dist`) is relatively low compared to the channel width.

In tests, a `cmgo.obj$par$bank.interpolat.max.dist` less than the average channel width was usually appropriate. Otherwise, the desired centerline segments produced by the Voronoi polygonization can protrude the bank polygon (Fig. 25a) and thus do not pass the initial filter of the centerline calculation (see section 3.3), since this filter mechanism first checks for segments that lie fully within the channel polygon. This creates a gap in the centerline, which results in an endless loop during the filtering for dead ends. Thus, if problems with the calculation of the centerline arise, an increase of the spatial resolution of bank points via `cmgo.obj$par$bank.interpolat.max.dist` is advised to naturally smooth the centerline segments (Fig. 25b).

```
cmgo.obj$par$centerline.use.reference = TRUE
cmgo.obj$par$centerline.reference     = "set1"
```

Codebox 6: the parameters to enable the reference mode for channel metrics calculations (only necessary for time series analyses).

Another problem can arise from an unsuitable setting during the calculation of transects. If the channel bed exhibits a sharp curvature a misinterpretation of the channel width can result (see Fig. 26). In that case, one of the red transects does not touch the left bank of the channel properly, thus leading to an overestimated channel width at this location. To prevent this, the span of the transect calculation can be increased. The results have to be checked visually by using one of the plotting functions of the package.

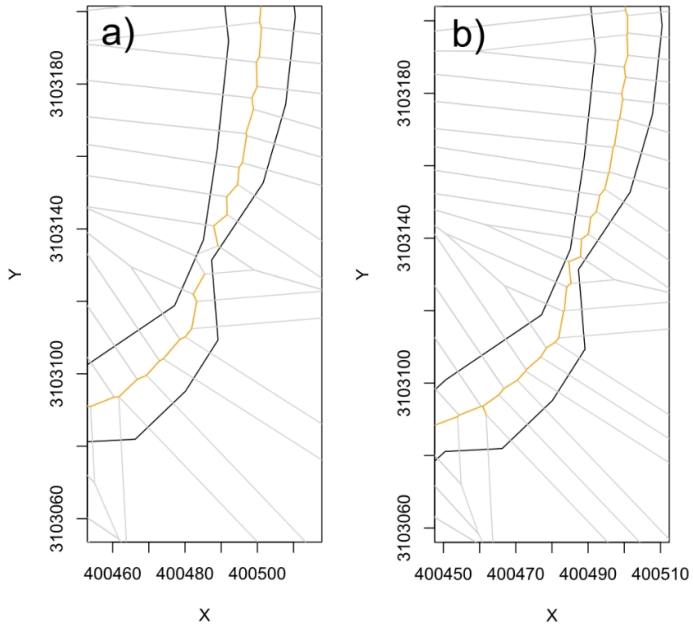

Fig. 25: a) a gap in the centerline occurs when the spacing of the bank points is too large compared to the channel width, b) the gap fixed by increasing the resolution of the bank points through the parameter `par$bank.interpolate.max.dist`.

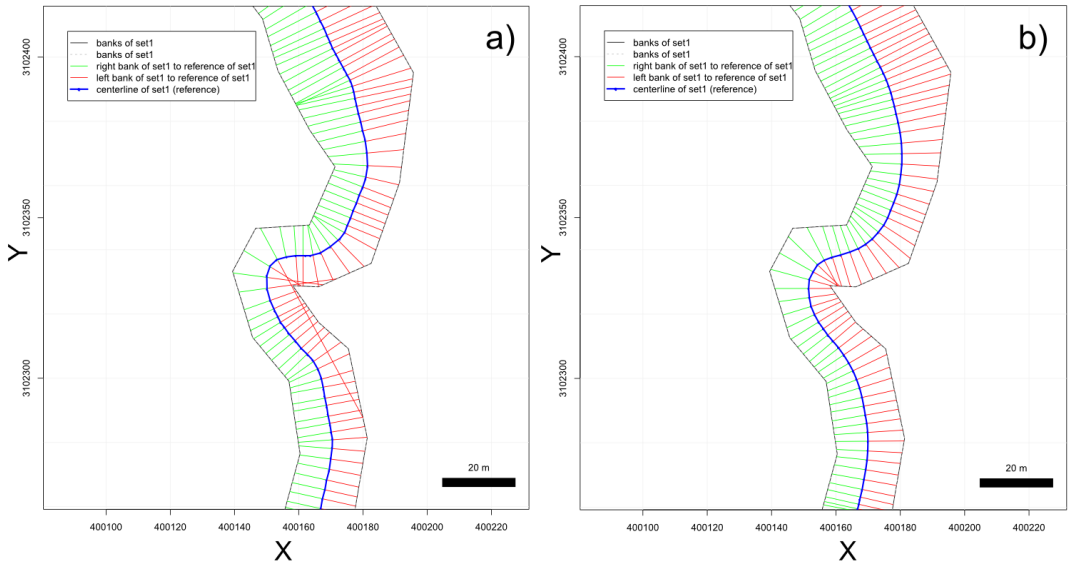

Fig. 26: a) the transects (perpendiculars to the centerline) do not intersect with banks properly, thus the channel width is overrepresented b) an increased transect span fixes the problem and channel width is identified correctly.

3.8 How to use the program: step by step instructions

cmgo can be used even without comprehensive R knowledge and the following instructions do not require preparatory measures other than an installed R environment (R Development Core Team, 2008). Once the R console is started, installation of the *cmgo* package is done with the `install.packages()` function (Codebox 7).

To quickly get started with *cmgo*, we provide four demo data sets. Using these data sets the following examples demonstrate the main functions of the package, but, more importantly, allow to investigate the proper data structure of the global data object. This is of particular importance when trouble shooting failures with custom input data.

The general execution sequence includes initialization, processing, and reviewing the results, with a standard execution sequence shown in Codebox 8. To switch from demo data to custom data, input files have to be placed in the specified input folder ("./input" by default) and `CM.ini()` has to be called without any arguments. Since the file format of the custom input files can differ from the expected default format, all program parameters regarding the data reading should be considered. A list of all parameters available can be accessed with `?CM.par` executed in the R console or can be found in the Appendix D. To change a parameter, the new parameter value is assigned directly within the global data object (e.g. `cmgo.obj$par$input.dir = "./input"`).

The plotting functions include a map-like plan view plot (`CM.plotPlanView()`), a line chart with the channel width (`CM.plotWidth()`) and, if available, a plot of the bank retreat (`CM.plotMetrics()`). The latter is only available in the reference centerline mode (see section 3.6.1).

```
# installation of dependencies (required only once)
install.packages(c("spatstat", "zoo", "sp", "stringr"))

# installation (required only once)
install.packages("cmgo", repos="http://code.backtosquareone.de", type="source")

# include the package (required for every start of an R session)
library(cmgo)
```

Codebox 7: installation and embedding of the package in R

```
# initialization: load data and parameters
cmgo.obj = CM.ini("demo")      # check the data structure with str(cmgo.obj)

# processing 15,23 cm
cmgo.obj = CM.generatePolygon(cmgo.obj)
cmgo.obj = CM.calculateCenterline(cmgo.obj)
cmgo.obj = CM.processCenterline(cmgo.obj)

# view results
CM.plotPlanView(cmgo.obj)      # plot a map with pre-defined extent
CM.plotWidth(cmgo.obj)         # plot the channel width in downstream direction
CM.plotMetrics(cmgo.obj)       # plot a comparison of bank profiles
```

Codebox 8: minimal example script to run cmgo with demo data set.

3.9 Evaluation of the data quality

We evaluated the quality of the derived channel width by cmgo to manually measured data and to the best documented and versatile product of our literature review RivMap (Table 5). First, we compared the evolution of the channel width derived by the two automated products showing that there is a general agreement (Fig. 27). We then identified 15 locations randomly (vertical dashed lines Fig. 27) where we assessed the channel width manually in a GIS (Fig. 28).

The channel width at the transects is generally well captured by the automated products (Table 3) as the mean errors are relatively low compared to the absolute width. However, compared to the manually derived average width of 3.49 m the average width of all transects deviates only -0.07 m for *cmgo* while it deviates -0.42 m for *RivMap*. Thus, *cmgo* performs generally better in deriving the channel width for the test channel reach and overall *RivMap* underestimates the channel width. This is also expressed in the smaller standard deviation of the differences which is 0.098 m for *cmgo* and 0.736 m for *RivMap*. The large scatter can also be observed in Fig. 27. Compared to the error of the in-situ measurements of the channel banks with a total station (1 cm) the precision of the channel width calculations by *cmgo* is within the same order of magnitude while it is an order of magnitude larger for *RivMap*.

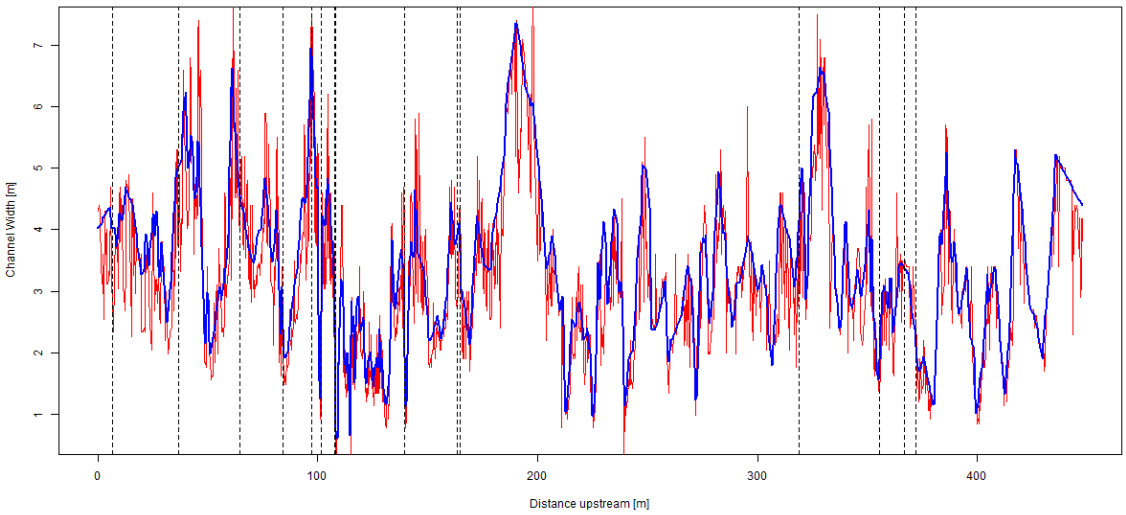

Fig. 27: Channel width as derived by cmgo (blue line) and RivMap (red line) for 1506 locations along a 449 m reach of a natural channel in upstream direction. The vertical dashed lines mark our points where we investigated the width manually in a GIS.

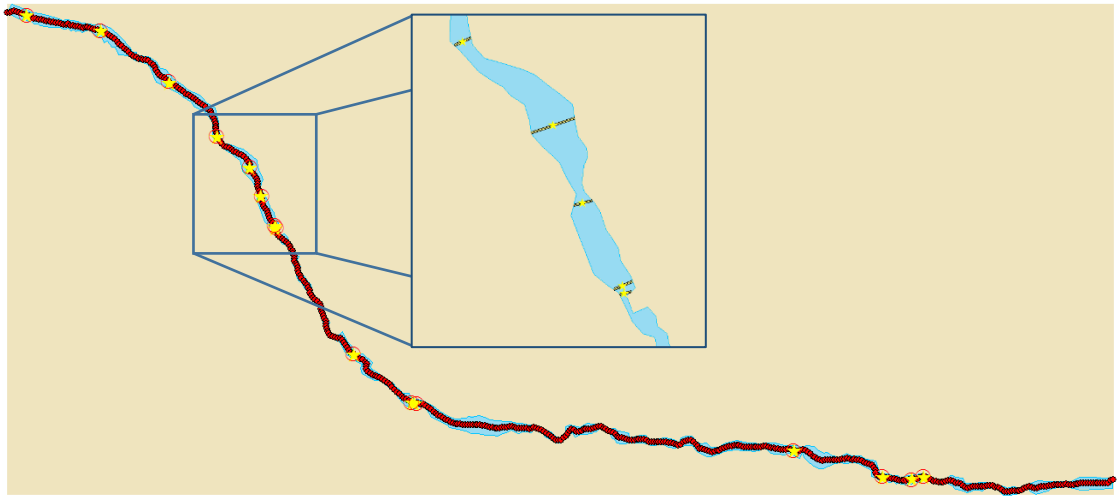

Fig. 28: Fifteen random locations (yellow stars) of the 1506 centerline points (red dots) where we evaluated the width manually in a GIS (example in the inlet) that are compared to the width of the automated products.

The channel centerlines of the two products differ in length. While the centerline of *cmgo* has a length of 449 m along the river reach, the centerline of *RivMap* has a length of 588 m (31% longer). Looking at the shape of the centerlines (Fig. 29) we argue that the centerline of *cmgo* better represents the channel in terms of large scale phenomena. It may for example be more accurate for reach-averaged calculations of bankfull flow. The centerline of *RivMap* contains a stronger signal of the micro topography of the banks due to the way the centerline is created (eroding banks). The difference in length also has an influence on slope calculations which will be lower for *RivMap*.

Transect [No.]	Manual approach [m]	cmgo width [m]	cmgo difference to manual [m]	RivMap width [m]	RivMap difference to manual [m]
1	4.01	4.02	0.01	2.83	-1.18
2	5.01	5.02	0.00	3.75	-1.27
3	4.57	4.55	-0.01	4.03	-0.54
4	2.66	2.59	-0.07	2.60	-0.06
5	6.79	6.83	0.04	5.37	-1.41
6	2.82	2.66	-0.15	2.12	-0.70
7	3.02	2.97	-0.06	2.55	-0.48
8	1.76	1.67	-0.09	2.60	0.84
9	2.27	1.93	-0.34	2.60	0.33
10	3.90	3.91	0.01	2.83	-1.07
11	3.82	3.66	-0.17	4.40	0.58
12	4.19	4.14	-0.05	3.04	-1.15
13	2.04	1.89	-0.15	1.34	-0.70
14	3.37	3.37	0.00	3.50	0.13
15	2.14	2.11	-0.03	2.50	0.36
avg.	3.49	3.42	-0.07	3.07	-0.42
st. dev.	1.340	1.399	0.098	0.997	0.736

Table 7: Channel width at 15 randomly selected locations along a natural channel. The width was identified manually in a GIS, by cmgo, and by RivMap. Differences of the width from the automated products were compared to the manual approach.

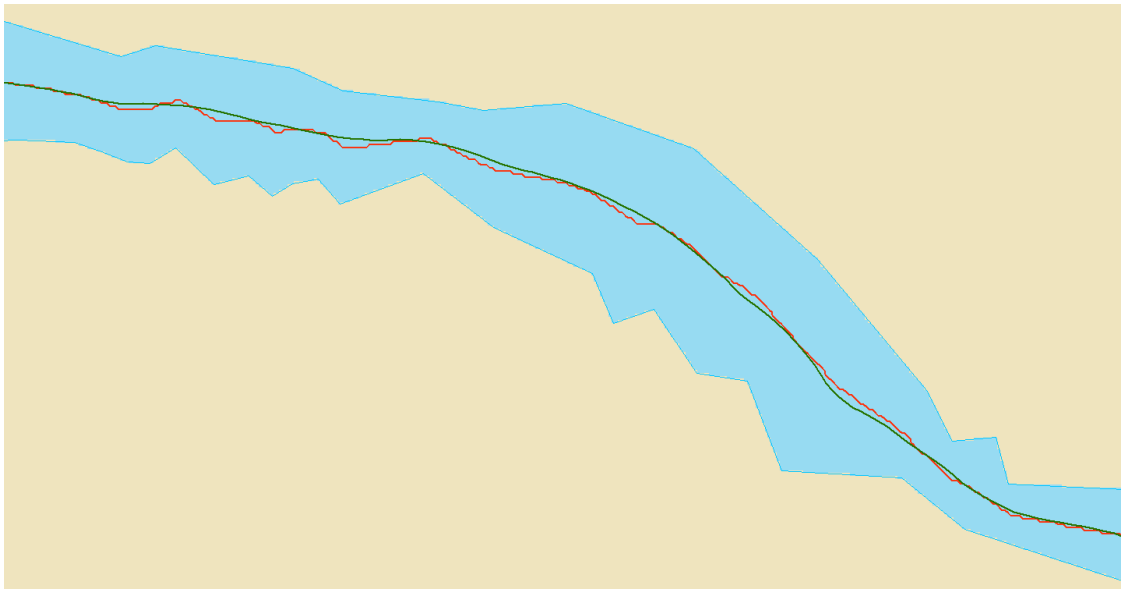

Fig. 29: The two different centerlines of the products cmgo (green line) and RivMap (red line) reveal differences in the shape that influence also the channel length.

3.10 Concluding remarks

The presented package *cmgo* offers a stand-alone solution to calculate channel metrics in an objective and reproducible manner. At this, *cmgo* allows for close look into the interior of the processing. All intermediate results are accessible and comprehensible. Problems that arise for complex geometries can be overcome due to the high degree of parametrization. *cmgo* qualifies for a highly accurate tool suited to analyze especially complex channel geometries. However, if complex geometries should be compared to each other, for example when analyzing the evolution of meandering channels, our product does not offer the ideal solution due to the style *cmgo* treats the reference of the channels. Thus, our product should be the tool of choice if precise measurements – both in location and quantity – are required and if geometrical and other spatial data should be statistically analyzed. However, when large time series of meandering rivers are the main purpose of the effort, other products, as for example the Channel Migration Toolbox, are more suitable.

Since *cmgo* does not come with graphical user interface only static map views of the channel can be obtained by scripting them. *cmgo* offers various plotting functions to do this which allow for predictable and reproducible plot. The downside of this approach is

that plots are naturally not interactive which is the case for GIS applications. For people who prefer this functionality an export of the intermediate and end results to GIS is recommended.

The only requirement for running *cmgo* is an installed environment of the open source framework R. Thus, the prerequisites are narrowed down to a minimum to facilitate an easy integration and wide a distribution for scientific or practical use. The license under which the package is provided allows modifications to the source code. The nature of R packages determines the organization of the source code in functions. This encapsulation comes at the cost of a sometimes untransparent architecture making it difficult to modify or understand the code. Thus, for advanced users, who desire a more flexible way of interacting with the algorithm, we refer to the raw source codes at GitHub (https://github.com/AntoniusGolly/cmgo).

3.11 Acknowledgments

We thank Michael Dietze for giving the helpful R-courses that facilitate the development of *cmgo* as an R-package and for the support during the debugging, Kristin Cook for providing the sample data for the demo data sets and Marisa Repasch-Elder for the guidance in MATLAB.

4 Article III: Testing models of step formation against observations of channel steps in a steep mountain stream

Authors: Antonius Golly [1] , Jens M. Turowski [1] , Alexandre Badoux [2] , and Niels Hovius [1,3]
Submitted to: Earth surface processes and landforms (Wiley)
Manuscript submitted: 8 November 2017

[1] German Research Centre for Geosciences (GFZ), Section 5.1 - Geomorphology, Telegrafenberg, 14473 Potsdam, Germany
[2] Swiss Federal Research Institute for Forest, Snow and Landscape (WSL), Zürcherstr. 111, 8903 Birmensdorf, Switzerland

Abstract

Steep streams often feature a step-pool morphology where the steps determine channel stability and dissipate the stream's energy, and thus are important for local flow hydraulics and bedload transport. Furthermore, steps play a key-role for the coupling of channels and adjacent hillslopes by controlling hillslope stability. Although step-pool systems have been investigated in various modelling and experimental efforts, the processes of step formation and destruction are still under debate. Theories of step formation consider a wide range of dominant drivers and can be separated into three domains favoring either hydraulic controls (**HC**), granular interactions during flow (**GI**) or random drivers (**RD**) as relevant factors for step initiation. A direct evaluation of these mechanisms with field observations is challenging, as step formation cannot be directly observed. Based on the physical mechanisms of the various formation models we derive diagnostic parameters and critically test them for a data set of 103 alluvial channel steps in a 550 m long channel section of a steep stream in Switzerland. We find that one class of alluvial steps form due to jamming in narrow and narrowing sections of the channel, while steps in wide and widening sections form around rarely mobile key stones. Therefore, these two models of step formation, which are often times seen as competing, apply in our study reach at the same time in different locations of the channel. A third class of steps is forced by logs. They are typically located close to the original growth position of the tree and therefore reflect strong channel-hillslope coupling. Wood-forced steps make up a minor fraction to the total number of steps, but contribute significantly to the cumulative step height and, thus, are relevant for the reach-scale flow resistance of the channel.

4.1 Introduction

Streams with gradients greater than 3% commonly have step-pool morphologies (Montgomery and Buffington, 1997), which reflect the complex interaction of flow hydraulics and sediment transport (Lenzi et al., 1999). During low flow conditions, steps determine channel stability (Abrahams and Li, 1995) and as major roughness elements they dissipate the stream's energy (Chin, 2003; Yager et al., 2012b), diminishing the ability of the river to transport sediment. During high flows, the shear stress exerted by the flow can exceed the critical shear stress that is necessary to break up these stable bed forms (Whittaker and Jaeggi, 1982; Chin, 1989; Chin and Wohl, 2005). This failure is crucial for the coupling of the channel with adjacent hillslopes because step destruction can induce hillslope failure through de-buttressing and thereby drive sediment supply to the channel (Schuerch et al., 2006; Molnar et al., 2010; Golly et al., 2017a). Thus, step dynamics have a two-sided impact on the sediment budget of a steep stream and a comprehensive understanding of stepped bedforms is essential to our comprehension of mountain channels. Yet, the development of step-pool structures is not thoroughly understood. Although step dynamics have been investigated in various modelling and experimental studies (e.g. Curran and Wilcock, 2005b; Zimmermann et al., 2010), the processes that lead to step formation and destruction are debated in the literature, and several different, competing models exists. Direct observations of step formation in natural environments are not available, for obvious reasons: direct observation is difficult and hazardous as we are lacking the tracking techniques to follow sediment particles during high flow events. These problems can be partly eliminated in experimental setups, but scaling effects may impact the processes at work (Curran and Wilcock, 2005b). Moreover, laboratory experiments have commonly been performed with constant water discharges, while such conditions do not reflect the complex hydrology of natural catchments that can be significant for the development of step-pool patterns (Lenzi, 2001; Turowski et al., 2009; Molnar et al., 2010). A critical review of observed step morphology in the field is required to discriminate the physical formation process, exploiting the process-form link.

In this study, we test different mechanisms of step formation by the step-pool morphologies observed in a natural steep stream. We do this by reviewing existing theories of step formation and derive from them the diagnostic parameters. With these parameters we evaluate the theorized step-forming processes with field data set of

channel steps of a natural steep mountain stream. We build this effort on the conceptual framework of the link between process and form common in (fluvial) geomorphology (Fig. 30a). Adapted to our case, we postulate a link between the transported sediment, the process of step formation, and the resulting step morphology. Since we are not able to identify the processes directly, we aim to detect them indirectly from the observed patterns of steps in a natural fluvial environment (Fig. 30b).

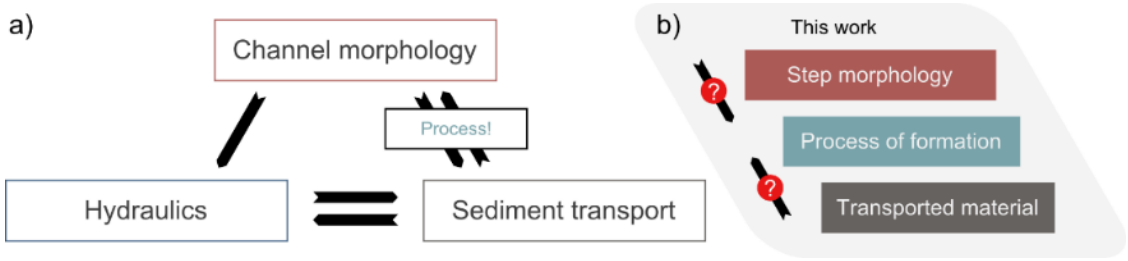

Fig. 30: a) Local flow hydraulics are determined by channel morphology, which in turn determines sediment transport. The latter link is bi-directional, meaning that sediment transport also has a direct effect on the flow hydraulics. Sediment transport determines channel morphology while the latter depends on the process (process-form link). b) Adapted to the focus of this study, the process is here the process of step formation, which we deduce by analyzing the morphology of channel steps while considering type and size of the transported material.

4.1.1 Theories of step formation

The role of steps in steep fluvial systems has been researched for decades for engineering purposes, and with regard to their local effects on flow hydraulics and sediment transport (Whittaker and Jaeggi, 1982; Chin, 1989; Yager et al., 2012b). This research raised awareness of these bedforms as dominant factors for the complex dynamics of high-gradient streams. It provided descriptive documentation of form and geometry of steps, based on which later studies could move towards a mechanistic explanation of their formation (Chin and Wohl, 2005). For example, many studies found an inverse correlation of average step length and slope, suggesting a link between formation and morphology of channel steps in mountain streams (Heede, 1981). However, analyses of other form parameters have led to contradicting results. For example, positive correlations of step length and channel width have been both confirmed (Chartrand and Whiting, 2000) and refuted (Wohl and Grodek, 1994). Similar outcomes have been found for step length and the size of step particles (Chartrand and Whiting, 2000). Hence, we have not fully

understood step formation and its mechanistic explanation is still under debate due to the numerous conditions under which steps form and the various shapes they can have (Curran and Wilcock, 2005b). Furthermore, studies that investigate the link between the step formation process and the form of steps in natural streams at a large spatial scale are rare and we are lacking a critical test of different theories of step formation against field data. Attempts to harmonize contradicting mechanisms occurring simultaneously within a single catchment – for example as different process domains – have been put forward (Zimmermann and Church, 2001), but have not been rigorously tested in the field.

Three classes of step formation models have been proposed. First, models that emphasize hydraulic controls, including maximization of flow resistance and the standing wave formation model (**HC**). Second, models that emphasize granular interactions like the jammed state model (**GI**). And third, models that assume that steps form around rarely mobile key stones or logs (**RD**). Here we introduce the different theories for which we derive the physical parameters later.

Hydraulic controls (**HC**): These models consider steps as the principal dissipators of energy (**HC.A**) in steep streams. They postulate that step formation occurs randomly and steps remain stable in patterns such that energy dissipation maximizes (Abrahams and Li, 1995; Chin, 1999a, 2002; Chartrand and Whiting, 2000; Lenzi, 2001). Alternatively, HC models postulate that steps form at hydraulic jumps (**HC.B**) analogous to antidunes in sand-bed rivers (Whittaker and Jaeggi, 1982), resulting in a constant step frequency. These so-called antidune models focus entirely on hydraulic conditions at the bed during high flows and require supercritical flow and completely submerged bed elements, which are rarely met in natural steep channels (Wohl and Grodek, 1994).

Granular interactions (**GI**): Models in this domain consider grain-grain and grain-bed interactions of the moving sediment as relevant processes for step formation. They incorporate the idea that sediment particles can interlock during transport and build stable force chains (Cates et al., 1998). This notion emerged from the observation that steps are often more stable than predicted, for example by the Shields criterion applied to individual grains. Specifically, the local hydraulic conditions at steps are often above the critical threshold of motion for the largest grains incorporated into the step (Komar and Li, 1988; Church and Zimmermann, 2007). The physical basis of

granular interaction models of step formation is the "jammed-state" hypothesis, where it is assumed that large grains are trapped preferentially at locations where the ratio of channel width and the diameter of the mobile grains (the "jamming ratio") is low (Church and Zimmermann, 2007; Zimmermann et al., 2010). Trapping is thought to occur through grain-grain interactions of mobile particles and is known as 'jamming' in the granular dynamics literature. The models can be extended to include further bed shape parameters such as the along-stream change of channel width – i.e. channel narrowing – upstream of the steps. These conditions increase the wall friction angle and thus influence the probability of jamming (To, 2002). Another crucial aspect in the application of GI models is the sediment supply during the flood events, which is difficult to measure or to model.

Random driver (**RD**): Models of this domain emphasize the random character of processes in the formation of steps. In this concept step formation occurs at the location of large clasts – or logs – with limited mobility against which other particles come to rest (Wohl and Grodek, 1994; Zimmermann and Church, 2001; Curran and Wilcock, 2005a). These "key-stones" are assumed to be introduced to the channel from adjacent hillslopes and to be immobile during step-forming floods. Their distribution along the channel is therefore determined by the supply of boulders and logs from hillslopes and is thus often considered to be random. The concept can be extended by the assumption that key-stones have limited mobility, i.e., they are mobile during the largest flood events but stable during sediment accumulating events. We consider this to be justified as large boulders can be mobile during floods (Lenzi et al., 1999; Turowski et al., 2009). In this alternative form, key-stones maintain their function of trapping further grains but are less bound to their point of entry into the channel from adjacent hillslopes. Rather, the location of key-stones may be determined by hydraulic conditions along the channel.

4.1.2 Deriving discriminatory parameters

Starting from the initial model hypotheses and using physical considerations, we now derive the diagnostic parameters (Table 8), which allow to discern the dominating step formation mechanism as listed in the previous section in a data set of natural channel steps. We number them in the form **XX.n**, where **XX** represents the model domain from Section 4.1.1 and **n** is the number of the specific test. In our analyses we focus on

geometrical parameters of channel and step morphology, as they are widely used in the literature and can be easily measured in the field. We do not rely on parameters derived from flow resistance considerations as they are often subject to large uncertainties in rough channels (Bathurst, 1985; Millar, 1999; Curran and Wohl, 2003; MacFarlane and Wohl, 2003).

HC.1, maximization of flow resistance: based on the hydraulic conditions in the channel during high flows, we can test for the hypothesis that steps act to maximize flow resistance. Abrahams et al. (1995) proposed a conceptual model in which the resistance of a channel to flow is greatest when the loss of elevation due to steps is maximized, assuming that total resistance is dominated by spill resistance. Thus, the mean step slope, expressed as $\overline{H_{step}/L_{step}}$, where H_{step} is the step height and L_{step} its length, should be equal to the overall channel slope $S_{channel}$ (Fig. 31). However, Abrahams et al. (1995) showed experimentally that the slope ratio $\langle\overline{H_{step}/L_{step}}\rangle/S_{channel}$ takes values between 1 and 2, since the height of a step is measured to the deepest point in the downstream pool and typically the bed gradients of pools are slightly positive. Hence, if this model applies, then we expect

$$1 \leq \langle\overline{H_{step}/L_{step}}\rangle/S_{channel} \leq 2. \quad (1)$$

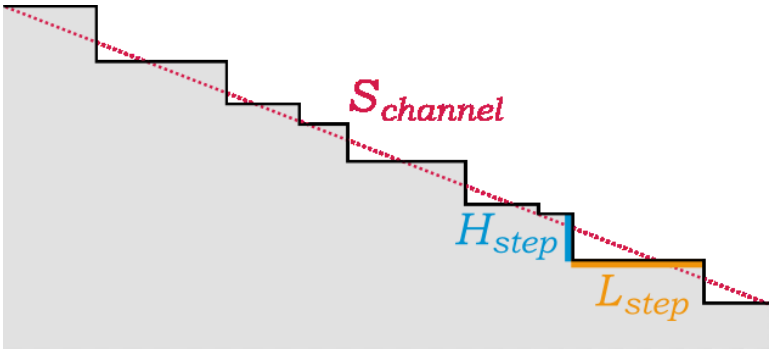

Fig. 31: After the concept of steps maximizing flow resistance (Abrahams et al., 1995) the overall channel slope ($S_{channel}$) should be equal to the average step slope (eq. 1). For successfully testing the concept of flow resistance optimization, however, step height (H_{step}) should correlate with the distance to the next step (L_{step}) on a per-step basis, aswell (eq. 2).

However, most realistic step distributions and geometries will yield a reach-averaged slope ratio between 1 and 2. Moreover, the maximization of flow resistance may be a bi-product of other step forming mechanisms. Therefore eq. (1) constitutes a weak test of the flow resistance maximization hypothesis. As a further test, we can analyze the maximization of flow resistance per step. This can be expressed by the correlation of the height of a step to the distance to the next step downstream which should go as the ratio of the average channel slope (Fig. 31), and therefore we expect for each step

$$H_{step}/d_{downstream} \approx S_c. \quad (2)$$

HC.2, standing waves: If the standing waves model applies, then the spatial distribution of step spacing should have a small standard deviation compared to the mean step spacing. The standing waves can be expected to occur at regular distances along the channel and steps should be located under or close to their maximum water surface elevation, i.e., underneath the standing wave. This implies that the mean step spacing is equal to the wavelength of the standing waves. If the waves are regular along the channel, both maxima and minima should occupy half of the total wave length. We assume that step spacing is normally distributed around the mean step spacing $\overline{d_{downstream}}$ and we specify that for a successful model test all steps within one (two) standard deviations need to be located underneath the wave maxima, corresponding to 68% (95%) of the steps. Then, the expected standard deviation σ_P of the distribution of step spacing $d_{downstream}$, should be less than 1/4 (1/8) of the mean step spacing and thus

$$\sigma_{P(d_{downstream})} \leq \frac{\overline{d_{downstream}}}{a} \text{ with } a = 4 \text{ and } a = 8. \quad (3)$$

Or, put differently, the correlation coefficient (mean/standard deviation) should be small, following

$$corr.coef. \leq b \text{ with } b = 0.25 \text{ and } b = 0.125. \quad (4)$$

GI.1, jamming ratio: In the jammed state hypothesis the controlling parameters are the properties of the grains that move, e.g. size and shape, and the local bed geometry, e.g. channel width. The lower the jamming ratio – $W_{channel}/d_{grain}$, where $W_{channel}$ is the channel width and d_{grain} is the diameter of the step forming grain – the higher is the

probability of the jamming of particles as the probability of building stable force chains increases (Beverloo et al., 1961). The critical ratio necessary for jamming to occur is typically in the range of 2 to 5 (To et al., 2001; Zimmermann et al., 2010). The size of the step forming grain can be estimated by the step height (Wohl and Ikeda, 1997; Chin, 1999b). The step height H_{step}, in turn, relates to the grain diameter with a factor of 1.2 (Chin, 1999b). Hence, we expect

$$W_{channel}/\left(H_{step} * 1.2\right) \leq 5. \quad (5)$$

GI.2, jamming ratio + wall angle: As the model of jamming assumes contact with the channel boundaries, the properties of the boundary, such as bank roughness (Zimmermann et al., 2010) or angle (To, 2002), matter. Thus, in addition to the absolute channel width at steps we computed the change of channel width ΔW over a distance Δx upstream of the step. We expect that downstream narrowing increases the probability of jamming and therefore steps formed by jamming should be commonly found in narrowing sections of the stream. Steps formed under this condition should preferentially show

$$\frac{\Delta W}{\Delta x} \leq 0 \quad (6)$$

where x is the along-stream coordinate in the downstream direction.

GI.3, jamming ratio + curvature: According to the jammed state model, steps form when mobile particles jam in the channel by building an arc spanning from left bank to right bank. As a result of the internal force conditions of steps that are formed by jamming, the plan view curvature κ should be curved upstream (To, 2002; Muthuswamy and Tordesillas, 2006). Thus, we expect

$$\kappa = curved\ upstream \quad (7)$$

RD.1, key-stones: The hypotheses based on random drivers are special with respect to their proof of concept. The stochastic nature of step formation could, in principle, be verified by demonstrating the randomness of the governing variables. However, randomness should also be observed for unrelated variables. Therefore, the original version of the key-stone hypothesis can be accepted only by rejecting all other hypotheses. With regard to our approach of analyzing a field data set, it remains

untestable. Hence, we use the combined version, in which large grains still have the ability to trap sediment particles even though they are semi-mobile (**RD.2**). Throughout this manuscript, we refer to this hypothesis as the key-stone hypothesis.

RD.2, semi-mobile key-stones: In this version of the key-stone hypothesis, key-elements are semi-mobile allowing for a relocation of grains during large floods. The final position of the key-elements, which then trap further grains to form a step, is controlled by the local bed shear stress τ_{bed} and step formation after this process is likely where the change of the shear stress decreases downstream, expressed as

$$\frac{\Delta\tau_{bed}}{\Delta x} < 0 \tag{8}$$

where *x* is the along-stream coordinate in the downstream direction.

The transport stage – the ratio of applied shear stress (property of the flow) and critical shear stress (property of the jammed grain) τ_{bed}/τ_c – has been argued to be a good parameter to confirm the jammed-state hypothesis (treated in the group GI, see also Zimmermann et al., 2010), assuming lower values for steps formed under jamming conditions. However, we argue that this ratio is not a good discriminator for the various theories because the transport stage minimizes if either the applied shear stress is low or if the critical shear stress is high. While the latter could apply to jammed grains, the former might occur for key-stones. Instead, we consider local shear stress τ_{bed}.

RD.3, key-stones + curvature: When key pieces come to rest and more sediment accumulates against their upstream side, the plan view geometry of the step should be altered consistently. Precisely, an triangular wedge or an arc should form, with its apex pointing in the downstream direction, and the key-piece located at its apex. Thus, after this theory we expect

$$\kappa = curved\ downstream \tag{9}$$

Test	*Domain*	*Concept*	*Discriminatory parameters*
HC.1	hydraulic conditions	maximization of flow resistance	$1 \leq \langle \overline{H_{step}/L_{step}} \rangle / S_{channel} \leq 2$, $H_{step}/d_{downstream} = S$
HC.2		standing waves concept	$\sigma_{P(d_{downstream})} \leq \frac{\overline{d_{downstream}}}{a}$
GI.1	grain interactions	jammed-state of grains	$W_{channel}/(H_{step} * 1.2) \leq 5$
GI.2		jammed-state + wall angle	$dW/dx \leq 0$
GI.3		jammed-state + curvature	$\kappa = curved\ upstream$
RD.1	random driver	key-stone (traditional)	*no discriminatory parameters*
RD.2		key-stone elements semi-mobile	$\Delta\tau_{bed} < 0$
RD.3		key-stone + curvature	$\kappa = curved\ downstream$

Table 8: List of step forming hypotheses and their testable parameters that we apply on our field data set of natural channel steps.

In addition to these considerations, the role of wood for steps has to be reviewed. In forested catchments steps often incorporate wood (Heede, 1972; Marston, 1982; Montgomery and Buffington, 1997), and wood steps can have a strong impact on catchment-wide sediment dynamics (e.g. Jochner et al., 2015). Although steps including wood can be higher than sedimentary steps in the same channel (MacFarlane and Wohl, 2003), it has been shown that the morphological and functional characteristics of steps including wood resemble those of boulder steps (Curran and Wohl, 2003). The role of wood in steps can be either non-structural (step contains wood) or structural (step formation was forced by wood) and typically a mixture of both step types is present within a single channel (Heede, 1981; Wohl et al., 1997). Accordingly, we collected an attribute for steps classifying the role of wood, if present (see section 4.2.). Steps forced by wood are marked as such throughout the results and we discuss the role of wood for each of the derived step formation models separately. Where wood has subordinate role, it does not significantly alter the mechanics of step formation, and hence, the resulting steps do not constitute a fundamentally different class. Instead, they can be associated to the above derived domains. We treat steps comprising wood identically to ones that do not, regarding the mentioned physical parameters, emphasizing the role of channel geometry in controlling step formation.

4.2 Field site and Methods

In this study we test the diagnostic parameters of step forming hypotheses, as listed in section 4.1.1, against high resolution field observations of step morphology collected in the Erlenbach. This steep mountain stream in the Alptal valley of the Swiss Pre-alps hosts an observatory for channel morphology and bedload transport (Turowski et al., 2009; Rickenmann et al., 2012; Beer et al., 2015). Its channel shows step-pool and occasional cascading reaches (Turowski et al., 2009; Molnar et al., 2010) and has high sediment supply (Turowski et al., 2009; Rickenmann et al., 2012). Bedload transport events are frequent with an average of ~20 events per year (Rickenmann and McArdell, 2007).

In the 0.74 km^2 headwater catchment we surveyed a ~ 550 m long reach of the Erlenbach main stream on March 13, 2015 with a total station. We measured with an accuracy of a few centimeters the 3D-position of the active channel bed and the thalweg (water flow path during low flow conditions), resulting in ~2000 point measurements with x,y,z-coordinates (Fig. 32). The margin of the active channel bed, determined by the transition from sediment cover to the vegetated riparian strip, was surveyed with an average spacing of 2.1 m. The measurement frequency was increased where rapid changes in the planform geometry of the channel bed occurred. The survey of the thalweg followed the protocol of Milzow et al. (2006). Measurements of the local minima of the cross-section profiles were collected approximately every ~1 m or where an obvious breakpoint in the long-profile occurred, e.g. a toe or crest of a step. The average spacing of the thalweg measurements is 0.65 m. The software package cmgo (Golly and Turowski, 2017) was used to derive principal local channel metrics for the entire study reach with a high spatial resolution. Using the measured bank positions, a channel centerline has been calculated with an average point spacing of 0.36 m. For every centerline point, channel width, width change, channel slope, bed shear stress and the bed shear stress change were calculated. Channel width is represented by the intersection of the channel banks with a transect perpendicular to the local centerline. The change of the width at a point P1 is the difference of a point P2 at a distance K upstream of P1 and the width at P1, divided by the horizontal distance between P1 and P2. Hence, positive (negative) values indicate widening (narrowing) of the channel in downstream direction. The normalization by distance emphasizes width changes when they occur over a shorter distance. Since the length scale K determines the value of the width change, an a-priori assignment of K likely prejudices

the observable processes of step formation. However, lacking a physical determination of this length scale we chose for *K* a value of twice the average channel width (~7 m) which we use for all *K* throughout this study. The local channel slope of a point P1 was defined as the average slope of the channel bed along the centerline upstream of P1, over a distance *K*. The upstream range of a given point instead of the range around the point, including downstream stretches, has been chosen because hydraulic effects are unlikely to propagate upstream in high-gradient channels. The bed shear stress was calculated for a discharge of 7 m^3/s, which has been estimated to be the critical discharge needed to break up steps along the Erlenbach main stream (Turowski et al., 2013a). The last flood exceeding this discharge occurred on 1st August 2010 (Turowski et al., 2013a), about 5 years before the measurement campaign. Flow velocity was estimated using the equation of Rickenmann and Recking (2011). A full derivation can be found in Appendix E0. The change of bed shear stress at a point P1 was calculated as the difference between the shear stress at a point P2 upstream of P1 within the range *K* and the shear stress at point P1.

Channel steps have been identified using the scale-free, rule-based algorithm by Zimmermann et al. (2008), which applies a series of geometric rules to the long-profile, including minimum step length, minim drop height and minimum step slope. A total of 103 steps were found in the long-profile, for which various metrics have been calculated (Table 9). The location of a step is defined by the thalweg point measurement that has been identified as the step crest (Fig. 32). The `step_height` of a step is the difference in elevation between the step crest and the deepest point in the downstream pool. The `step_length` of a step is defined here as the horizontal distance of the step crest to the crest of the next step downstream, and the `step_slope` is the fraction `step_height`/`step_length`. The values for the step parameters `width`, `width_change`, `channel_slope`, `tau_bed` are taken from nearest centerline points calculated by cmgo. As the average spacing of the centerline points (artificial line derived from banks) is 0.36 m, the average maximum distance from a step to a centerline point is 18 cm.

Step attribute	Unit	Source	Description
location	m	automated[1]	x-y-z coordinate of step crest
step_height	m	automated[1]	distance between step crest and deepest point in pool
step_length	m	automated[1]	distance between crest of step and crest of next step downstream
step_slope	m/m	automated	height/length
width	m	automated[1]	width of the channel at step
width_change[2]	m/m	automated[1]	upstream change of the channel width in downstream direction
channel_slope[2]	m/m	automated	slope of the bed upstream of the step over the range K
tau_bed	Pa	automated	pressure exerted on the bed by the flow at a discharge of 7 m3/s
tau_bed_change[2]	Pa	automated	change of tau_bed in downstream direction over a range K
curvature	<class>	manual	plan view curvature
wood_role	<class>	manual	classification of the role of wood: <no_role>, <included>, <structural>
wood_transport	<class>	manual	classification of the transport state of wood: <not transported>, <possibly transported>, <likely transported>
wood_ori	<class>	manual	cross-sectional orientation of wood: <stream-parallel>, <transverse>, <vertical>

Table 9: The parameters we collected for each of the 103 steps in the channel survey of 2015. Data have been collected manually and by automated methods: [1] direct output of the software tool cmgo (Golly and Turowski, 2017), [2] this measure requires a length scale which has been set to twice the average channel width.

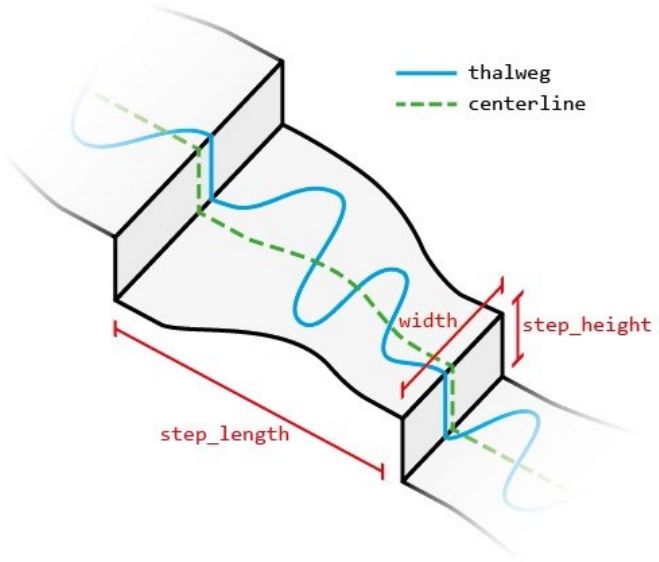

Fig. 32: Sketch of the parameters defining step geometry as used in this study.

Fig. 33: a) A step in which wood plays a structural role, and b) a step that consist entirely of alluvium and only minor amounts of smaller wood fragments that do not have a structural role.

Further step parameters have been collected manually from a three-dimensional model of the reach, constructed from a photogrammetric survey on Aug 2, 2015. The development of this model is described in Appendix F. The largest flood between this survey and the geodetic survey in March 2015 had a maximum water discharge of 1.1 m^3/s, well below the mean annual peak discharge (~2 m^3/s), and did not break up channel steps. Thus, all 103 steps identified by the algorithm from the long-profile could be confirmed in the

model. The step parameters manually collected from the model are planform curvature, the role of wood, the transport state of wood and the orientation of wood in the channel (Table 9). The curvature is the plan view curvature of the step wall. Classes are defined as "straight", "curved downstream" and "curved upstream". The class "straight" was assigned when the crest of the step is not obviously curved across the channel. The role of wood in a step (wood_role) was judged by eye, and classified as "not present", "included" and "structural". This classification is based on principal criteria of the shape, size and orientation of wood pieces (Fig. 33a). "Not present" was assigned for sedimentary steps that did not show wood. Wood-bearing steps were separated into "included" and "structural". "Structural" was assigned when a wood piece is anchored on both channel banks or if a vertical piece is anchored in the channel bed and trapping sediment. We refer to these steps also as wood-forced steps. Otherwise, the class "included" was assigned if wood was present, but not of structural importance. The transport state of the wood was classified into "not transported", "possibly transported" and "likely transported". "Not transported" was assigned when the major part of important wood pieces perpendicular to the stream was located outside of the channel bed (e.g. a fallen tree from an adjacent hillslope) or if vertical wood debris has intact bark, branches and leaves. "Likely transported" was assigned, when wood pieces were stream parallel, indicating in-stream relocation, or if wood pieces had apparent signs of physical or biological decomposition, indicating long residence times in the channel. The label "possibly transported" was assigned if none of the afore-mentioned categories could be confidently assigned.

During hypotheses testing, we compare various metrics of subsets of steps. For example, we evaluate the distributions of jamming-ratios for different classes of transported state. Whenever we give p-values, those were derived using the univariate, two-sample Kolmogorov-Smirnov test (Birnbaum and Tingey, 1951).

4.3 Results

Testing the various models introduced above we now give the results of the geometrical parameters of the 103 channel steps found in the studied reach of the Erlenbach. Of these steps, 59 are sedimentary, containing no wood, 16 include wood which is not-structural and in 28, wood is essential to the step structure (wood-forced steps) (Fig. 34). Despite the low number of wood-forced steps, their cumulative step height (30.34 m) is similar to that of sedimentary steps (34.92 m). We present the morphological analyses in the order

in which step formation hypotheses have been introduced above, starting with the hydrologically controlled models.

In the Erlenbach the average ratio of $\langle \overline{H_{step}/L_{step}} \rangle / S_{channel}$ for all steps is 1.29 (Fig. 35), which lies within the expected window of 1 and 2. For individual steps, however, there is large scatter, with ratio values ranging from 0.15 to 4.34 and the inter-quartile range spans from 0.69 to 1.93 (Fig. 35c). We tested the proposed metric of H_{step}/L_{step} also on a per-step basis (Fig. 36), as this reflects the effects of local hydraulic conditions. The root mean square error of the expected step length is 7.2 meters and the R^2 to the expected mean channel slope is -2.58.

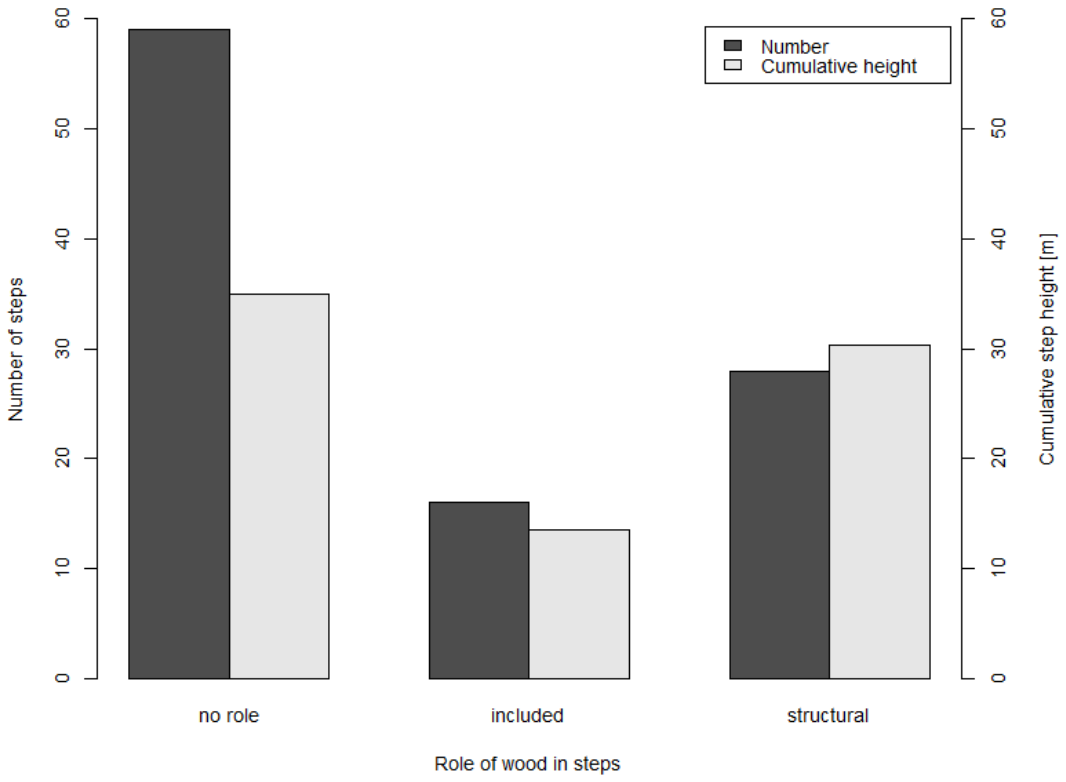

Fig. 34: Total number (dark gray columns) and cumulative height (light gray) of sedimentary steps and steps including wood.

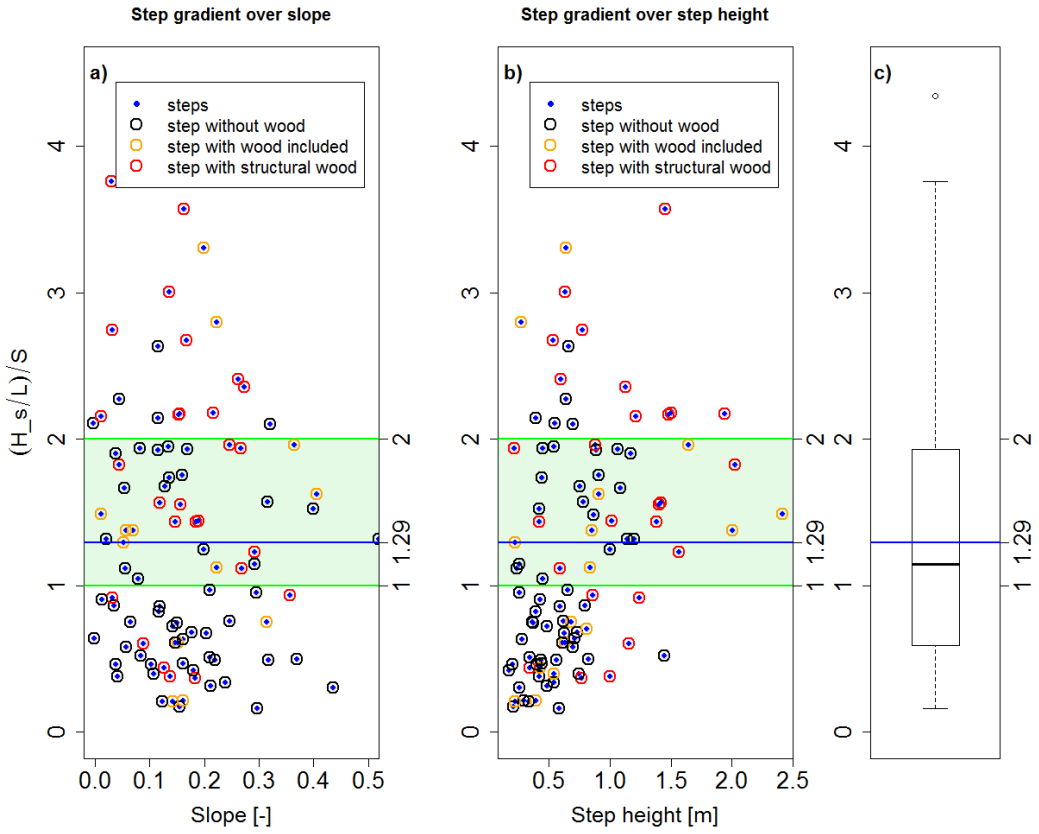

Fig. 35: The slope ratio of [Hs/Ls]/S plotted against a) channel bed slope, measured over a distance of 7 m upstream of the step crest, and b) the step height. c) Boxplot of the distribution of [Hs/Ls]/S. With a value of 1.29, the median of [Hs/Ls]/S is within the expected range of 1 to 2, the ratios for individual steps show large scatter and only 34% of the steps fall within the range. On average, wood steps seem to have a higher ratio (Hs/Ls)/S than sedimentary likely due to a higher average height (Fig. 34).

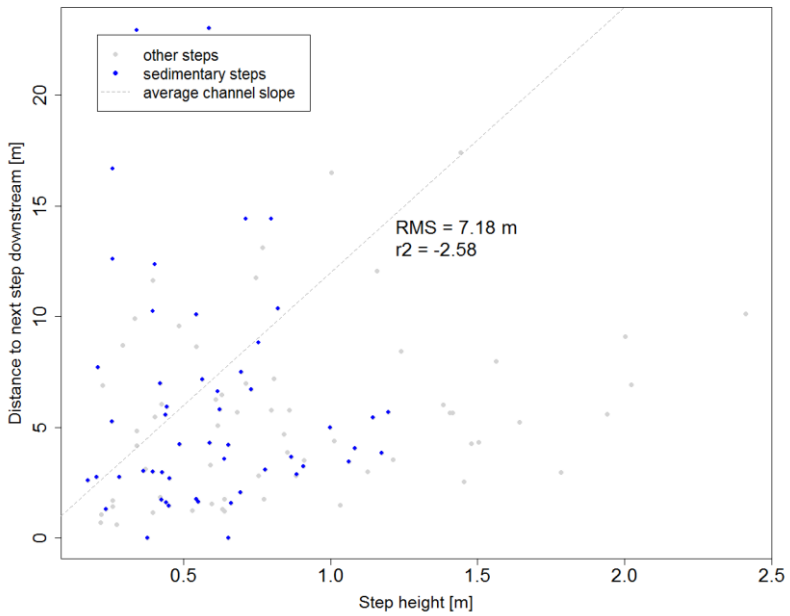

Fig. 36: Height of the individual steps and the distance to the next step crest downstream shows no clear correlation as the linear fit to the average channel slope (dashed line) yields an RMS of 7.18 m.

Channel steps have a mean spacing (distance of each step to the next step downstream) of 5.17 m with a standard deviation of 3.78 m (Fig. 37). The coefficient of variation (standard deviation divided by mean) is 0.73.

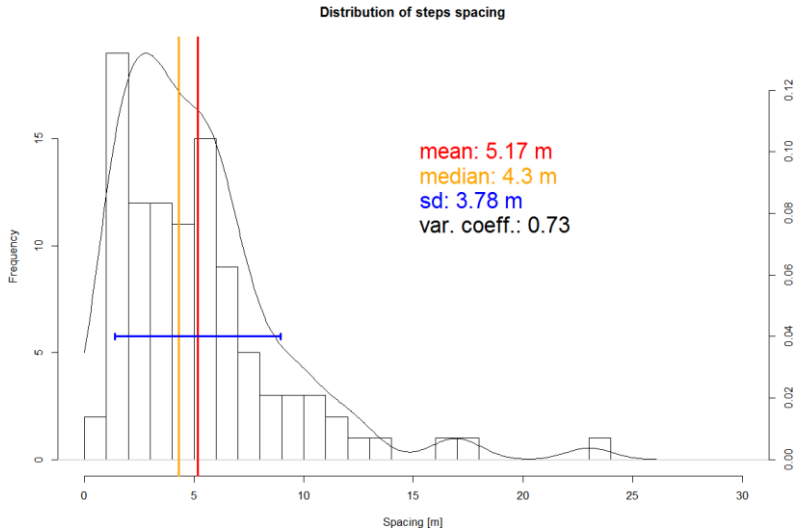

Fig. 37: Frequency and density of the distribution of steps spacing shows a large variation around the mean.

The jamming ratio was calculated using the ratio of step height multiplied by 1.2, which is a proxy for the diameter of the step forming grain (Wohl and Ikeda, 1997; Chin, 1999b), and the channel width at the location of the step. The mean jamming ratio of all steps is 5.87, with an inter-quartile range from 2.53 to 8.37 (Fig. 38b). In total, 56 out of the 103 steps have jamming ratios lower than 5. These tend to be located along narrow channel sections, with a mean width of 3.05 m below the mean width of the whole surveyed channel reach of 3.63 m. The mean channel width at steps with a jamming ratio greater than 5 is 4.75 m. Wood appears to systematically affect the distribution of step jamming ratios (Fig. 38a). 24 of 28 (86%) steps in which wood plays a structural role have jamming ratios less than 5, with a relatively narrow spread of values (Fig. 39). The lowest median jamming ratio was found for wood-forced steps, and the highest median for sedimentary steps without wood (Table 10). However, below the critical jamming ratio the number of sedimentary steps (23) is similar to the number of steps with structural wood (24). Of the steps with a jamming ratio smaller than 5, the median width of steps comprising wood (included and structural) is higher than the median width of sedimentary steps (Fig. 40).

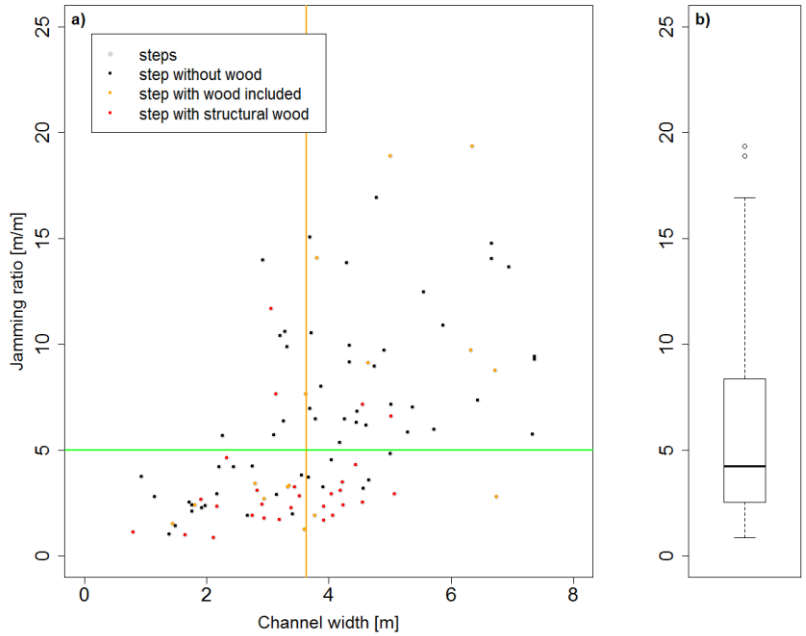

Fig. 38: a) Jamming ratios for the 103 steps of our study reach are positively correlated with absolute channel width. About half (43%) of the steps with low jamming ratios have wood as a structural element. The orange vertical line denotes the average channel width of 3.63 m. The horizontal green line denotes the critical jamming ratio of 5. b) A boxplot of the jamming ratios for all 103 steps.

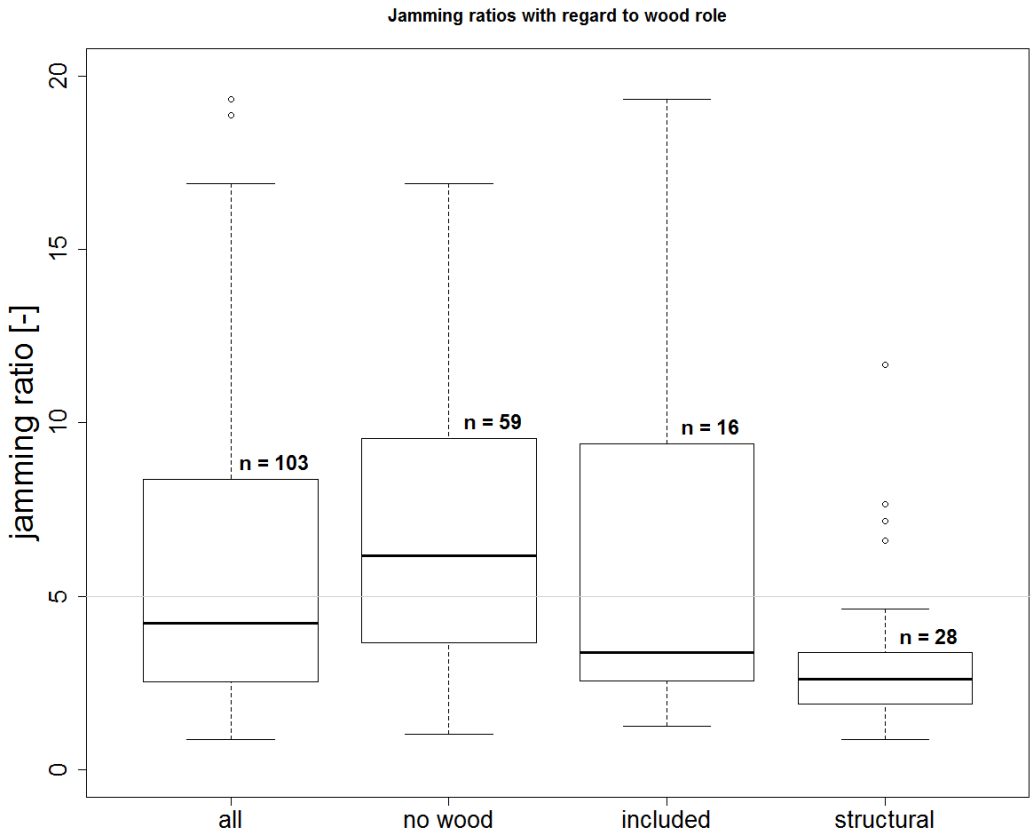

Fig. 39: Boxplots of the jamming ratios for all steps and separately for the three classes of the role of wood. Statistics are given in Table 10.

Set	**all**	**no wood**	**wood included**	**wood structural**
mean	5.87	6.82	6.88	**3.3**
median	4.22	6.17	3.36	**2.6**
25th percentile	2.53	3.65	2.55	**1.89**
75th percentile	8.38	9.56	9.4	**3.37**

Table 10: Statistics of jamming ratios for all steps and subsets classified by the wood role, minima in bold. Boxplots in Fig. 39.

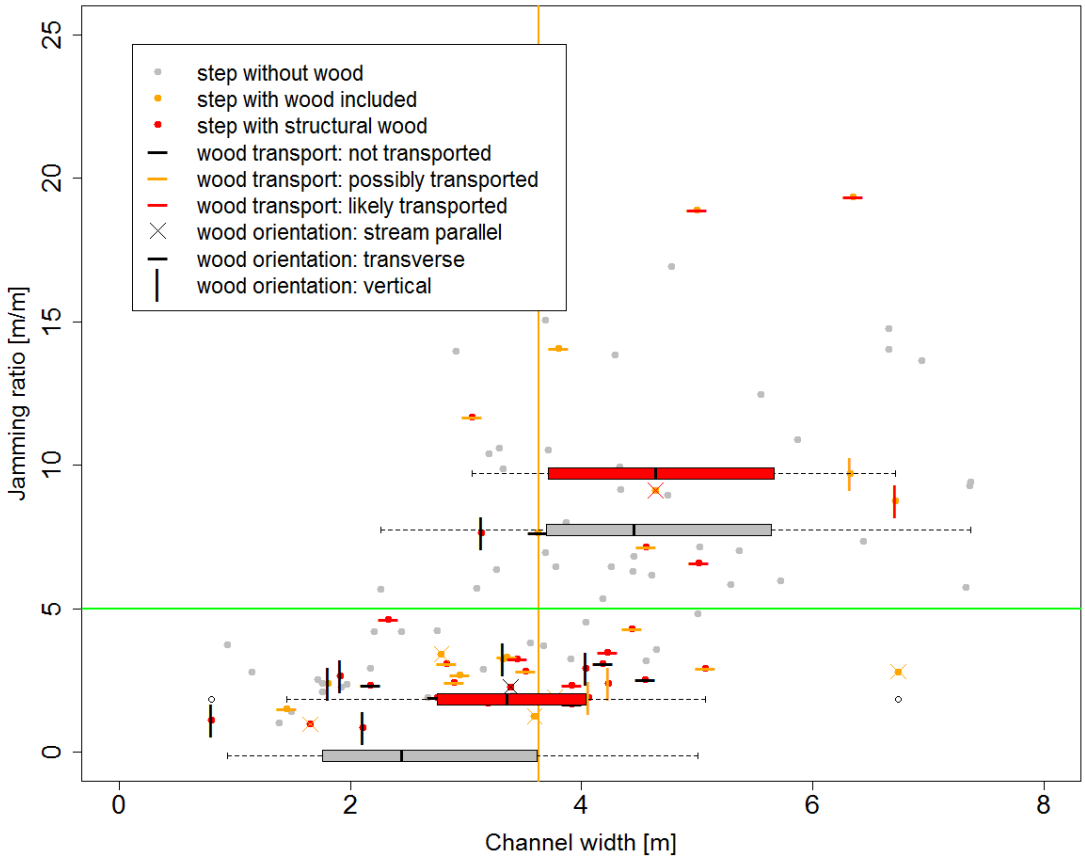

Fig. 40: Jamming ratios for different classes of wood role (color of points), wood orientation (type of overlay icon, e.g. horizontal bar) and the transport state of wood (color of overlay icon). For 42% of the steps below the critical jamming ratio that incorporate wood the wood has not been transported. The boxplots show the distribution of channel widths for sedimentary steps (gray boxplots) and wood-bearing steps (red boxplots) below and above the critical jamming ratio of 5.

Next we explore the change of the channel width upstream of a channel step with regard to the jamming ratio. The channel tends to become narrower where the jamming ratio is below the critical value of 5 (Fig. 41): the median channel width change is -0.05 m/m. By contrast, above the critical jamming ratio the median is +0.08 m/m. The distributions above and below the critical jamming ratio of 5 are significantly different ($p = 0.0077$).

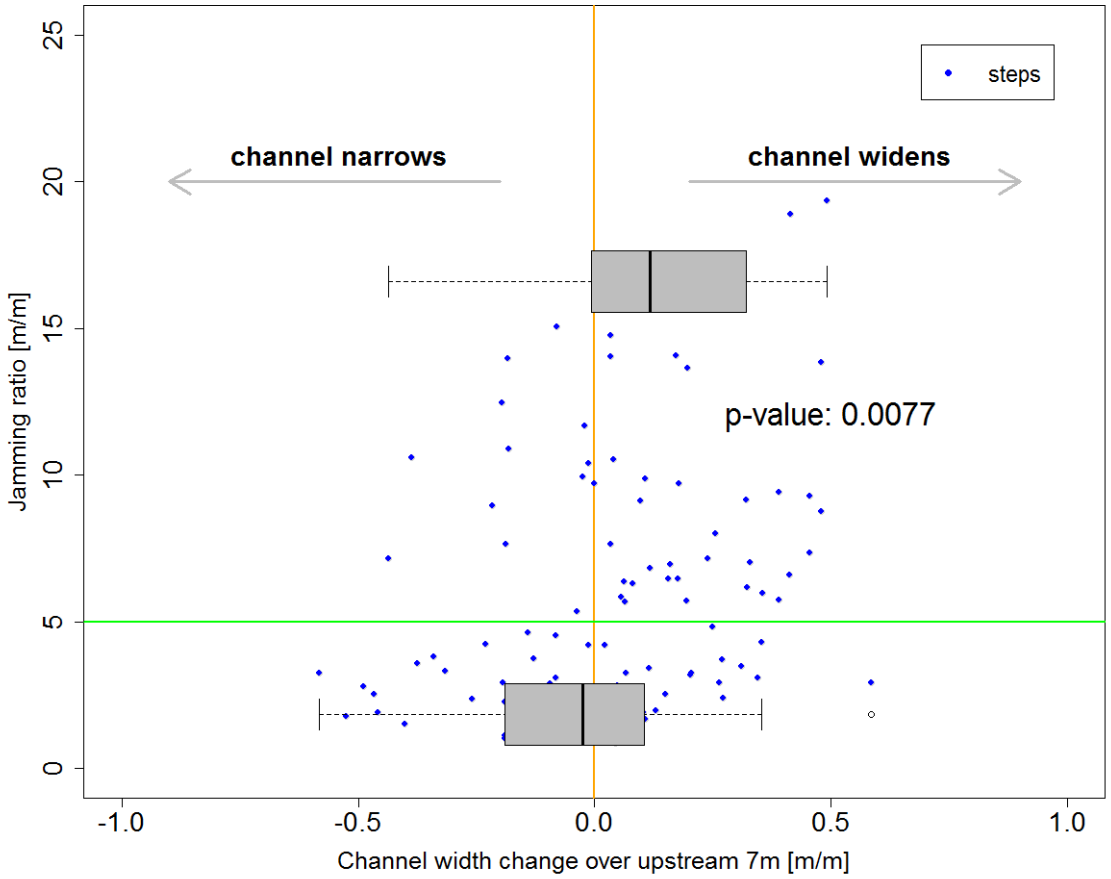

Fig. 41: Jamming ratio plotted against channel width change upstream of the step. The channel is more likely to narrow (widen) where the jamming ratio is below (above) the critical value of 5 (p = 0.0077). The green line indicates the critical jamming ratio of 5. The orange line indicates the transition from stream sections that narrow to those that widen.

	channel width change	
Set	jamming ratio <5	jamming ratio > 5
mean	-0.04	0.13
median	-0.03	0.12
25th percentile	-0.19	-0.01
75th percentile	0.10	0.32

Table 11: Statistics of channel width change below and above the critical jamming ratio of 5. Boxplots in Fig. 41.

We now explore the planform of the step in the context of channel metrics. Upstream curved steps have a lower median than other steps (Fig. 42a). This difference increases if only sedimentary steps (steps without wood) are considered (Fig. 42b). Combining the jamming ratio with the absolute channel width (Fig. 43), we find that sedimentary steps with an upstream curvature locate where the channel is narrow and the jamming ratio is small (Table 13). Conversely, where the channel is wide or the jamming ratio high, sedimentary steps are more likely curved downstream. The pattern for wood steps (included or structural) is fundamentally different (Fig. 44) and most of these steps have a straight planform geometry (Table 14).

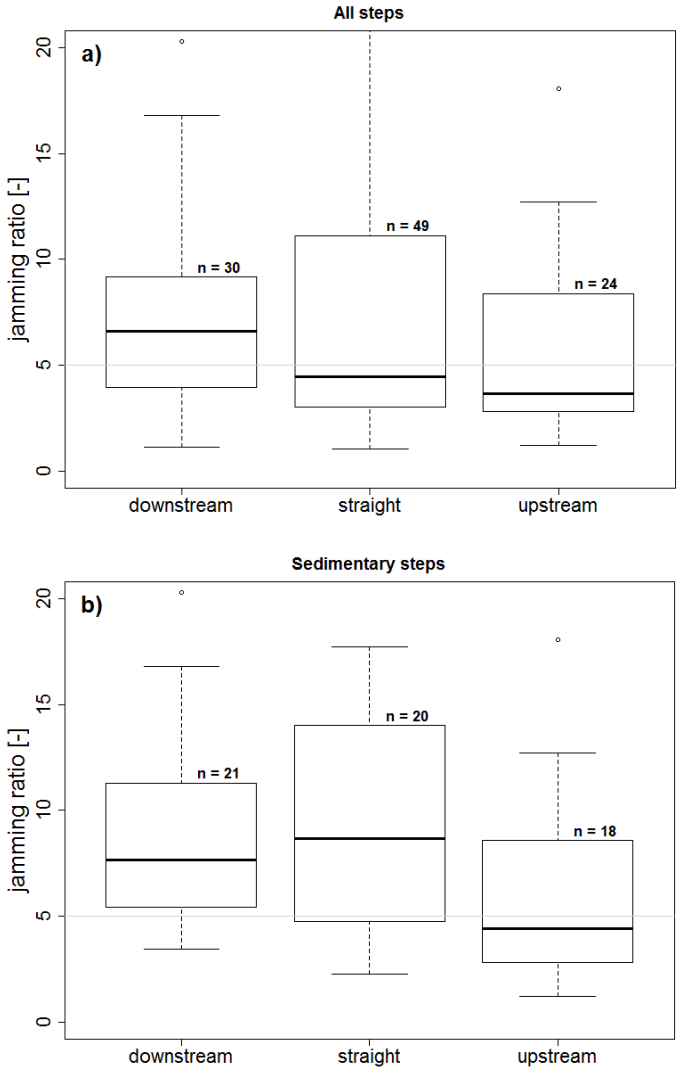

Fig. 42: Boxplots of jamming ratios by class of step curvature for a) all 103 steps, and b) for the 59 sedimentary steps only. Statistics are given in Table 12.

	all steps (Fig. 35a)			sedimentary steps (Fig. 35b)		
Set	downstream	flat	upstream	downstream	flat	upstream
mean	7.11	7.59	**5.87**	8.51	9.53	6.33
median	6.63	4.49	**3.37**	7.65	8.67	4.43
25th percentile	3.98	3.05	**2.83**	5.41	4.77	2.84
75th percentile	9.18	11.13	**8.39**	11.29	14.01	8.57

Table 12: Statistics of jamming ratios for all steps sorted by class of curvature. Boxplots are shown in Fig. 42.

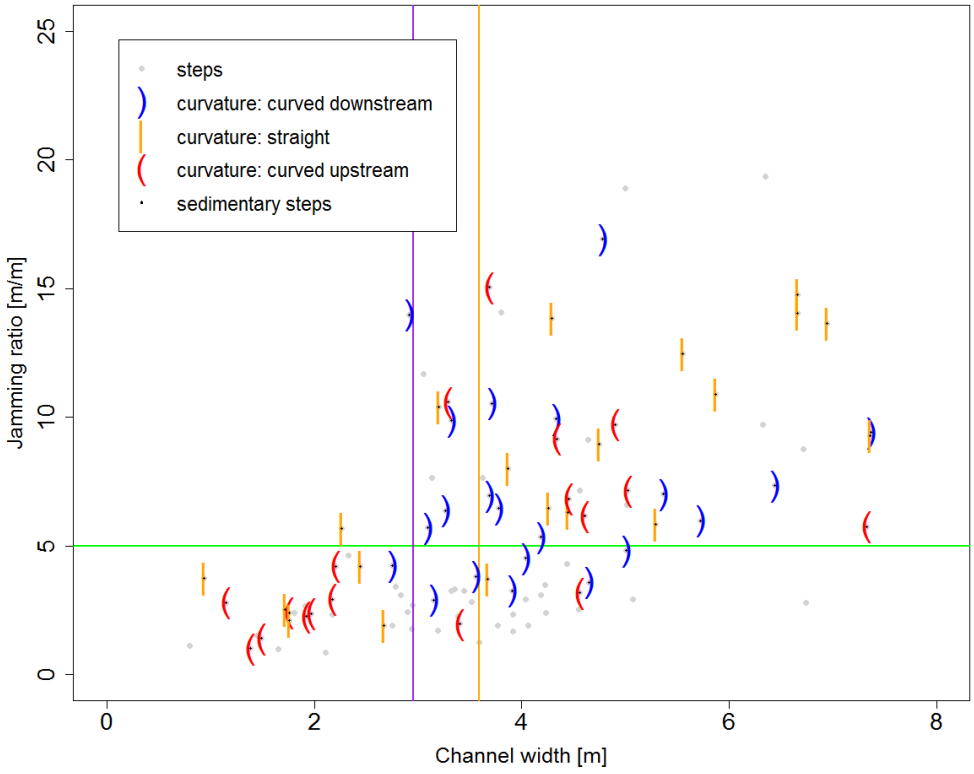

Fig. 43: The curvature of the 59 sedimentary channel steps plotted in the space of jamming ratio and channel width. Upstream curved steps (red brackets) cluster where the jamming ratio is low (jamming likely) and the channel is narrow (statistics in Table 13). Brackets depict curvature of steps assuming a flow direction from left to right. The vertical purple line indicates a channel width of 2.96 m, corresponding to the jamming width considering the average step height (proxy for relevant boulder size) and the critical jamming ratio of 5 of our data set. The vertical yellow line indicates the average channel width of 3.59 m which was used for calculating the absolute numbers of steps in each domain listed in Table 13.

	jamming ratio				channel width			
Set	**< 5**		**> 5**		**< 3.59 m [1)]**		**> 3.59**	
curved upstream	**10**	**44%**	8	22%	**10**	**42%**	8	23%
curved downstream	7	30%	**14**	**39%**	7	29%	**14**	**40%**
straight	6	26%	14	39%	7	29%	13	37%
total	23	100%	36	100%	24	100%	35	100%

Table 13: Numbers and percentages of step curvature for the 59 steps without wood in different classes of channel width and jamming ratio. [1)] A channel width of 3.59 m corresponds to the mean width of the surveyed section of the Erlenbach channel.

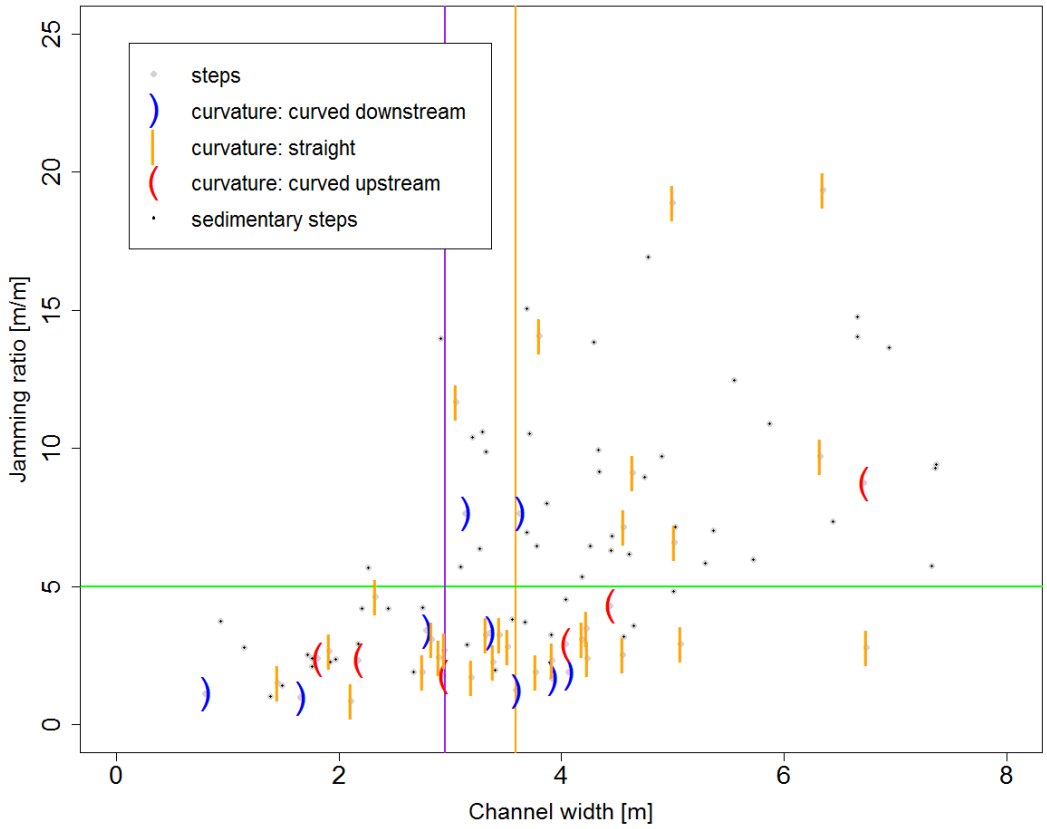

Fig. 44: Curvature of the 44 wood steps (wood included or structural) plotted in the space of jamming ratio and channel width. The majority of steps with wood have a straight planform geometry (statistics in Table 14). The vertical purple line indicates a channel width of 2.96 m, corresponding to the jamming width considering the average step height (proxy for relevant boulder size) and the critical jamming ratio of 5 of our data set. Brackets depict curvature of steps assuming a flow direction from left to right. Absolute numbers of steps in each domain are listed in Table 14.

	jamming ratio				channel width			
Set	**< 5**		**> 5**		**< 3.59 m [1)]**		**> 3.59**	
curved upstream	5	15%	1	9%	3	14%	3	14%
curved downstream	7	21%	2	18%	5	23%	4	18%
straight	**21**	**64%**	**8**	**73%**	**14**	**64%**	**15**	**68%**
total	33	100%	11	100%	22	100%	22	100%

Table 14: Count and percentages of step curvature for the 44 steps with wood (included and structural) in different classes of channel width and jamming ratio. [1)] The width of 3.59 m corresponds to mean width of the surveyed section of the Erlenbach channel.

We further test the local shear stress – the energy exerted by the water at step forming discharge of 7 m^3/s – at a step. First, we explore how the local channel width impacts the change in shear stress in the downstream direction, showing a broad, negative trend (Fig. 45a). Similarly, for sections in which the channel widens, the shear stress drops in the downstream direction (Fig. 45b). This reduction in shear stress correlates with the jamming ratio. The shear stress decreases significantly at steps that form above the critical jamming ratio of 5 with a median of -106.4 Pa. However, it decreases slightly, with a median of 40.6 Pa, where the jamming ratio is subcritical (Fig. 46). The distributions of local bed shear stress change above and below the critical jamming ratio of 5 are significantly different ($p = 0.0187$).

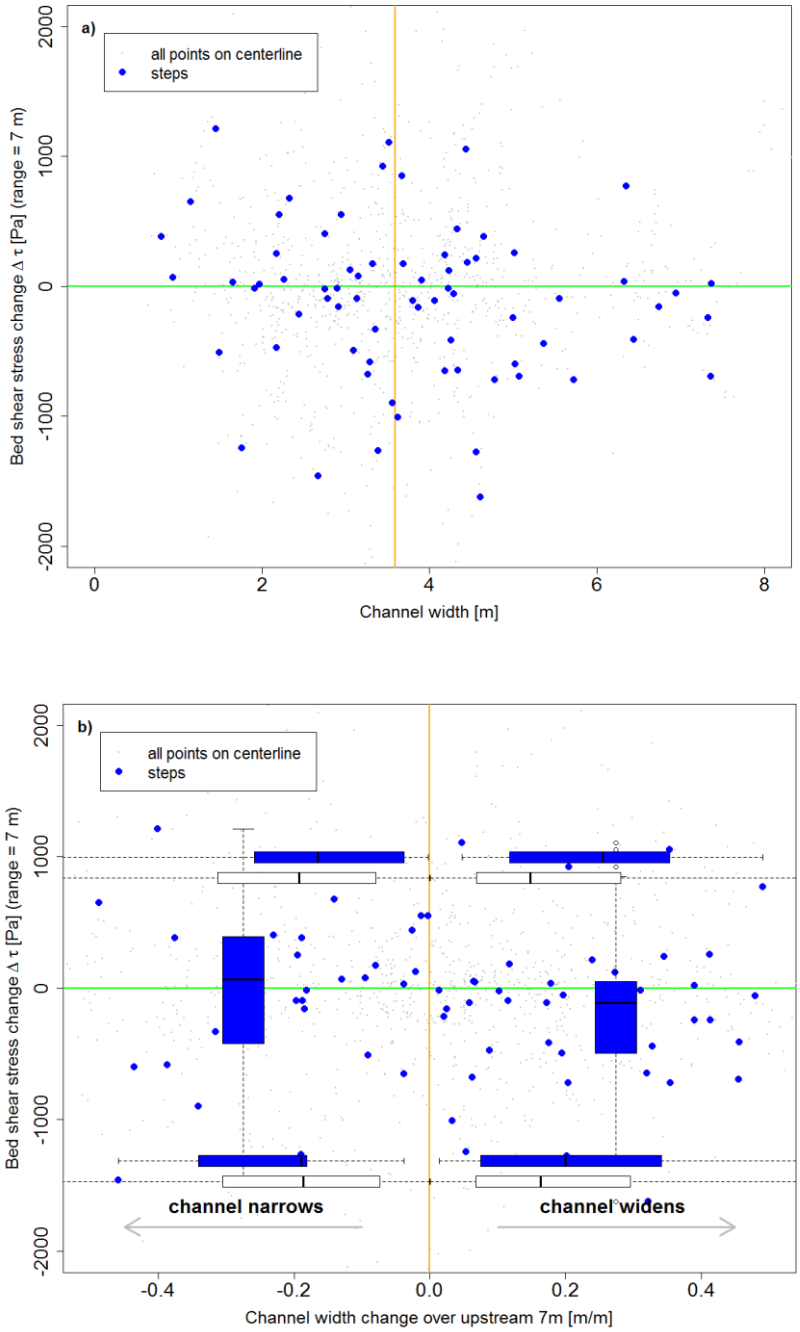

Fig. 45: a) The change of the bed shear stress $\Delta\tau$ and the absolute width for the 103 channel steps (blue dots) and all other centerline points (gray dots) shows consistently larger widths for negative $\Delta\tau$. b) Similarly, $\Delta\tau$ tends to be negative where the channel widens. The horizontal boxplots show that when $\Delta\tau$ is negative the channel is preferentially widening at steps (blue bars) than at other locations along the stream (white bars). Also, sections that widen (narrow) have negative (positive) bed shear stress change (vertical boxplots).

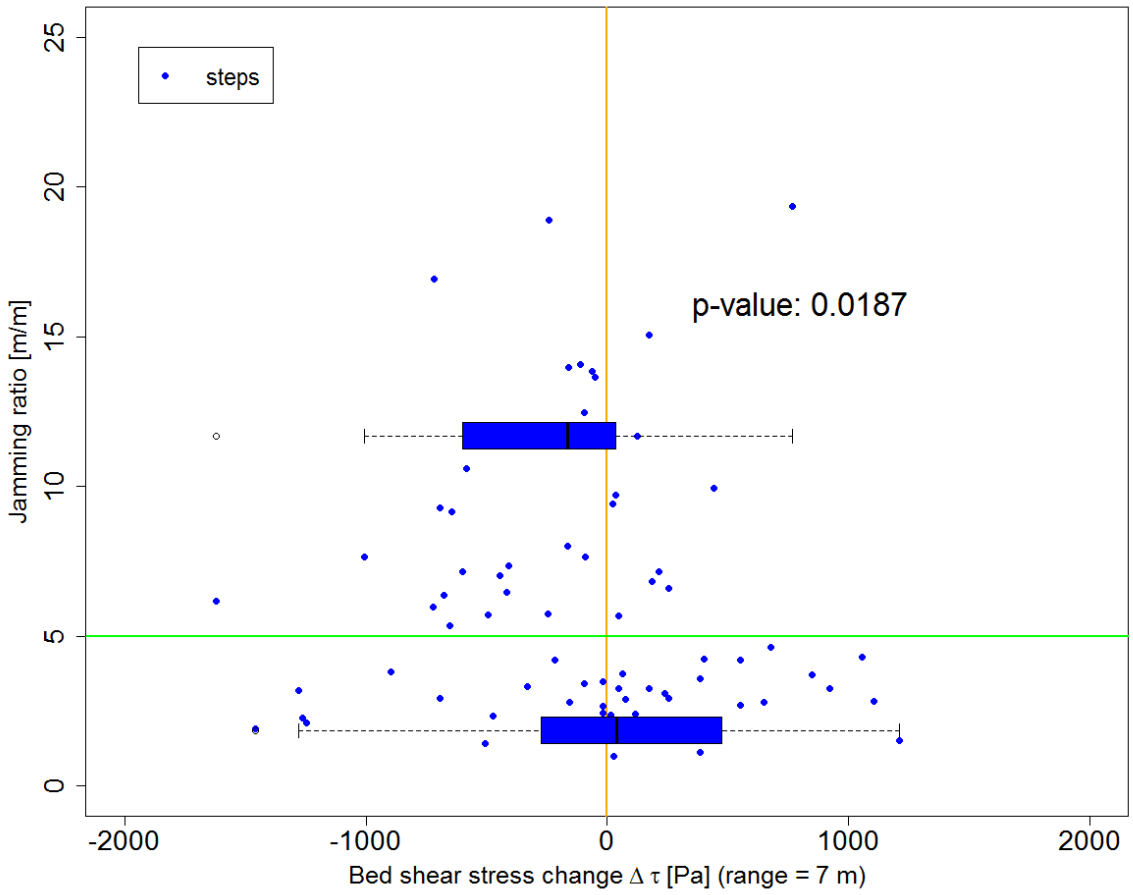

Fig. 46: The jamming ratio and the change of shear stress at the steps (blue dots). Below the critical jamming ratio of 5, the shear stress change Δτ at steps is widely distributed, with a slightly positive median of 40.6 Pa. Above the critical jamming ratio of 5 the distribution of Δτ shows less variability and a trend towards negative Δτ with a median of -106.4 Pa. The distributions are significantly different (p = 0.00187).

4.4 Discussion

The results presented in section 3 can be used to evaluate step formation models. We do this in the order of the list Table 8 in section 4.1.2, and finish with a general discussion of the implications of our findings.

4.4.1 Evaluation of model tests

Hydraulic controls (**HC**): Models in this class consider step occurrence as a function of local hydraulic conditions. For the test of the concept of flow resistance maximization (**HC.1**),

we found a slope ratio $\langle\overline{H_{step}/L_{step}}\rangle/S_{channel}$ = 1.29, which is within the expected range of 1 to 2. We assessed the proposed metric not only on the reach scale but also on a per-step basis (Fig. 35), because the model of flow resistance maximization should reflect the local hydraulic conditions. There is large variability of the slope ratio for individual steps and only 34% of steps along the surveyed section of the Erlenbach have a slope ratio between 1 and 2. The slope ratio does not correlate with channel bed slope (Fig. 35a) or step height (Fig. 35b), neither for the totality of steps, nor for sedimentary or wood-bearing steps separately. We argue that validating a model that emphasizes the local flow hydraulics with reach-averages is not adequate and constitutes a weak test, especially since a $\langle\overline{H_{step}/L_{step}}\rangle/S_{channel}$ ratio of around 1.29 can be expected for most natural step geometries and distributions. Thus, based on the results considering the individual steps we consider flow resistance maximization to be an unlikely driver of step formation and will not discuss it further.

The test of the standing waves model (**HC.2**) is based on the downstream spacing of steps. In the Erlenbach, we found a large standard deviation of step spacing of 3.78 m, corresponding to a coefficient of variation of 0.73 (Fig. 37). This is much larger than the value of 0.25 (0.125), which we expect when 68% (95%) of the steps are located under wave maxima. Only 59% of surveyed steps have a spacing that deviates less than the mean spacing from the expected value and would therefore be located under a standing wave in the stream water surface. Hence, we reject the standing wave model as an explanation for step formation in our study reach. Prior studies have also rejected the standing wave model for natural streams, because the necessary hydraulic conditions are not met in rough channel beds that are common in steep streams (Wohl and Grodek, 1994).

Granular interactions (**GI**): These models consider grain-grain and grain-channel bed interactions during transport conditions as dominant controls on step formation. The discriminant parameter for grain interaction-based models (**GI**) is the jamming ratio (**GI.1**). We find a wide range of jamming ratios for the 103 steps in our study reach (Fig. 38). For 54% of steps, the ratio is less than 5 – which is assumed to be the threshold for jamming caused by grain-grain or grain-channel interactions (To et al., 2001; Zimmermann et al., 2010). Such steps occur, on average, in narrower stream sections than do steps with higher jamming ratios. Jamming is likely the dominant physical process of formation for steps with a jamming ratio below 5. However, jamming does not explain the

entire population of steps along the Erlenbach, as 46% of the steps have a jamming ratio above 5 (Fig. 38). The steps that form at a jamming ratio above the critical threshold imply a mechanism of formation fundamentally different to jamming. Thus, we argue that jamming is not the only mechanism of step formation. The tests of wall angle (**GI.2**) and the curvature (**GI.3**) support this conclusion: for the steps that form at a low jamming ratio the channel narrows (**GI.2**), and the difference of channel width change above and below the critical jamming ratio of 5 is statistically significant (Fig. 41). Similarly, the curvature test (**GI.3**) confirms the role of jamming for the same populations of channel steps (Fig. 43): the upstream curved steps represent forms similar to force chains and the majority of curved steps with a jamming ratio below 5 are curved upstream (Table 13). However, this applies only for sedimentary steps; steps comprising wood are mostly straight (Table 14, Fig. 44). 33 of the 56 steps (59%) with jamming ratios less than 5 incorporate wood. Due to the slightly higher median channel width of these 33 wood-bearing steps (Fig. 40), it seems that wood jamming works mechanically different than sediment jamming. Thus, wood-bearing steps need to be considered separately from sedimentary steps. Of the 33 wood-bearing steps attributed to jamming, 14 incorporate wood pieces that have likely not been transported by the stream. The orientation of the dominant wood pieces in these steps is either horizontal or vertical, and never stream parallel. The step formation mechanism may be controlled by the lateral supply of large wood logs. These promote jamming in narrow but not in wider than average channel sections, and log length rather than step height may be the relevant parameter (Abbe and Montgomery, 2003; Jochner et al., 2015). Hence, we argue that of the steps with sub-critical jamming ratios only the sedimentary steps were initiated by jamming in the original mechanistic sense. Wood-bearing steps, with low jamming ratios may function mechanistically similar to the one of jammed sedimentary steps, but they have a different step geometry with a straight planform and a greater step height and occur over a large range of channel widths (Table 14). Their association with wood pieces that have not been fluvially transported (Fig. 40) suggests that these steps develop where logs have been supplied from the adjacent hillslope, not far from their original growth position. This interpretation is in agreement with findings from previous studies in the Erlenbach (Jochner *et al.*, 2015; Golly *et al.*, 2017a).

Random drivers (**RD**): The random driver mechanism involves trapping of grains against a key obstacle in the channel. This should generate steps with a downstream curvature

(**RD.3**). The majority of curved steps at wide channel sections have a high jamming ratio and are curved downstream (Table 13, Fig. 43). This suggests that the formation of steps in these channel reaches may be explained by the key-stone hypothesis. This population of steps is complementary to the one assigned to the jamming mechanism. The analysis of the bed shear stress change at steps (**RD.2**) supports this interpretation, as there prevail depositional conditions: for steps at wider than average channel sections, bed shear stress tends to decrease over the 7 m upstream of the step (Fig. 45a). No such trend is apparent for steps in narrow channel sections. Similarly, for sections that widen locally, the bed shear stress is negative (Fig. 45b). Steps likely form at these locations because of deposition, and thus favor the concept of semi-mobile keystones (**RD.2**).

4.4.2 Interpretation and implications

In summary, we find that maximization of flow resistance is unlikely to be the principal driver of step formation along the Erlenbach main channel. Instead, we find evidence for both granular interaction (GI) controlled steps and depositional key-stone steps (RD) (Fig. 47). A first domain of steps tends to occur in sections of the channel that are both narrower than the average channel width and have a decreasing channel width upstream of the step. Channel steps in this first domain were attributed to jamming. Flow energy changes at these locations have a minor impact on step formation, and bed shear stress is constant or slightly increasing downstream (Fig. 46), indicating that for jamming steps, depositional conditions are not required. This would also explain the large variability of the Shields ratio (transport stage) that has been observed in other field-tests of the jammed state hypothesis (Zimmermann et al., 2010). Steps in a second domain are controlled by large wood pieces recruited from hillslopes. These steps follow the same channel geometries and hydraulics as observed for the first domain of steps, suggesting that the mechanism of jamming works in a similar way. A third domain of steps occurs in wide channel sections with increasing channel width where depositional conditions prevail. These steps may form around key obstacles that have been deposited there due to locally decreasing flow energy. Steps of the third domain seem to rarely include wood.

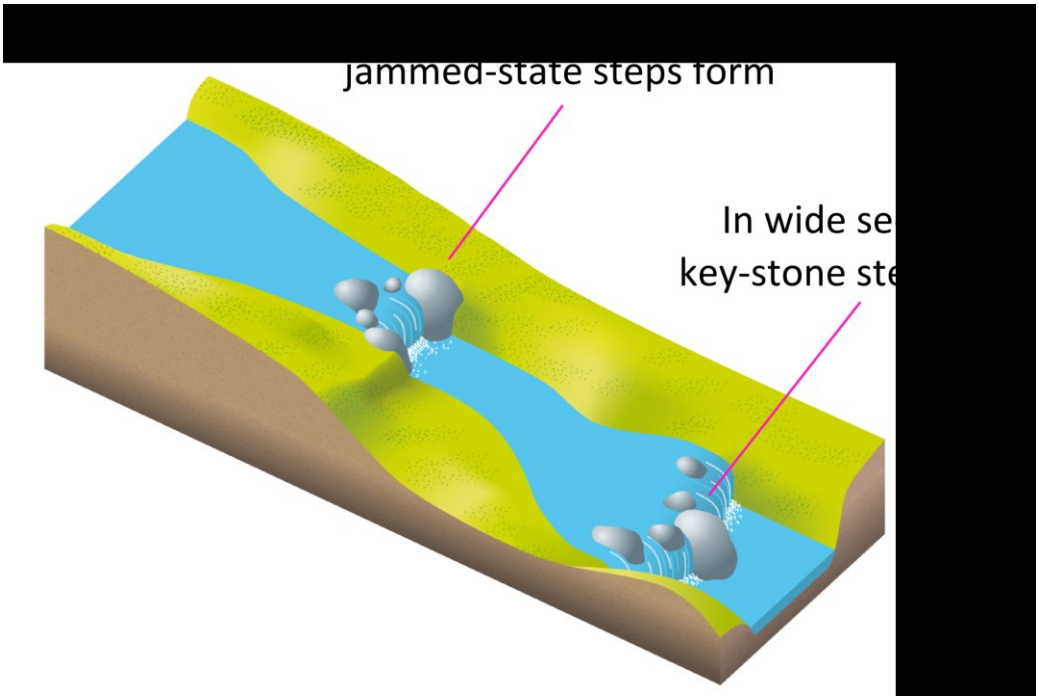

Fig. 47: Two different domains of step formation mechanisms were detected: in narrow channel sections, where the channel narrows, steps form due to jamming and build upstream curved steps. Further, steps form at wide sections where flow energy is decreasing, causing key-stones to deposit and forming steps with downstream curved planforms.

We interpret these findings as evidence that the population of channel steps along the studied stream reach cannot be attributed to a single process of step formation. The mechanisms of step formation can be described by the jammed-state hypothesis and by the keystone hypothesis, which operate in the Erlenbach catchment at the same time at different locations along the channel. The hydraulic conditions necessary for these two step formation mechanisms are contrary. Thus, a single conceptual framework of step formation cannot explain our observations.

Wood plays an important role in the formation and location of channel steps along the surveyed reach of the Erlenbach. Although wood-forced steps make up a small fraction of the step population (27%), their cumulative height is approximately the same as that of the more frequent sedimentary steps. Hence, wood-forced steps contribute significantly to the overall flow resistance of the channel. The type and properties of the incorporated wood suggest that wood-forced steps form close to the entry points of logs into the channel, at least in the Erlenbach (cf. Jochner et al., 2015). Their number and location is

therefore a direct function of tree fall on adjacent hillslopes and advection of material into the channel. This leads to the conclusion that both the biological activity on channel-bounding hillslopes, and the location and strength of hillslope-channel coupling may act as strong controls on the hydraulics of the stream. At least in the Erlenbach, hillslope activity is in turn driven by channel processes (Golly *et al.*, 2017a), emphasizing the importance of feedbacks between the channel and the hillslopes for the dynamics of mountain channels.

The fact that steps form at various geometrical conditions and through different processes has implications for the modelling of step-pool streams. Models that include only a single step formation process (Lenzi, 2001; Zimmermann et al., 2010; Saletti et al., 2016) have limited use. Moreover, when comparing model results to natural or experimental data, observed variability of the controlling parameters may be wrongly attributed to stochastic influences on step formation (Zimmermann et al., 2010). Instead, it is likely a result of the spatial (and temporal) variability of the underlying processes. Our observations suggest that modelling efforts should combine several step formation mechanisms. Following this proposition, the experimental design of ongoing research on step-pool formation considers multiple step formation domains (Saletti 2017, UBC, pers. commun.).

4.5 Conclusions

We analyzed a set of alluvial channel steps in a natural stream and explored the link of channel geometry and step morphology with regard to the existing knowledge on step formation processes. Our data included not only relevant parameters of the steps – such as step height or wood content – but also precise information on local channel geometry, such as width and downstream width change. Based on the observational evidence, we reject hydraulically based theories for the formation of 103 channel steps of the steep mountain catchment. We found evidence for steps both formed by jamming (sedimentary and wood induced) and sediment accumulation around key-stones and we attributed individual steps in our study reach to one of these two models. With this result we confirm earlier calls (Chin, 1999a; Chin and Wohl, 2005; Curran, 2007) for a broader perspective on step formation in natural streams as step formation is unlikely to be driven by the same mechanistic principle everywhere. We argue that the various step formation theories should not be treated as competing theories. Instead, several step formation mechanisms

are active in the study reach at the same time, but at different locations with characteristic local channel geometries.

In our study, we evaluated not only absolute metrics (e.g. channel width and bed shear stress) describing step occurrence, as used in previous studies. We evaluated also derivatives of these quantities, such as the variability of the channel width or bed shear stress, and demonstrated their importance for step formation. This represents a new approach that could be incorporated into modelling efforts of step formation.

The parallel occurrence of different formation mechanisms has implications for the temporal dynamics of step-pool systems. For example, after exceptional floods that break up the majority of channel steps (Turowski et al., 2009), we can advance new hypotheses on the chronological development of new channel steps. First, steps that form due to jamming are most likely to develop, even during the flood event itself, as this mechanism requires mobile particles and is insensitive to high shear stresses. Once formed, these steps can resist high flow energies. Second, during subsequent intermediate floods, key-stone steps should form, as they require depositional conditions and the accumulation of sediment. Similarly, wood steps induced by channel-hillslope coupling should form over time. To verify these hypotheses, a time-series of channel long-profiles following an exceptional event can be used to analyze step formation and resilience of the different classes of formation processes. Following an exceptional flood, we would expect that the relative number of jammed-state steps compared to key-stone steps decreases over time. In addition, based on our findings, jammed-state steps are expected to be more stable. Here, however, the interaction of adjacent steps may play an additional role (Waters and Curran, 2012). Both the temporal evolution of step-pool channels and the mechanistic effects of series of steps on hydraulics and sediment transport need further investigation using field and laboratory studies.

4.6 Acknowledgments

This study would not have been possible without the valuable help of many people, both in the field and during discussions. We thank Gilles Antoniazza, Roman Gerbero and Kari Steiner for the assistance during the laborious long-profile measurements performed in the Erlenbach. We thank Pat Thee for the thorough post-processing of the geospatial data and Fabian Fleischer for the post-processing of the stereo-images to generate the three-

dimensional model of the Erlenbach. We also thank WSL (Manfred Stähli, head of Mountain hydrology and mass movement) for the support with equipment and infrastructure throughout this study. Finally, we also thank Claire Masteller for the supportive and constructive comments on the manuscript.

5 Article IV: The evolution of step-pool systems after an exceptional flood event

Authors: Antonius Golly [1] , Jens M. Turowski [1] , Alexandre Badoux [2]
Status: Early draft

[1] German Research Centre for Geosciences (GFZ), Section 5.1 - Geomorphology, Telegrafenberg, 14473 Potsdam, Germany
[2] Swiss Federal Research Institute for Forest, Snow and Landscape (WSL), Zürcherstr. 111, 8903 Birmensdorf, Switzerland

Abstract

Previous work has shown that channel steps observed in a natural steep channels form under a range of hydraulic and geometrical conditions, which can be assigned to different physical processes. A given set of channel steps observed in the field can thus be separated into classes of step forming mechanisms based on principal channel and step morphological metrics. Given the plurality of step forms present at one instant of time, the question is raised how such channel step compositions evolve temporally, for example after large floods that destruct and re-organize most steps. Here we present preliminary data on the temporal evolution of alluvial channel steps of a steep stream with regard to previously derived diagnostic parameters of step formation. We find that previous hypotheses on the evolution of channel steps, e.g. the maximization of entropy, cannot be confirmed. Instead, the temporal evolution of channel steps can be best explained with previous observations based on channel-hillslope coupling: in this model steps form after large channel disturbances as a result of channel widening, to be later accompanied by jammed-state steps.

5.1 Introduction

The channel beds of steep mountain streams often feature coarse clasts and logs, and commonly exhibit step-pool morphologies (Montgomery and Buffington, 1997). These roughness elements reflect the complex interaction of flow hydraulics and sediment transport (Lenzi et al., 1999), determine channel stability (Abrahams and Li, 1995) and dissipate the stream's energy (Chin, 2003; Yager et al., 2012b). Steps also represent crucial links in the coupling of channel and adjacent hillslopes, whereat step destruction can induce hillslope failure through de-buttressing and thereby drive sediment supply to the channel (Schuerch et al., 2006; Molnar et al., 2010; Golly et al., 2017a). Beside their important role for the sediment dynamics of steep streams, field observations of step destruction and formation remain scarce. A recent study has shown that step formation mechanisms can be tested with measurable, physically-based parameters (Golly et al., 2017b, under review). A comparison with a field set of 103 depositional channel steps revealed that steps formed under multiple step forming processes are present within a natural study reach of a steep stream. To understand the role of steps for the reach-scale sediment dynamics and the long-term re-organization of steep streams to extreme events, the temporal progression of step formation needs to be investigated. However, the temporal evolution of channel steps remains poorly studied. Previous studies on the temporal evolution of channel steps have hypothesized a self-organized autogenic process of step formation (Chin and Phillips, 2007). Chin and Phillips (2007) postulated that a previously undifferentiated, planar channel bed developed first an irregular step-pool bedform and later a series of steps and pools of consistent size and spacing. In terms of the system's entropy – defined as the Shannon entropy – the channel bed evolution can be expressed as an initial increase in entropy (from planar bed to irregular step pattern) and a later decrease (irregular to structured step pattern). However, this study was based on few field observations of an artificially manipulated (flattened) stream. Step-pool morphology was surveyed at a single point in time, years after the restauration efforts. Further, the processes that drive the evolution of the channel towards a regularly stepped bed have not been described. Thus, it is unclear whether such an increase in entropy should also apply for natural channels, for example for channels with pronounced channel-hillslope coupling. Regularly spaced step patterns as a possible end state of step organization have been rejected based on process considerations and detailed field observations in a steep mountain stream (Golly et al., 2017b, under review). Also, this

concept does not differentiate between step forming mechanisms. A view on step pools and their temporal evolution based on a single process of formation might be limited (Golly et al., 2017b, under review), as the multiplicity of formation mechanisms has impacts on the morphodynamics of step-pool streams.

Here, we present data on the temporal evolution of alluvial channel steps adjusting after an exceptional flood event in 2010 within a 550 m reach of steep mountain stream in Switzerland using bi-annual surveys of the stream. The flood event in 2010 had a recurrence interval of ~20 years and its peak discharge exceeded the critical discharge to move the largest clasts found in the stream bed (Turowski et al., 2013a). Thus, most of the steps might have been mobilized during that flood.

5.2 Methods

All measurements were performed in the Erlenbach (see paragraph 4.2). The long-profiles of the studied reach were collected during 13 total station surveys between 2010 (after the flood event) and 2017 (Table 15) of which 7 were collected in spring and 6 in autumn. These surveys were the only available long-profiles of that stream reach with a high spatial resolution of the thalweg points with an average spacing of about 0.5 m. Surveys prior to 2010 followed a different protocol and yielded an average spacing of 1 m. The coarse resolution of these surveys was excluded since an automated identification of channel steps did not yield comparable data sets.

Most of the surveys prior to 2013 did not include measurement of the channel banks. Where these measurements are missing, the channel banks of the temporally closest bank measurement was used. For the first survey in 2013, this was the bank measurement of September 2013 and for all other surveys without bank measurements, this was the data of July 2012. Although the channel bed does not show signs of lateral migration throughout the entire measuring period, the local channel width can differ considerably between consecutive surveys. Thus, the use of bank data from other surveys likely introduces an error on the channel width estimations at steps, and this error cannot be quantified. The approach affects all calculations using local channel width, most importantly the jamming ratio. However, other step metrics, such as spacing and the step height, are not affected. Channel steps were identified by the automated algorithm by Zimmermann et al. (2008),

resulting in a total number of steps for the individual surveys between 70 (2010a) and 114 (2013b) (Table 15).

	2010b	*2011a*	*2011b*	*2012a*	*2012b*	*2013a*	*2013b*	*2014a*	*2014b*	*2015a*	*2015b*	*2016a*	*2017a*
Date	3 Sep	22 June	18 Nov	20 July	29 Oct	4 June	11 Sep	9 Apr	15 Nov	13 May	1 Oct	20 May	3 June
Thalweg survey	•	•	•	•	•	•	•	•	•	•	•	•	•
Channel bank survey	-[1)]	-	-	•	-	-	•	•	•	•	•	•	•
Number of thalweg points	889	903	773	975	919	800	934	801	929	951	1191	1030	1035
Number of steps	70	98	94	99	86	92	114	90	90	103	96	100	97
Peak discharge before survey [m³/s]	**10.6**	1.7	3.1	0.8	1.4	2.3	1.9	1.5	4.8	2	1.1	0.9	1.6

Table 15: Total station surveys performed in a 550 m long reach of the Erlenbach as used for this study. Previous studies have not been included as thalweg surveys followed a different protocol with a resulting courser spatial resolution. [1)] When channel bank surveys were not available, the banks of the temporally closest surveys have been taken. This introduces an error in the calculated channel width at the steps.

Steps have been separated into classes regarding their assumed mechanism of formation. Golly et al. (2017b, under review, chapter 4 of this thesis), showed based on the examination of diagnostic parameters and a comparison to field data that several classes of steps exists within a natural channel at a given time. These classes are determined by their mechanism of formation, while jammed-state steps and key-stone steps prevailed. It has also be shown, that the jamming ratio – ratio of channel width at the step and diameter of the step forming grain – is suitable for discriminating step classes and a critical jamming ratio of five serves as a threshold to separate these classes into jammed-state steps and key-stone steps. Hence, in this study the jamming ratio is used to classify the most dominant step formation mechanisms. The step forming grain has been approximated with the steps height multiplied by 1.2 (Chin, 1999b).

The Shannon entropy was derived for multiple categories of channel reach features such as pools, steps and runs (remainder of the channel bed) following the considerations of Chin & Phillips (2007):

$$H = -\sum p_i \ln p_i \quad (1)$$

where H is the Shannon entropy and p_i is the proportion of the total in each category *i*. That means, for the three categories steps, pools and runs:

$$H = -Rel_{step} * \ln Rel_{step} - Rel_{pools} * \ln Rel_{pools} - Rel_{runs} * \ln Rel_{runs} \quad (2)$$

where Rel_x is the relative length of that category with regard to the total channel length.

The water discharge was measured with a calibrated water gauge at the retention base at the catchment's outlet (Fig. 7).

5.3 Results

The flood before the first survey had a peak discharge of 10.9 m3/s (Fig. 48), which was caused by precipitation event totaling 56.6 mm of rain. The recurrence interval of this flood event was estimated at ~20 years and the peak discharge lies above the characteristic discharge competent to transport grains larger than the average step-forming grains (Nitsche et al., 2011; Yager et al., 2012b; Turowski et al., 2013a). The flood history with peak discharges is shown in Fig. 49.

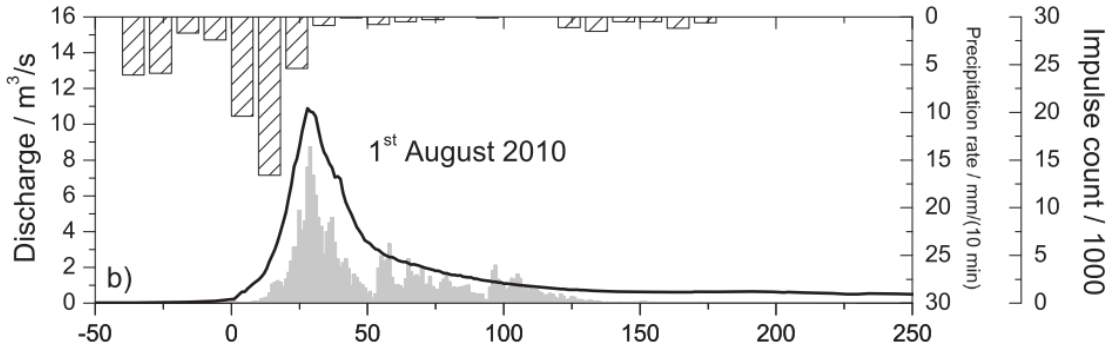

Fig. 48: Hydrograph, precipitation and impulse counts caused by sediment transport of the exceptional flood on 1st of August 2010 (from Turowski et al., 2013c).

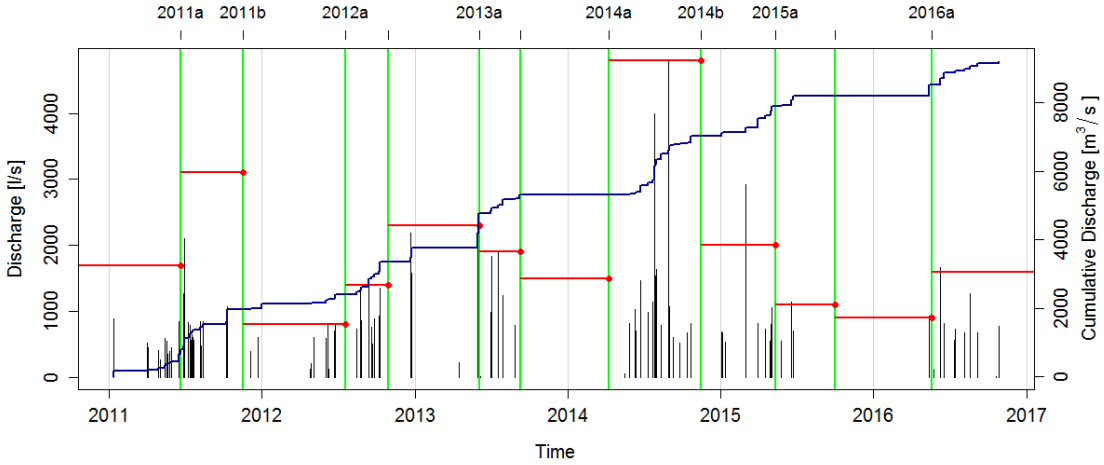

Fig. 49: History of floods (black bars) between the surveys (green lines). The red bars indicate the maximum peak discharge prior to the surveys. The blue line indicates the cumulative discharge over the measuring period. The red lines are based on 1-min discharge data while the black bars and the blue line is based on 10-min discharge data. Due to this difference in the source there is a mismatch.

The number of steps is with 70 identified steps lowest during the first survey (2010b) after the exceptional flood event (Fig. 50). In consecutive surveys this number averages at 97 steps for each survey but no significant upwards or downwards trend in the long-term mean is obvious throughout the measuring period (Fig. 50). However, a seasonal pattern seems to occur as the number of steps is more often higher in the spring survey than in the autumn survey.

There is no clear trend in the distribution of the spacing of steps, either (Fig. 50, Fig. 51), although the spring/autumn seasonality seems to appear also in this metric. The highest median step spacing was observed in the survey immediately after the exceptional flood in 2010. The histograms of the step spacings can be found in Appendix G.

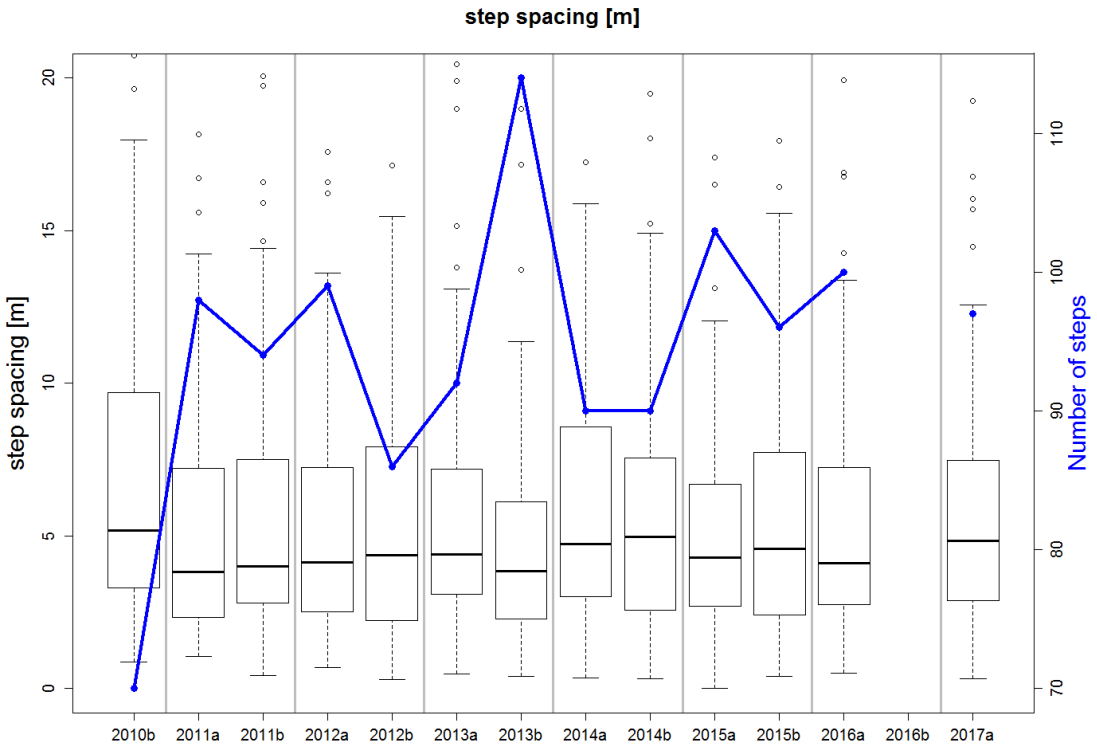

Fig. 50: Number of steps (blue curve) and the distributions of step spacing (boxplots). No survey was taken in the autumn of 2016 (2016b).

The Shannon entropy was calculated for all 13 surveys (Fig. 52), and in addition to the resulting H, also the individual length of the categories pool length, step length and runs (rest of the channel bed) as a fraction to the total channel length is presented. An increase of the entropy after the first survey past the exceptional event can be observed (Fig. 52), which suggests that the entropy has significantly decreased immediately after the event. This is opposite to what would be expected after Chin & Phillips (2007). The Shannon entropy seems to be more sensitive to changes in relative pool length, because the relative run length is quite constant throughout the measuring period.

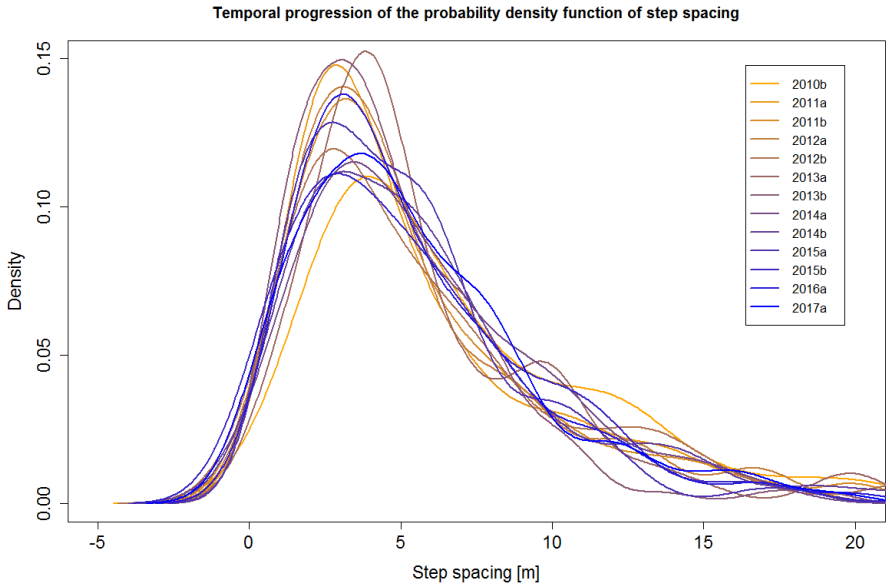

Fig. 51: Temporal progression of the probability density functions of step spacing. Histograms can be found in Appendix G.

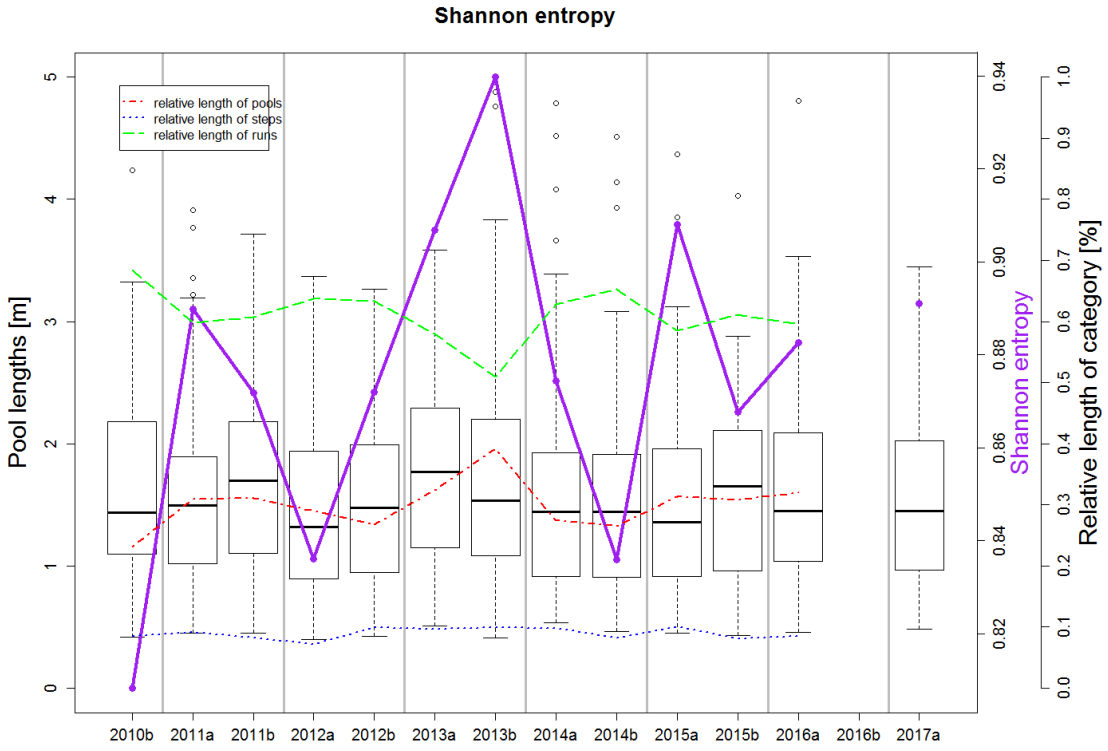

Fig. 52: The Shannon entropy (purple line) for the 13 surveys. The dashed lines give the fractions of the individual categories (pool, step and runs) compared to the total channel length.

The median jamming ratio of the identified steps are above the critical value of 5 for all surveys before autumn 2013 (Fig. 53). After that point they are always below that critical value except for the survey of spring 2016. A separation of steps into classes of the assumed mechanism of formation has been performed based on the jamming ratio (see article III). The fraction of steps attributed to jamming is low (41%) in the beginning of the measuring period (Fig. 53, red line) and is decreasing in the following 1.5 years, before increasing. It reaches 50% first in the survey of autumn 2013 and peaks with 60% the following year (spring 2014). This indicates that jamming steps are less common immediately after exceptional events and develop only after a delay time.

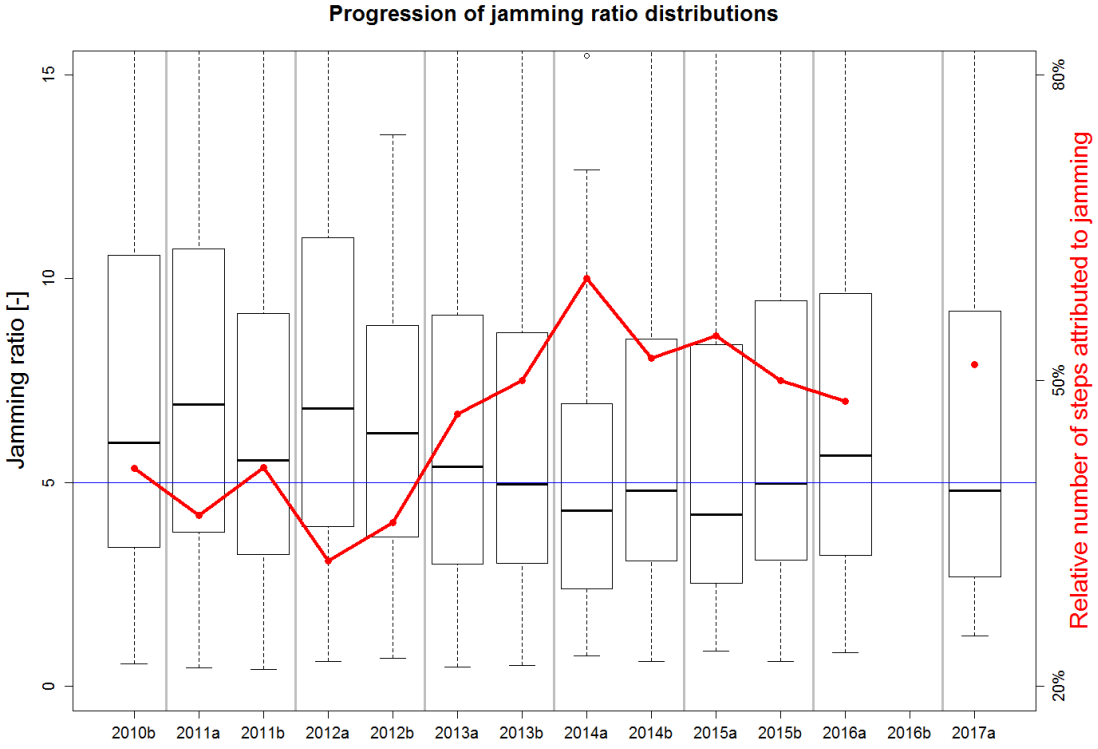

Fig. 53: Evolution of jamming ratio distributions of the identified steps of the 13 surveys.

To further investigate the reason for the evolution of the jamming ratios, next the channel width (Fig. 54) and step height (Fig. 55) are explored. The average channel width is highest for the 2012 survey of the channel banks (Fig. 54). Note, that the channel bank survey of spring 2012 was taken as a reference also for four other surveys. Hence, the evolution of the width should not be interpreted as being elevated for several years. However, the higher width for 2012 in comparison to later years are a clear result.

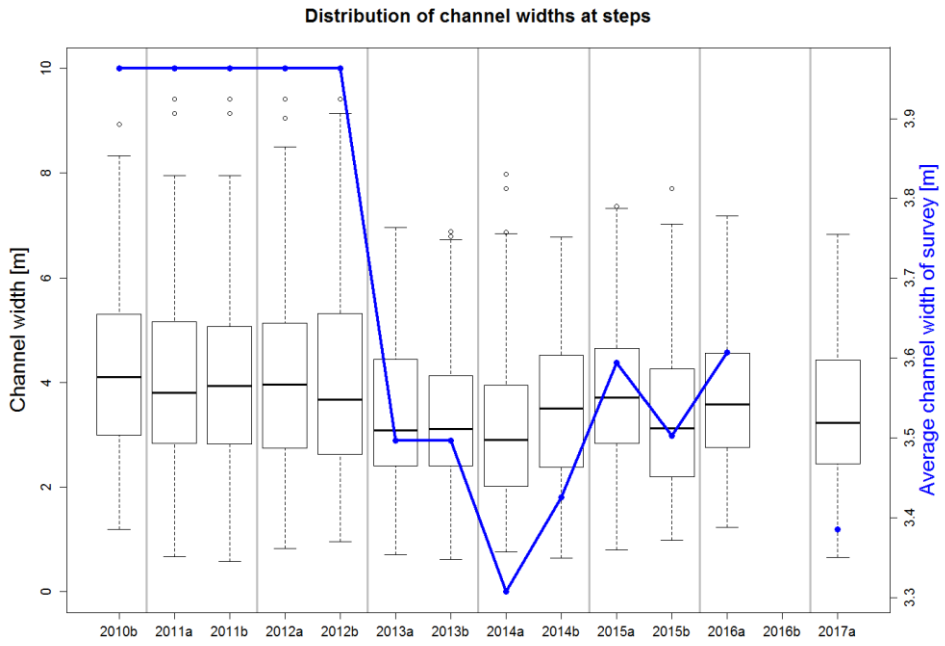

Fig. 54: Distributions of channel widths at steps over the 13 surveys. Note the difference in the axes. Left and right axis are both in meters but range is different. The left axis is valid for the boxplots while the right axis is valid for the blue line.

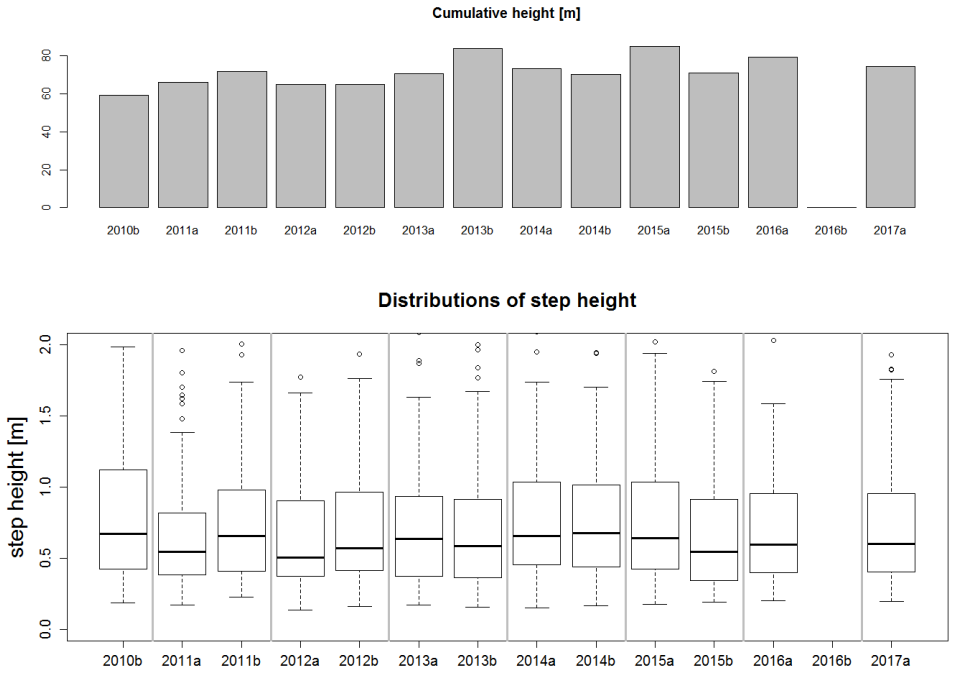

Fig. 55: Cumulative step heights for the 13 surveys (gray bars upper panel) and distribution (boxplots lower panel).

Similar to the reach-averaged channel width, the mean channel width at steps was higher in 2012 than in the later years (boxplots of Fig. 54). The highest median of the channel width at steps was reached in the spring of 2012, the first survey after the exceptional event in August 2010.

The distribution of step heights show the second highest median in the first survey in autumn 2010 (Fig. 55) with a cumulative step height of 59 m. Although, this is the smallest cumulative step height (which averages at 67 m during the following surveys), it is relatively high considering the low number of steps during that survey (70 steps compared to the mean number of steps of 97 found in the years 2011 to 2017).

5.4 Discussion

Based on the results of the 13 field surveys of long profile and channel banks it seems unlikely that the Erlenbach shows an autogenic self-organization towards flow resistance maximization as has previously been suggested (Chin & Phillips 2007). Neither the evolution of step spacings (Fig. 50, Fig. 51), nor of the Shannon entropy (Fig. 52) shows a clear trend in the temporal evolution. The step spacing is lowest immediately after the exceptional flood in 2010, but this is a direct result of the small number of steps, as these metrics are directly related. In the case of a self-organization of the stream bed towards flow resistance optimization, the interquartile range of the distributions of step spacing should constantly decrease. This seems not to be the case (Fig. 50, Fig. 51). The evolution of the Shannon entropy of unstructured channel beds according to Chin & Phillips (2007) should first increase to then later decrease as a result of homogenization of inter-step distance and step height. Although the Shannon entropy prior to the exceptional event in 2010 is not known, the entropy value of the 2010b survey is very low compared to the average mean of the following surveys (Fig. 52). Thus, the results present an evolution of the Shannon entropy opposite to the expectation of Chin & Phillips (2007).

Based on the jamming ratio a classification of steps regarding their mechanism of formation has been applied (Fig. 53). A previous study has shown that the jamming ratio serves as a valid discriminator of different step formation processes, separating steps formed by jamming from those formed around key-stones (Golly et al., 2017b). It was hypothesized that step formation after the destruction of most of the channel steps might occur first due to jamming and later, during consecutive flood events, due to the deposition

of key stones. The temporal evolution of the fraction of steps formed by jamming, however, shows an opposite trend (Fig. 53). It seems that key-stone steps dominate the overall number of steps in the aftermath of large exceptional floods. Only after a relaxation time of 1.5 years this trend is reversed and steps attributed to jamming processes show growing importance. Three years after the exceptional event the ratio is balanced (50% jamming steps and 50% key-stone steps) with a continuing increase of steps formed by jamming.

The effect of the exceptional flood event in 2010 on reach-averaged channel width (Fig. 54, blue line) and channel width at steps (Fig. 54, boxplots) allows for an interpretation of the cause of the growing importance of steps formed by jamming. It has been demonstrated that wide-spread step destruction, which has likely occurred in the large flood, has a strong impact on the channel hillslope coupling (Golly et al., 2017, chapter 2 of this thesis). Furthermore, the observed feedback cycle of channel-hillslope coupling led to a significant increase in the local channel width (paragraph 2.3). Key-stone steps form dominantly in wide channel sections, where depositional conditions prevail. It seems likely that keystone steps formed in or after the 2010 flood in locations where the channel widened due to step erosion and the activation of channel hillslope coupling. This agrees with the findings, that key-stone steps dominate during the early surveys following the exceptional event (Fig. 54). Channel width at these locations seem to stay elevated for some time as the newly built step (formed due to the key-stone process) buttresses the hillslope and stabilizes it again, as previously observed. This interpretation of the evolution of step-pool systems after large floods agrees with the observation of elevated step heights (Fig. 55), which are reportedly amplified due to the channel-hillslope coupling feedback cycle (2.3).

5.5 Conclusion

We presented preliminary analyses on a seven year data set of long profiles of a natural steep stream. The time series followed a year that had an exceptional flood event that eroded most of the channel steps. On these long profiles steps have been identified and a number of step metrics have been compiled. Previously suggested concepts of the response of channels to bed disturbances have been tested. The result suggest neither a consistent progression of the channel towards a homogeneous step spacing, nor the increase of the Shannon entropy after the exceptional flood. Furthermore, classes of step regarding their mechanism of formation have been identified based on the critical

jamming ratio. It has been shown, that the relative number of jamming steps are significantly lower than the long term average. After a relaxation phase of 1.5 years, key-stone steps become increasingly important. This result refutes previous speculations on the temporal evolution of dominant formation mechanisms following a large flood. The pronunciation of key-stone steps in the aftermath of the exceptional floods is related to a generally wider channel bed. This might related to channel-hillslope coupling feedbacks which are expected to occur after large exceptional floods.

6 General conclusion

At the beginning of this project the vast majority of research on the Erlenbach was focused on the last 50 m of the channel upstream of the retention basin. Most research was concerned with the amount of sediment transported out of the catchment and its local effects. Studies about processes within the catchment were limited to a few studies (Schuerch et al., 2006; Yager et al., 2012a; Jochner et al., 2015). In this thesis a broad approach has been chosen to gain insights into the complex system of steep mountain rivers. The effort includes in situ field observations (article I), the development of quantitative scientific tools (article II), the reach-scale analyses of step-pool morphology (article III) and its temporal evolution (article IV). With this work our view on the processes within the catchment has been advanced. It follows a discussion on research questions regarding the individual articles (1.2.1 to 1.2.3), as well as how the articles support the general objectives raised in this thesis (paragraph 1.2.4).

6.1 Channel-hillslope coupling

In the first article on the controls and feedbacks of channel-hillslope coupling (section 2) an important process of sediment generation in the Erlenbach has been identified addressing the research questions Q 1 to Q 3, which are repeated as a quick reminder.

> Q 1: Which processes are responsible for activating the sediment sources and mobilizing sediment?

Sediment is mobilized from the hillslopes adjacent to the channel, which are compromised by processes occurring in the channel. The main control on hillslope stability and sediment input rate was not the slope-internal hydrologic regime – e.g. controlled by rainfall or snow cover – but the local base-level of the channel. The vertical incision of the stream bed, in the form of the erosion of an alluvial channel step, led to debuttressing of the hillslope and triggered sediment mobilization. The direction of the coupling of channel and hillslope was bi-directional. First, in an upsystem link the channel compromised hillslope stability. Second, the hillslope responded with sustained sediment input (Fig. 18).

> Q 2: Are the processes of sediment generation threshold processes or continuous?

The process of sediment release into the channel was spatially and temporally discrete. The spatial extent of the failing hillslope correlated with the length over which debuttressing occurred. Furthermore, once initiated the progression of the mass wasting (hillslope collapse) was independent of the trigger (bed lowering). This re-defines the role of the hillslopes as sediment sources, which previously have been considered to exhibit creeping behavior controlled by hillslope-internal hydrology (Schuerch et al., 2006).

Q 3: If they are threshold processes, what floods are required to trigger them?

The flood that triggered the channel-hillslope coupling process had a recurrence interval of ~5 years, demonstrating, that for this process small and intermediate flood events are relevant in contrast to rare, exceptional events. This makes the observed mechanism a frequent and important process that needs to be understood and captured in the conceptualization of steep mountain streams, e.g. for the modelling of sediment dynamics.

6.2 Methods and tools for analyses of high-resolution geometry

The development and test of a framework to assess the high-resolution field data from the Erlenbach was a substantial and inevitable part of this dissertation (section 3). The research question emerging from the first study demanded new solutions to run statistical analyses on the step geometry. The simple question of the distance of two steps in the channel bed cannot be straightforwardly answered without a precise definition of the reference for the distance along the channel bed, since the Euclidean distance between two step crests can deviate from their straight distance, when considering channel meandering or the lateral position in the channel bed. Apart from this simple example a precise calculation of local slope, channel width or their derivatives was inaccessible with existing tools. Hence, the following research questions arose.

Q 4: Can we develop a scientific standard by defining principal channel metrics in an objective and reproducible manner?

A definition of principle channel metrics has been proposed. This definition includes first, the calculation of a channel reference, and, second, the variability of channel metrics (e.g. channel width via transects) along that reference. Several user-defined parameters in these concepts allow for the applicability and adaptability of the method also to complex

channel topographies with high small-scale variability. The definitions advance currently existing tools, which are often based on static or arbitrary concepts.

> Q 5: Can we resolve the local channel width and slope as well as their local change in downstream direction with the necessary detail required for scientific research?

Algorithms have been developed to derive the objective reference line of a channel – the channel centerline – based on the channel banks. This reference allows for further calculations of channel metrics (local width, local slope and their derivatives) and secondary features (measured long-profile, thalweg, knickpoints, etc.). The results have been quantitatively tested against manual measurements and the results from other channel metric tools, showing the closest match to the manual measurements for the newly developed approach.

> Q 6: Can we provide a structured framework for the analyses of channel geometry and secondary geomorphological features?

A standalone tool, developed as an R package with the name *cmgo* was developed. The framework can integrate multiple, repeated surveys (time series of geometrical data), as well as analyze secondary features that are separately collected (in our case that were data of depositional channel step properties). The feature catalog of *cmgo* has been critically compared to numerous existing tools, while *cmgo* showed the widest functional range (Table 5). The tool has also been published under a free copyright license to make it available for the community of fluvial geomorphology.

6.3 Step-pool systems

Facilitated by the development of the technical basis capable to handle and process high-resolution geometry of a natural steep stream, the morphometry of a set of natural depositional channel steps has been investigated (section 4).

> Q 7: What are the characteristic morphological step metrics (step parameters) that are indicative for the various step forming theories?

In this study, step formation mechanisms have been evaluated by performing various test of physically based parameters to the observations of natural channel steps. The tested

parameters include both parameters that have been previously suggested and examined, as for example the step height to channel width ratio (jamming ratio), and innovative ones. For example, the downstream change of the channel width upstream of a step has been proven to be a valid discriminator of step classes. The parameters indicative for step formation mechanism are jamming ratio, channel width change, planform curvature, the change of bed shear stress along the channel upstream of a step, and presence of wood in a step.

Q 8: How do those theorized parameters compare with a set of natural channel steps observed in the field?

The assessment demonstrated that any single parameter was insufficient to characterize the entire population of channel steps. Instead, in a natural setup of steps multiple parameters are required to classify step groups. Good explanation can only be accomplished if a multivariate approach is chosen, which explains why previous attempts to harmonize theory and observation failed. The physical nature of the parameters allow to draw a conclusion from the parameters to a mechanistic explanation of step formation in our study reach.

Q 9: Of the models of step formation suggested in the literature, which one or which ones apply in natural stream?

The field observations have shown, that a single formation process for all steps is unlikely. In a natural environment, steps form through different mechanisms and for a range of hydraulic and geometric conditions. These mechanism include ‘jamming’ processes in narrow and narrowing sections and depositional ‘key-stone’ steps in wide and widening channel sections (Fig. 47).

In addition to the baseline study on step-pool systems the temporal evolution of steps in the aftermath of an exceptional flood have been investigated. The research question as answered by article IV were answered as follows.

Q 10: How do patterns of channel steps evolve after exceptional floods that mobilize most of the channel steps?

The temporal analyses of step patterns showed that the number of steps significantly decreased as an immediate effect of a large flood (Fig. 50), and, consequently, the step spacing was increased during the first year after the flood (Fig. 51). However, the cumulative height was only slightly affected, indicating that the remaining steps were individually higher (Fig. 55). Furthermore, in the year after the large flood most steps formed at a higher channel width and had generally a low jamming ratio (Fig. 53). Although, the number of steps and the step spacing show seasonality (more steps in spring than autumn) a drifting trend is not observable past three years after the large flood.

Q 11: Do entropy concepts previously suggested prevail in natural steep streams?

Two concepts have been tested with the preliminary tests: the concept of a development of a regular step spacing and the concept of a peaking Shannon entropy (first increase then decrease) following large flood events. Both concepts were rejected based on the data. The distribution of spacings did not converge to a constant, and the Shannon entropy showed a behavior opposite to the previously suggested concept (Fig. 52).

Q 12: What step forming mechanisms dominate in which phase of the recovery after exceptional floods?

Directly after the exceptional flood the fraction of channel steps formed by jamming are reduced compared to the steps formed by key-stones (Fig. 53). This proves a previous hypothesis of pronounced jamming steps after large flood events wrong. A reason for the delayed development of key-stone steps might be the fact that the of jamming steps require sediment transport and a larger number of sediment transport event increases the probability of jamming.

6.4 Sediment dynamics

The findings from the observed feedback cycle in the coupling of channel and hillslopes (article I) can be used to discuss the initially outlined uncertainties in the prediction of sediment sourcing and transport.

Q 13: What are the implications of the characteristics of channel-hillslope coupling processes on the sediment dynamics?

The characteristics of the mass wasting mechanism identified in the first article (section 2) shapes our understanding of the sediment dynamics on the reach scale. Multiple mass wasting processes have been identified acting on different spatial and temporal scales (Fig. 56). A cavity failure as a spontaneous and singular event was observed immediately after the step destruction occurring within minutes (see also Fig. 58B). Concentrated mudflow on the hillslope surface was observed also only after the step destruction, lasting throughout the response period of the hillslope. Finally, the deep seated movement of the collapsing hillslope delivered the highest amount of sediment to channel. After initiation, this process was never disrupted.

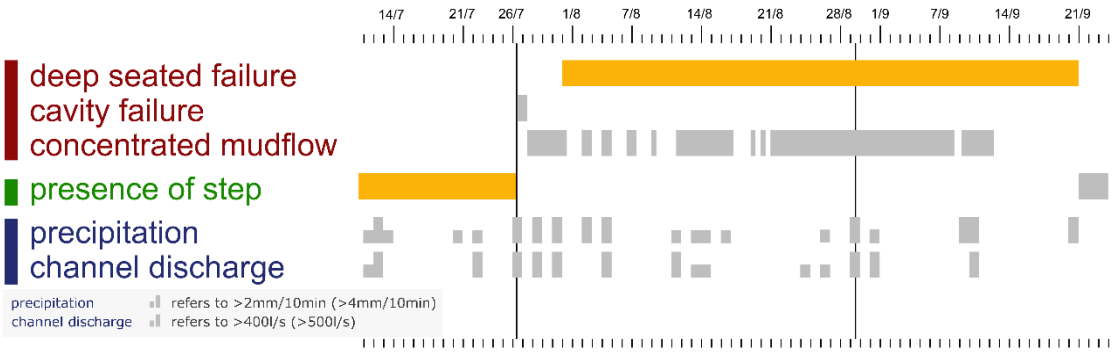

Fig. 56: Gantt chart of the different mass wasting processes (group of red items) in comparison to the step presence (green item) and classified precipitation and discharge events (blue items). All mass wasting processes occur only after step destruction, and are thus threshold processes. None of the processes show a direct correlation with the hydrologic regime.

The threshold nature of the process shows that the sediment input from the hillslope does not scale with the magnitude of floods. Hence, hillslope sediment supply should not be modelled as a linear function of water discharge. A flood might be competent to break up depositional steps in a reach, but it might also depend on the individual stability of the step and on its location with respect to landslide-prone banks whether or not such a feedback cycle is induced. This highlights the importance for sediment dynamics of fundamental research on step morphology and formation to assess and predict step stability (article III).

The findings can also be used to discuss the relative timing of sediment transport rates of the dominant mass wasting process (hillslope collapse) and water discharge. Between the trigger of the coupling process – the step failure – and the hillslope failure, there was

considerate delay period of 40 hours. Thus, peaks of sediment transport rates cannot necessarily be expected during the triggering event, but rather during flood events successive to the triggering event. However, considering the lag time until hillslope response started (3 days) and the time it lasted (40 days) there is a minimum time when sediment provided through this process is available. Successive floods that occur within the lag or response period will not gain sediment from the channel-hillslope coupling process.

The spatial scale of the observations shed light on the sediment composition found in the stream, e.g. the grain size distribution of the material released to the channel can be comprehended. Due to the spatial scale of the failure (hillslope scale) fractions of grains up to meters could potentially be mobilized if present in the hillslope substrate. This allows for the entrainment from the sediment sources of much larger grains than for example possible through washout – e.g. driven by surface runoff – and helps to explain the bed composition which is coarse in comparison to the grain size distribution of the hillslope surfaces.

The documented process emphasizes the role of hillslopes in the catchment as relevant components for reach-scale sediment dynamics. Thus, the characteristics of hillslopes and the processes of their coupling with the fluvial system should be incorporated into models of landscape evolution.

From this research, new questions emerged. The notion that steps are important links in the coupling of sediment sources and transport zones attracted interest in the evolution of channel steps, their formation and stability. Such an assessment must be based on detailed analyses of step occurrences in a natural environment. However, the technical basis to perform these analyses was not yet established. Considering the high variability of the topography of steep streams (1.2.2) a framework to manage, process and evaluate the high-resolution field data from different sources was required. This call was satisfied with the second study of this thesis (section 3).

6.5 Technical tools in geomorphology

In this doctoral project a substantial amount of time and resources were invested into the development of a technical framework for the generation and analyses of geometrical data from the studied channel. This raises the following question.

> Q 14: Does the development of technical tools advance the way we design studies of the morphometry in steep mountain streams?

The motivation for developing methods and tools for the data analyses originated from the lack of existing tools. A deep and thorough investigation on how previous studies were set up and performed revealed two facts. First, existing tools were not capable to perform the data processing of the high-resolution geometry data of the Erlenbach. For example, the channel centerline generation was not accurate with existing tools due to a lack of parametrization and or the way, the centerline was derived. Second, the local channel metrics that govern the prediction of channel step formation were not established metrics, but were innovative and their calculation was facilitated only by the development of the framework. For example, the local change of the channel width was shown to be an important discriminator of step formation mechanisms. We argue that the high variability of the channel banks of the Erlenbach can be found in most steep streams and hence, that the development and publication of a highly parametrizable tool was a valuable achievement of this dissertation. Possible applications of the tool are discussed in the outlook section (paragraph 6.8).

6.6 Channel width variations

The findings suggest that the variations in channel width represent a link between the channel-hillslope coupling observations and the step forming mechanisms, raising the following question.

> Q 15: How do temporal and spatial variations of the channel width fit in the context of channel-hillslope coupling mechanisms and the evolution of step-pool systems?

The spatial variations of the local channel width has been shown to play a crucial role in the formation of channel steps (article III). Where the channel is wide (and widening in downstream direction) depositional conditions prevail, forcing key-stones to deposit and

the formation of steps around them. However, the local channel width, in turn, is affected by channel-hillslope coupling processes that are induced by step failure (article I). It has been documented (see paragraph 2.3) that the channel width doubled after the hillslope failure. Hillslope stability could only be re-established through the formation of a new step, which buttressed the unbalanced hillslope. This observation is in agreement with the identified step classes from article III, where lateral input of material produces steps in narrows sections. However, combining the findings of the step formation mechanisms with observations of the feedback mechanism, other end member states for a given channel section with a channel step and a hillslope are conceivable: after step destruction, hillslope destabilization and channel widening, the conditions for depositing key-stones are met. If sediment is trapped by this key-stone during following floods fast enough before the channel narrows due to the hillslope collapse, a key-stone induced step would form. Such a step would arguably stabilize the hillslope preventing further narrowing due its collapse. Hence, the terminal stage for channel-hillslope coupling would be constituted by a completely different mechanism. Furthermore, although in both end states a step would form, it forms by a different mechanism.

6.7 Long-term evolution of channel steps

In the fourth article (section 5) the observation was presented that channel steps are reduced in number after the occurrence of exceptional flood events able to destruct most of the channel steps. The remaining channel steps seem to be formed rather due to key-stones then due to jamming. This single observation could not be interpreted without precise system and process knowledge of the morphodynamics of a steep stream. The question was raised:

> Q 16: How can the temporal progression of different step types be explained by the previous findings of this work?

In combination with the first article on the channel-hillslope coupling an explanation of the evolution of steps with regard to the formation mechanism can be attempted. Field observations have been presented showing that the channel width is increased by the factor two after the destruction of an alluvial channel step (paragraph 2.3). Such feedback cycles are likely to be induced in many locations of the stream during and immediately after an exceptional flood event. The widened channel sections might then invite key-

stones to deposit which form due to the local flow hydraulic conditions (depositional conditions). The formed steps might then be capable of stabilizing the hillslope through debuttressing and prevents the hillslope at an early state to further narrow the channel bed. This emphasizes a second end-state of the channel-hillslope coupling feedback, in which the hillslope is also stabilized by a step, but this step has formed due to a key-stone. This explanation agrees with the increased channel step height following the exceptional flood (Fig. 55), because step height is reported to be amplified through the channel-hillslope coupling process. During consecutive floods sediment is routed through the stream increasing the probability of jamming and to form jamming steps. A balanced ratio of key-stone and jamming steps are observed after a relaxation phase of three years after the exceptional flood event.

6.8 Outlook

The observations and results obtained through this thesis have also highlighted the need for further research on several key aspects which are presented below.

6.8.1 Step stability

It has been shown, that floods of a relatively small magnitude with a recurrence interval of 5 years are competent to break up steps to initiate a feedback cycle in channel-hillslope coupling (article I). The investigation and documentation of the feedback cycle was based on an observation of a hillslope and a channel section with time lapse cameras. The selection of this particular hillslope was arbitrary as the event was unprecedented and not expected. At the time of the flood and feedback mechanism taking place no further hillslopes were monitored within the catchment. This leaves two questions open. First, it is unclear how many of the steps in the Erlenbach stream have been eroded during the flood. Generally spoken, the question is whether all floods with a recurrence interval of 5 years are able to break channel steps, or if a certain channel step type is more prone to collapse. It has been hypothesized that jammed steps are more stable than key-stone steps (see also paragraph 4.5), but direct field observations of the destruction of channel steps are required to confirm this hypothesis. Second, it is questionable whether all step destructions cause hillslope destabilization. Although, it has been estimated that this feedback mechanism could be relevant for the reach scale sediment supply (paragraph 2.4) such a generality would require systematic examination with further field observations.

6.8.2 Relevant spatial scales for step formation

Innovative measures have been introduced to integrate field observations of step occurrences with pre-existing and newly developed ideas of step formation mechanisms (paragraph 4.1.2). The measures – e.g. the downstream change of channel width or the change of the local bed shear stress – require a spatial length scale over which they are derived (paragraph 4.2). The relevant scale for example for the local flow hydraulics is unclear and an a-priori choice of this length scale must always be critically viewed. In the lack of physical constraints on that scale, a length of twice the channel width has been arbitrarily used. The relevant scale could also depend on the particular process of step formation. For example, the length scale to calculate width channel changes for steps that form under key-stone conditions might differ (e.g. long distance to develop depositional conditions) compared to jammed-state steps (e.g. small variations of the channel width matter). However, a physically-based evidence for this length scale should be derived using field measurements or lab experiments to confirm and investigate the right scale.

7 Acknowledgments

First of all I would like to thank all my colleagues of section 5.1. – Geomorphology and adjacent groups at the GFZ. These were over the last four years a lot of different people, all of which were inspiring and an essential to my education and development: Christoff Andermann, Camilla Francesca Brunello, Aaron Bufe, Arnaud Burtin, James Collins, Kristen Cook, Mitch D'Arcy, Michael Dietze, Robert Emberson, Theresa Grunwald, Niels Hovius, Luc Illien, Almuth Janisch, Christoph Kappler, Sophie Lagarde, David Maas, Odin Marc, Claire Masteller, Johanna Menges, Oliver Rach, Marisa Repasch-Elder, Sam, Joel Scheingross, Dirk Sachse, Taylor Schildgen, Anne Schöpa, Steffi Tofelde, Jens Turowski and Iris van der Veen. You guys developed a good working environment in the young and growing group making it fun and productive to work in. Big thanks also to the GFZ tech staff Alexander Lachmann (representative for workshop) and the HR staff Nicole Kernchen (representative for HR), for pulling all the strings in the background to produce our special field gear and to enable our last-minute field trips. Thanks also to Stefan Lüdtke and Michael Dietze for constant support on R. Although I won't use ggplot2 ever in my life again, I appreciate your teaching :). I also thank the two interns I supervised during my PhD time Clemens Schmitt and Fabian Fleischer for the valuable work they did for us. For

the creation of the nice landscape sketches I thank Tom Baumeister. For the use of figures in this thesis I thank Dieter Rickenmann and Jens Turowski.

An extensive part of this doctoral project took place in Switzerland and I received a lot of support from many people of the WSL. I thank Manfred Stähli for equipment and infrastructure from his group and Alexandre Badoux for four years of mentoring and help on the articles. I am also very thankful for the expertise the colleagues at WSL shared with me: Johannes Schneider for the help on the RFID antennas, Pat Thee for the preparation of the data of the total station surveys, Luzi Bernhard for providing the climate data, and Bruno Fritschi and Stefan Boss for technical support in the Erlenbach. I also thank the many field assistants for their time and support on the laborious total station surveys: most of all I thank Kari Steiner, who was with me for most of the surveys. Without him and his excellent chainsaw the Erlenbach would still be undiscovered. I will keep these adventures in great memory. Further, I thank for field support Norina Andres, Gilles Antoniazza, Alexander Beer, Martin Böckli, Simon Etter, Roman Gerbero, Florian Heimann, Christoph Heim, Daniel von Rickenbach, Matthias Speich, and Anil “godfather of soil mechanics” Yildiz, as well as all their supervisors for letting them…

I also thank my colleagues from other institutions, who in many ways helped to support this project with man power, ideas or motivation: Matteo Saletti (ETH), Peter Molnar (ETH), Elowyn Yager (UI), Manual Antonetti (WSL), Fabian Walter (ETH) and Eric Larose (ISTerre).

Finally I like to express my greatest gratitude to the person who was most responsible for the success of this project and the quality my education: my PhD supervisor Jens Turowski. I was lucky to establish a work and private relation with one of the most genuine and honest persons I have met and it was a pleasure to graduate and progress under him. He took not only numerous chances to actively improve and critically review his supervising skills, but also invested a significant part of his time personal discussions and written reviews almost on a daily basis. I am very thankful for his thorough support and his incredible engagement for his students and science in general. I’ll end with his favorite emoji, which is now also mine.

:o)

Appendix

The appendices include all supplementary material from the articles I to III (A. to C.) as well as supplementary information for the general conclusion (D).

A. Sample of the three-dimensional model

A demonstration of the final model created from the Erlenbach stream can be found online. The video is hosted on YouTube and gives an impression on resolution and extent.

https://www.youtube.com/watch?v=w_N_Yaf2rCA

Fig. 57: Online video of the three-dimensional model of the Erlenbach.

B. Landslide Movie (article I)

The movie shows the time lapse images which have been the principal observations the first manuscript was based on. It is available under:

http://www.geosociety.org/datarepository/2017/2017090_Movie_DR1.mp4

Please, note: the movie was originally submitted to the journal Geology as Appendix S1. Providing the video separately on a public platform would be a copyright infringement after the journal's legal terms. Thus, we link to their repository here.

C. High resolution time lapse images of hillslope (article I)

These versions of key phases of the monitored hillslope have been originally submitted as Appendix S2 to the journal Geology and are available under:

http://www.geosociety.org/datarepository/2017/2017090.pdf


2014-07-12 6pm
A
Step before flood
Initial patch outline


2014-07-26 4:30pm
B
Bank failure during flood


2014-08-01 6pm
C
Channel widening

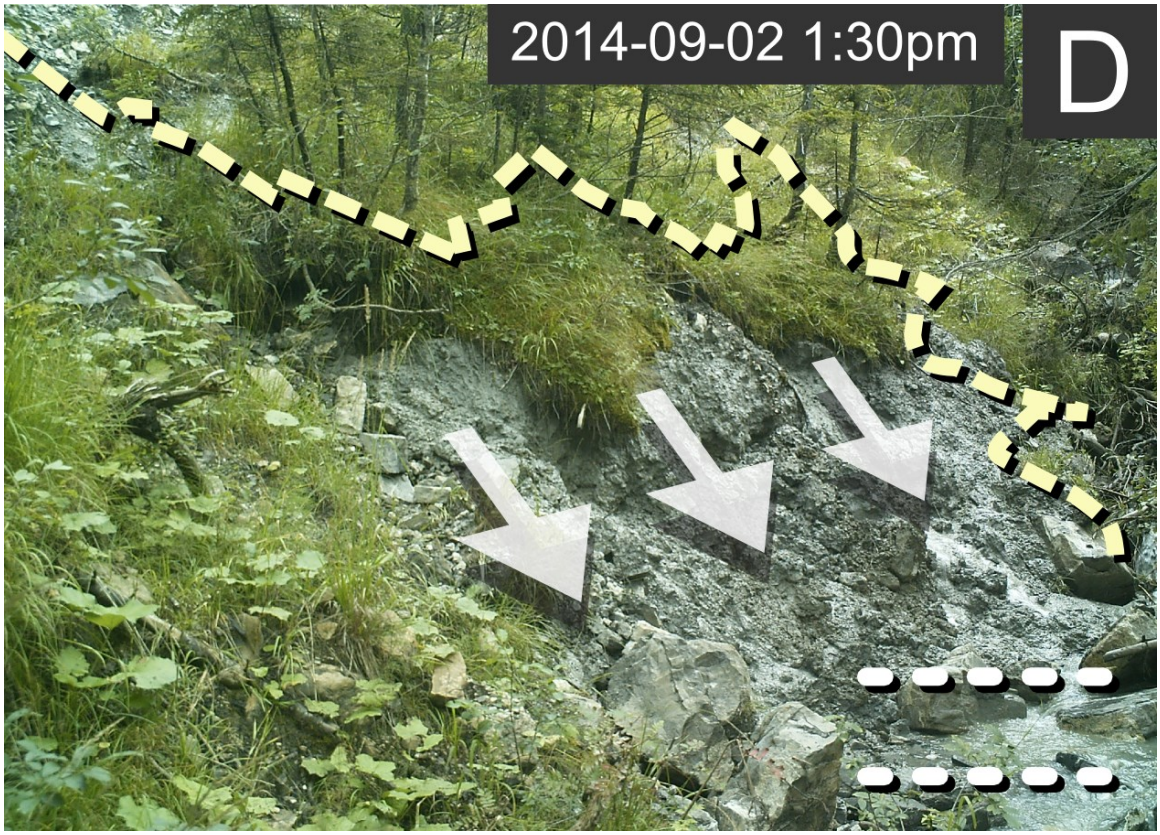
2014-09-02 1:30pm
D

Fig. 58: High resolution versions of the images of Fig. 17.

D. Parameters (article II)

The following list contains the entirety of parameters that can be adjusted in *cmgo* in the version as submitted to ESURF for the article II. Please note, that this list might have been updated meanwhile. The most recent version can always be found on the GitHub page:

https://github.com/AntoniusGolly/cmgo

```
par.default = list(

    # name of the parameter set
    name                        = "default",

    # workspace
    workspace.read              = TRUE,        # if [TRUE] it is tried to load the global data object from a workspace file in CM.ini()
    workspace.write             = FALSE,       # if [TRUE] a workspace with the global data object will be written in CM.writeData()
    workspace.replace           = FALSE,       # if [TRUE] a workspace will be replaced when existing in CM.writeData()
    workspace.filename          = "user_workspace.RData", # the filename used in CM.ini() and CM.writeData()

    # input settings
    input.dir                   = "input",     # the directory from which all input files will be read in by CM.ini()
    input.sep                   = "\t",        # the column separator sign, e.g. ",", ";", "\t" (tab) passed to read.table
                                               # (?read.table for more information)
    input.col.easting           = "POINT_X",   # the column name for the x-value
    input.col.northing          = "POINT_Y",   # s.a.
    input.col.elevation         = "POINT_Z",   # s.a.
    input.units                 = "m",         # units of input coordinates (will be used for axis labels in plotting functions)
    input.col.bank              = "Name",      # the column name of the side (left/right bank)
    bank.code.left              = "left",      # the string code used for the left bank
    bank.code.right             = "right",     # the string code used for the right bank
    bank.reverse.left           = FALSE,       # reverse bank points of left bank from input data
    bank.reverse.right          = FALSE,       # reverse bank points of right bank from input data

    # output settings
    output.replace              = FALSE,       # if [TRUE] the output files are replaced when existing in CM.writeFiles()
    output.write.centerline     = FALSE,       # if [TRUE] the geometry of the centerline will be written in CM.writeFiles()
    output.write.metrics        = TRUE,        # if [TRUE] the calculated channel metrics will be written in CM.writeFiles()
    output.write.metrics.d      = TRUE,        # switch on/off the variable d.r and d.l (distances from centerline to banks)
    output.write.metrics.w      = TRUE,        # switch on/off the variable w (channel width)
    output.write.metrics.r      = TRUE,        # switch on/off the variable r.r and r.l (direction factor of d.r and d.l)
    output.write.metrics.diff   = TRUE,        # switch on/off the variable diff.r and diff.l (distances between two banks)
    output.write.steps          = FALSE,       #
    output.write.steps.shp      = FALSE,       # write an ESRI shapefile of steps

    output.dir                  = "output",
    output.dir.shp              = "output/shp",
    output.sep                  = "\t",


    # enable/disable plots
    plot.polygoncheck           = TRUE,        # if [TRUE], a three-column plot is generated showing the entire river and both ends to
                                               # roughly check the polygon consistency (see also CM.generatePolygon())

    plot.planview               = TRUE,        # create a plan view overview plot
```

```
    plot.planview.secondary     = TRUE,        # in the plan view plot, add a secondary data set for comparison (will be displayed in
                                               # dashed lines)
    plot.planview.bankpoints    = FALSE,       # in the plan view plot, add the bank points of a data set
    plot.planview.bankpoints.interpolated = FALSE,       # in the plan view plot, add the interpolated bank points of a data set
    plot.planview.polygon       = TRUE,        # in the plan view plot, add the channel borders
    plot.planview.voronoi       = FALSE,       # in the plan view plot, add Voronoi polygons in plan view plot
    plot.planview.cl.original   = FALSE,       # in the plan view plot, add the rough centerline (before smoothing)
    plot.planview.cl.smoothed   = TRUE,        # in the plan view plot, add the smoothed centerline
    plot.planview.cl.points     = FALSE,       # when a centerline is plotted should the points representing the line be emphasized
    plot.planview.cl.tx         = FALSE,       # in the plan view plot, add a label with the number next to the centerline points
    plot.planview.cl.selection  = TRUE,        # if [TRUE] and plot window is determined by cl points (see documentation) the cl points
                                               # are highlighted
    plot.planview.transects     = FALSE,       # in the plan view plot, add transects (perpendiculars to centerline)
    plot.planview.transects.len = 20,          # give the length of transects in the unit of the input coordinates
    plot.planview.dist2banks    = TRUE,        # in the plan view plot, add transect segments from centerline to the banks (left and right)
    plot.planview.grid          = TRUE,        # in the plan view plot, add a grid in the background
    plot.planview.grid.dist     = 20,          # the distance of the grid lines in the unit of the input coordinates
    plot.planview.legend        = TRUE,        # in the plan view plot, add a legend
    plot.planview.legend.pos    = "topleft",   # keyword to position legend (see ?legend)
    plot.planview.scalebar      = TRUE,        # in the plan view plot, add a scale bar (width of one plot.planview.grid.dist)
    plot.planview.use.names     = TRUE,        # if [TRUE] set names will be used for display, otherwise "set1", "set2", etc.

    plot.metrics.use.names      = TRUE,        # if [TRUE] set names will be used for display, otherwise "set1", "set2", etc.

    # plot options
    plot.zoom                   = TRUE,        # if [TRUE] the plan view plot is zoomed in (see also CM.plotPlanView())
    plot.zoom.extent.length     = 140,         # zoom window extent for the plan view plot in the unit of the input coordinates
    plot.zoom.extent            = "e1",        # applied zoom window name (see also CM.plotPlanView())
    plot.zoom.extents           = list(        # presets (customizable list) of zoom windows
      e1  = c(400480,  3103130),
      e2  = c(399445,  3096220),
      e3  = c(401623,  3105925)
    ),
    plot.cl.range               = "cl1",       # applied zoom cl range (see also CM.plotPlanView)
    plot.cl.ranges              = list(        # presets (customizable list) of cl ranges
      cl1 = c(1235,    1260)
    ),
    plot.cl.range.use.reference = TRUE,        # determines whether to look for reference centerline [TRUE] or current centerline when centering around
cl.range
    plot.to.file                = FALSE,       # if [TRUE] all plots will be copied to file devices
    plot.to.pdf                 = TRUE,        # if [TRUE] the plot will be saved as pdf
    plot.to.png                 = TRUE,        # if [TRUE] the plot will be saved as png
    plot.index                  = 0,           # numbering for filenames (see also CM.plotPlanView())
    plot.directory              = "plots/",    # directory for saving plots if plot.to.file = TRUE
    plot.filename               = "documentation", # plot file name

    # model parameters
```

```
    force.calc.voronoi          = FALSE,       # if [TRUE] the voronoi polygons are always re-calculated and never taken from cache
    force.calc.cl               = FALSE,       # if [TRUE] the centerline is always re-calculated and never taken from cache
    bank.interpolate            = TRUE,        # if [TRUE] the provided bank points are linearly interpolated to generate a denser
                                               # polygon (see CM.generatePolygon())
    bank.interpolate.max.dist   = 6,           # if bank.interpolate is [TRUE] this is the maximum distance all bank points will have
    bank.reduce                 = FALSE,       # if [TRUE] the provided bank points are reduced by points that are closer to each other
                                               # than bank.reduce.min.dist
    bank.reduce.min.dist        = 0.5,         # if bank.reduce is [TRUE] this is the minimum distance all bank point will have
    bank.filter2.max.it         = 12,          # number of the maximum iterations for filter 2 to prevent the program to run infinitely
    centerline.smoothing.width  = 7,           # smoothing window width of mean filter in number of observations (see
                                               # CM.calculateCenterline())
    centerline.local.slope.range= 15,
    transects.span              = 3,           # span of centerline points used for calculating the transects (see CM.processCenterline())
    centerline.bin.length       = 5,           # for simplifying the centerline give the spacing in the unit of the input coordinates
                                               # (see CM.reduceCenterline())
    centerline.use.reference    = FALSE,       # sets method for calculating distance centerline to banks, if [FALSE] (default) each river
                                               # profile will be compared to its own centerline, if [TRUE] the centerline of
                                               # centerline.reference will be taken (see CM.processCenterline())
    centerline.reference        = "set1",      # sets the reference data set if centerline.use.reference is [TRUE]
    calculate.metrics           = TRUE,        # if [TRUE] all centerline metrics are calculated (see CM.processCenterline())
    force.calc.metrics          = FALSE,       # if [TRUE] the metrics  are always re-calculated and never taken from cache

    # step identification after Zimmermann et. al 2008 [Zimmermann, A.E., Church, M., and Hassan, M. a., 2008, Identification of steps and
    # pools from stream longitudinal profile data: Geomorphology, v. 102, no. 3–4, p. 395–406, doi: 10.1016/j.geomorph.2008.04.009.)]
    steps.identify              = TRUE,
    steps.verbose               = FALSE,       # should there be
    steps.thalweg.dist          = "3d",        # chose method of distance calculation "3d" or "2d"
    steps.minimum.step.length   = 2.25,        # as percentage of Wb [%]
    steps.maximum.step.length   = 200,         # as percentage of Wb [%]
    steps.minimum.pool.length   = 10,          # as percentage of Wb [%]
    steps.minimum.residual.depth= 0.23,        # as percentage of Wb [%]
    steps.minimum.drop.height   = 3.3,         # as percentage of Wb [%]
    steps.minimum.step.slope    = 10,          # average slope + 10 degree [°]
    steps.bank.full.width.fix   = TRUE,        # TRUE: use a fix bank full width for the whole stream, FALSE: calculate from banks
    steps.bank.full.width       = 3.7,         # [m]
    steps.average.slope.fix     = FALSE,
    steps.average.slope         = 12.5,        #8.34, #12.5,         # [°]

    # ignore
    dummy = TRUE

)
```

E. Derivation of bed shear stress (article III)

```
# constants
rho = 1000 # [kg/m^3] density of water
g   = 9.81 # [m/s^2] gravitational constant
Q   = 7    # discharge [m3/s]
D84 = 0.4  # [m] approximated with D90 from Molnar et al. 2010


S   = slope_by_cmgo # derived by cmgo
w   = width_by_cmgo # derived by cmgo


### dimensionless unit discharge (Rickenmann et al., 2011)
q   = Q / w
qss = q / ( g * S * (D84 ^3) ) # Rickenmann et al., 2011 (Fig. 11)


### dimensionless flow velocity from Rickenmann et al., 2011 (Fig. 18a, C domain)
Uss = 1.55 * ( qss ^ 0.706)


### flow velocity
U   = Uss * ((g * S * D84)^(1/2))


### flow depth (continuity)
d   = q / U


### hydraulic radius
Rh  = (d * w) / (2*d + w)


### the bed shear stress
tau_bed = rho * g * Rh * S
```

F. Generation of the 3D-model of the study reach (article III)

We performed two different types of surveys in the Erlenbach over the 550 m long study reach (see section 4.2 Field site and Methods). In the field we measured with a total station (Leica Nova MS50 MultiStation) the location of the thalweg, the channel banks (Fig. 59 a+b) and 88 marker points (Fig. 59 c+d), for which the accuracy is in the range of a few centimeters. The marker points consist of a head with three 2 x 6 cm reflective tapes and an 60 cm long aluminum pole. The markers were deployed in the field (Fig. 59 e) on both sides of the channel with an average spacing of 6 m. These marker points act as reference points for the second survey, performed in the Erlenbach. A three-dimensional digital model has been developed from a photography survey (Fig. 59 h). During this survey, the channel bed has been captured with two digital cameras (Canon PowerShot D20, Fig. 59 g) mounted to a 3 m long portable pole (Fig. 59 f). With this equipment nearly 6000 images have been taken from the 550 m long channel reach over two days with discharge at baseflow conditions. The calculated overlap of the images was 5.3, meaning that on average every channel bed point was captured in 5.3 images. The images have been post-processed with Agisoft PhotoScan Pro (e.g. Crosby, 2016) to generate a complete, and fully quantitative three-dimensional model. First, the 6000 images have been manually filtered, where low-quality photos and photos that point outside the channel have been removed. The 550 m reach has then be separated into 16 chunks (spatial subsets) to increase performance of the Agisoft software. The filtered set of images (~5000) haven been sorted into these 16 chunks and the reference points (markers) have been manually identified in all images, where they appear (on average in 5.3 images). In addition, the list of x,y,z-coordinates of the 88 markers have been loaded into Agisoft. The processing of the chunks in Agisoft works as follows. First, tie points are automatically identified in the imagery of each chunk, which means that identical objects are identified within the photo set. Next, based on this sparse point cloud of tie points, a dense point cloud is generated where subsequently more points are added.

Fig. 59: a) the Leica total station during a typical survey of long profile, channel banks and fix point markers in the Erlenbach, b) assistant holds the reflector required for thalweg and bank survey point measurements, c),d) preparation of reference markers, e) reference markers deployed in the study reach, f) the 3 m long mount of the digital cameras used for the photogrammetric surveys, g) the camera mount on top, h) the final 3d model of the reach created based on the photogrammetric images created with Agisoft PhotoScan Pro.

Of this point cloud, a polygon mesh is generated by fitting triangle faces into the point cloud. This mesh is the final geometrical model of the channel. To better distinguish objects in the model, the texture of the faces have been compiled based on the original set of images, yielding a photo-realistic model (Fig. 59 h). For more information on the processing we refer to the user manual of the software tool of Agisoft Photoscan Pro (http://www.agisoft.com/downloads/user-manuals/).

The model has been loaded into ESRI ArcScene (ESRI, 2017), together with the geometrical data of the thalweg survey and the steps features, identified by the automated algorithm of Zimmermann et al. (2008). The agreement of the geometry of the total station measurements – which have an accuracy of a few centimeters – and the channel bed of the three-dimensional model was very high, leading to the conclusion that the model also has an accuracy of a few centimeters. From the model we measured and collected the parameters plan view curvature, wood_role and wood_ori, presented in section 4.2.

G. Histograms of step spacings

We give here the full list of histograms of step spacings as well as their statistics. The results (discussed in paragraph 0) show that there is no clear trend towards a uniform step spacing after large flood events.

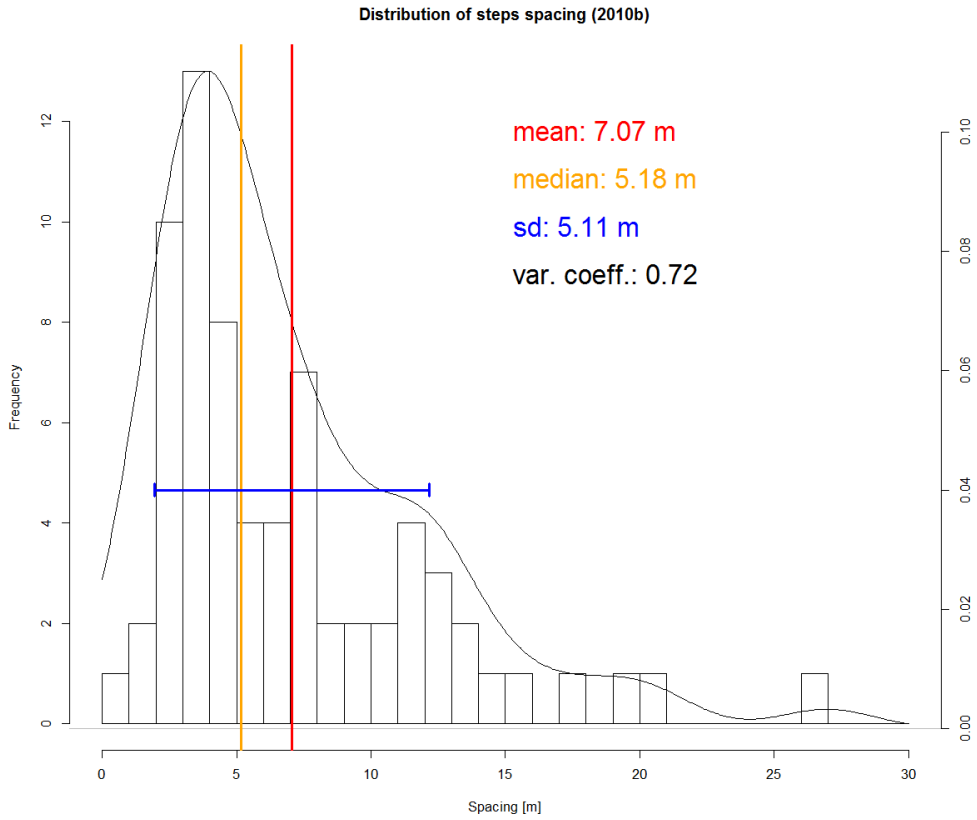

Fig. 60: Histogram of step spacing of the 70 steps of the 2010b long-profile survey.

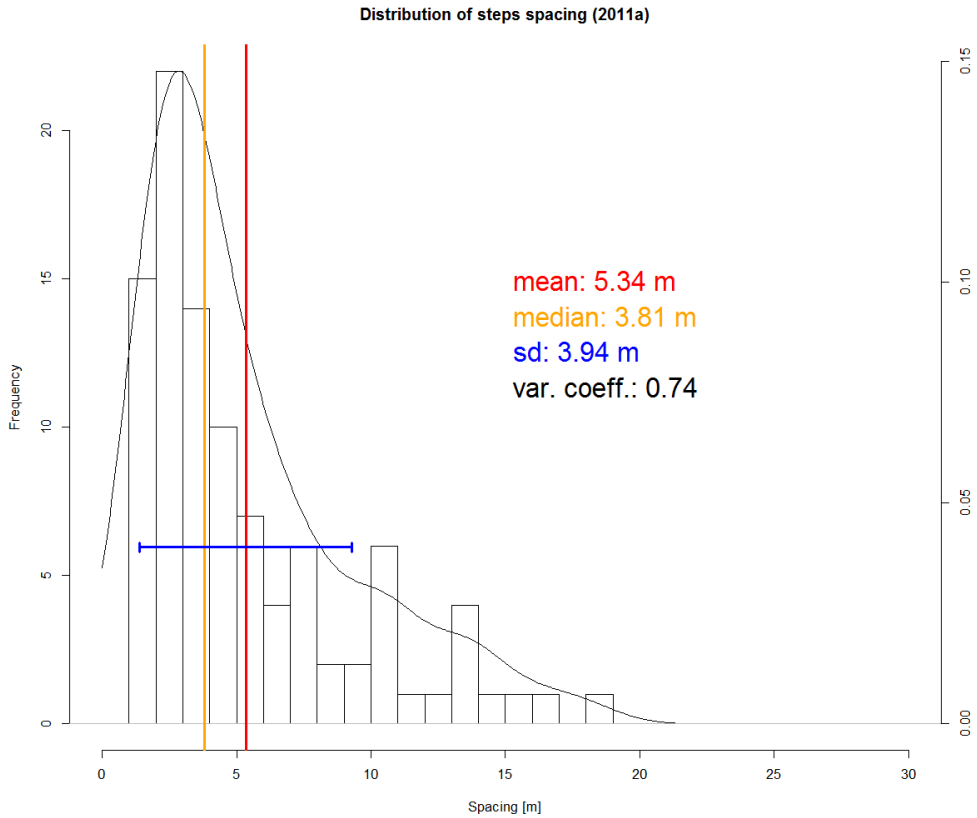

Fig. 61: Histogram of step spacing of the 98 steps of the 2011a long-profile survey.

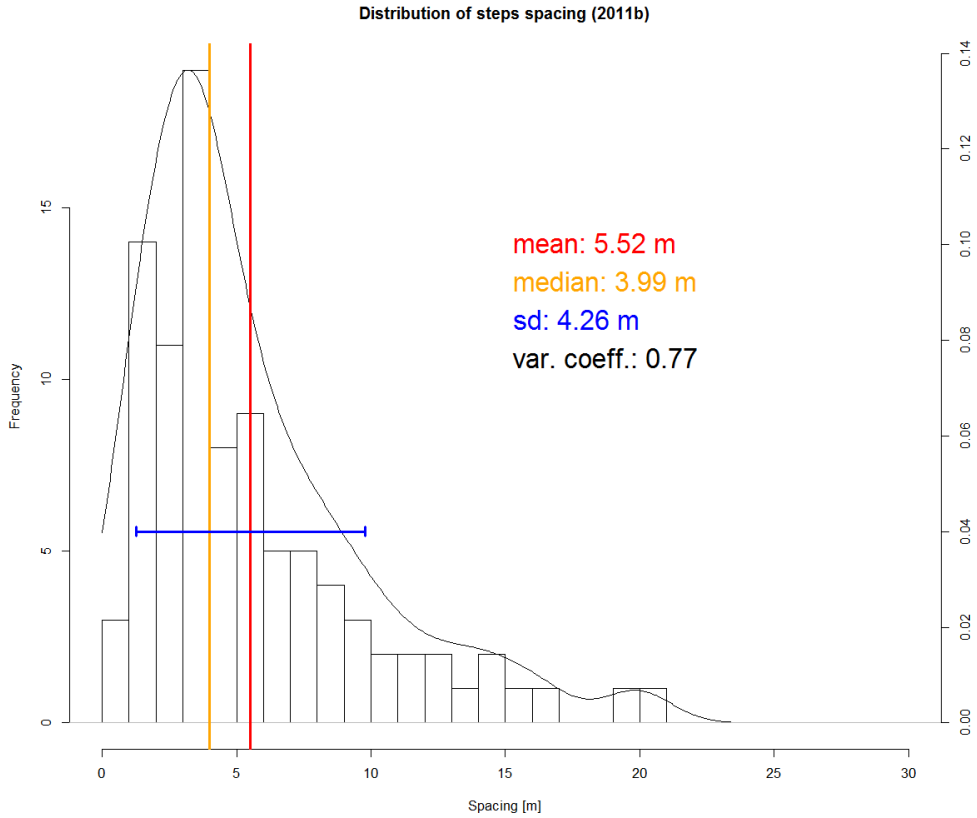

Fig. 62: Histogram of step spacing of the 94 steps of the 2011b long-profile survey.

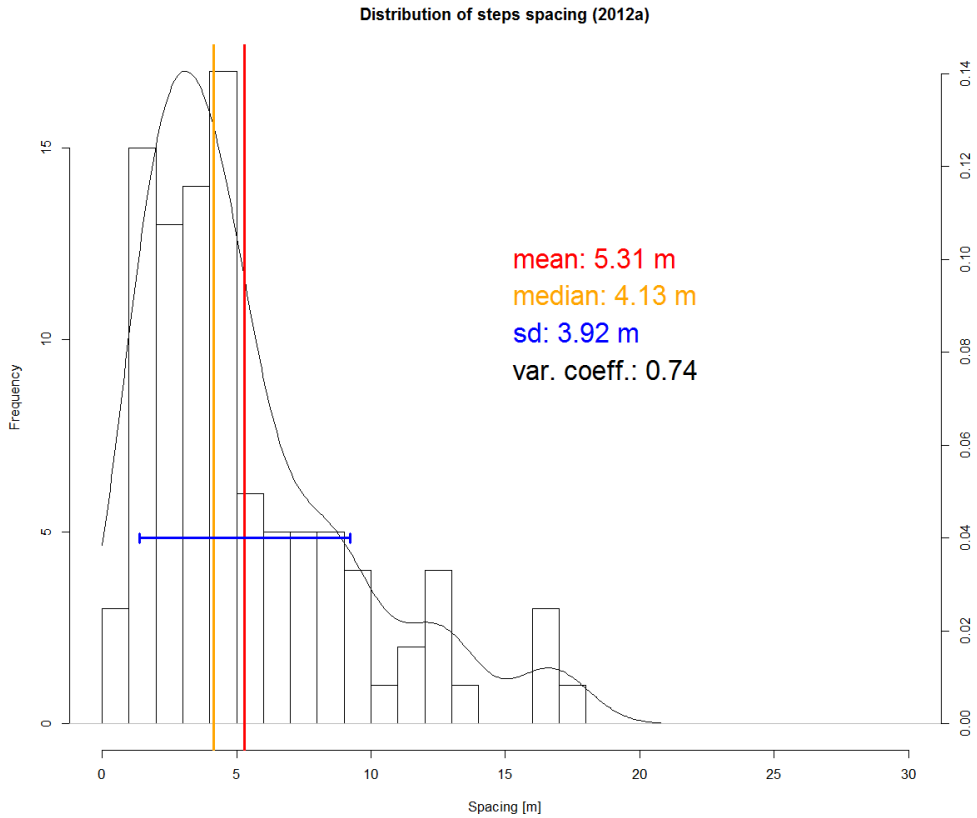

Fig. 63: Histogram of step spacing of the 99 steps of the 2012a long-profile survey.

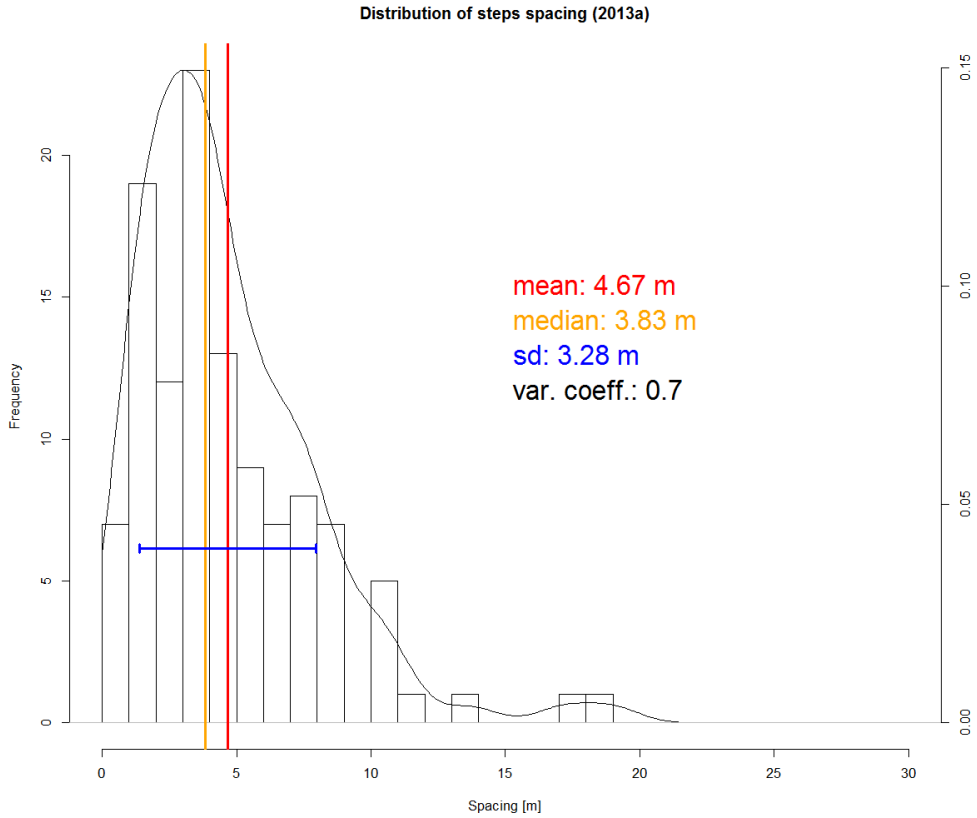

Fig. 64: Histogram of step spacing of the 92 steps of the 2013a long-profile survey.

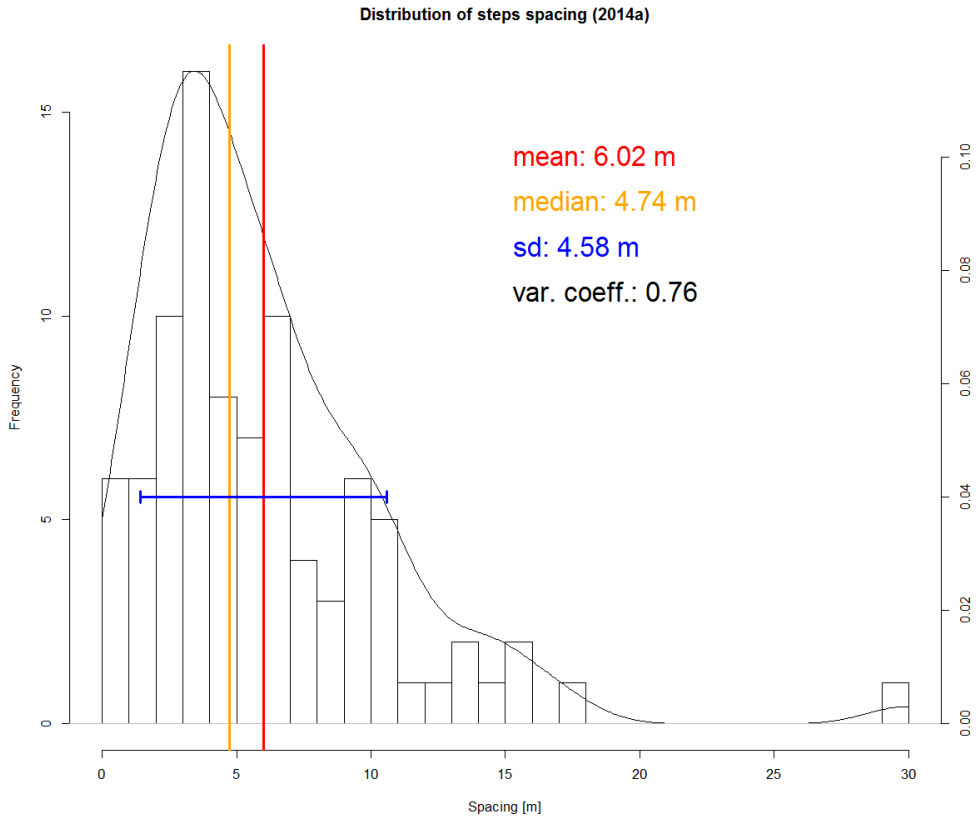

Fig. 65: Histogram of step spacing of the 90 steps of the 2014a long-profile survey.

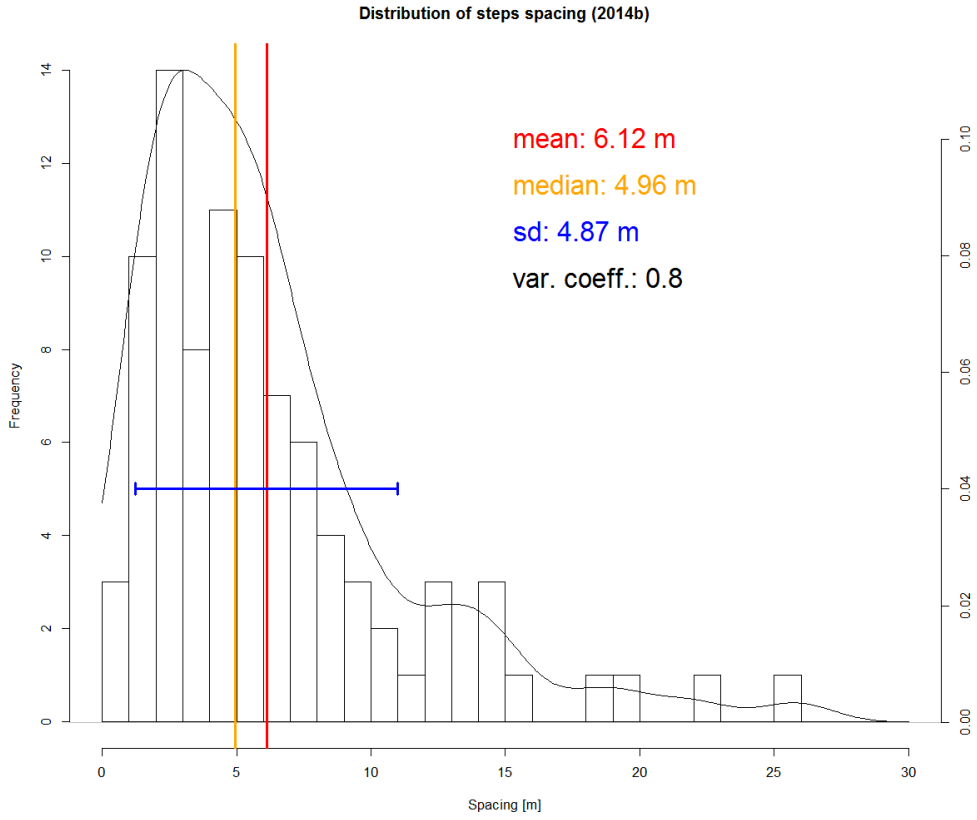

Fig. 66: Histogram of step spacing of the 90 steps of the 2014b long-profile survey.

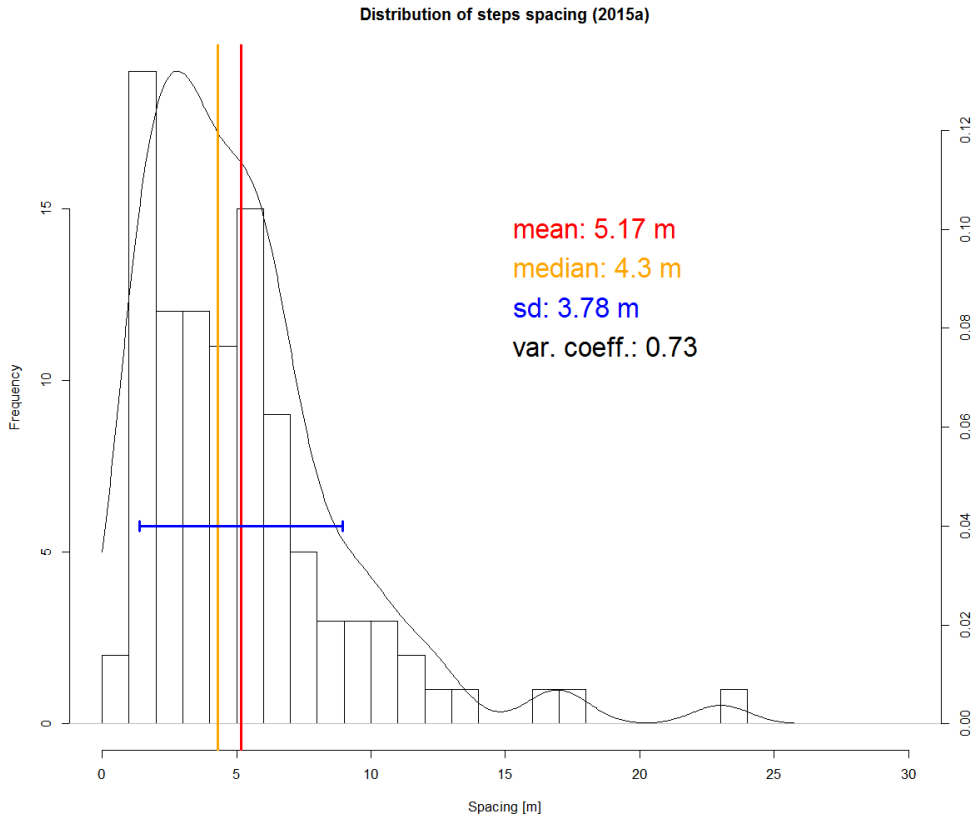

Fig. 67: Histogram of step spacing of the 103 steps of the 2015a long-profile survey.

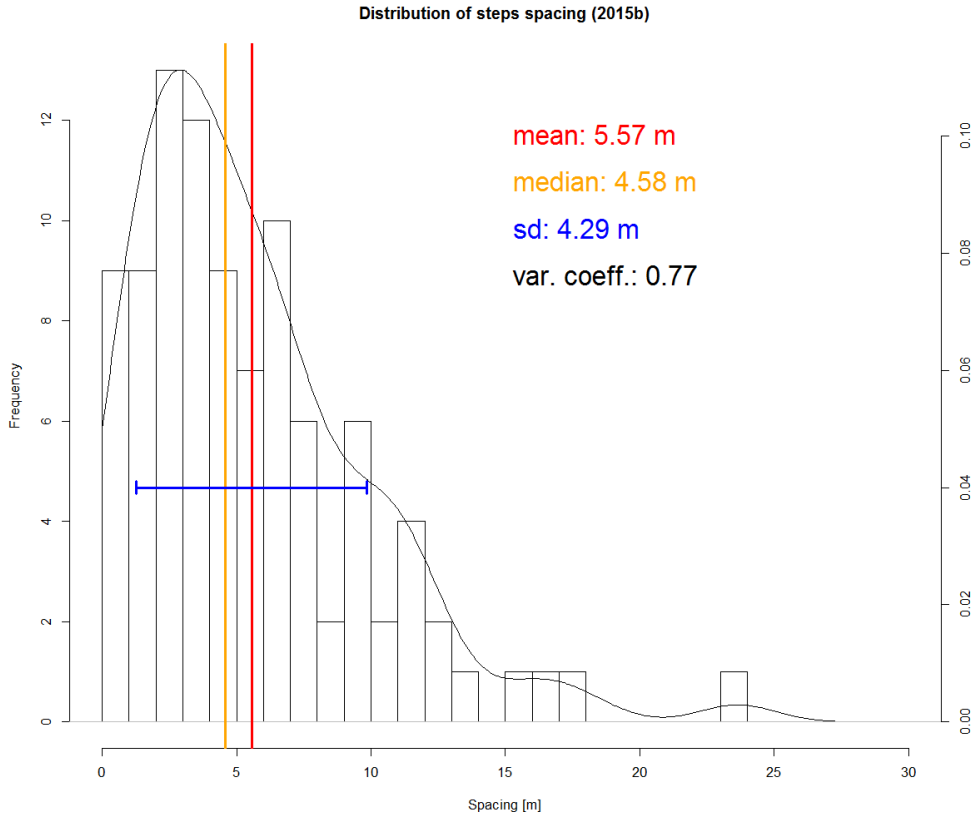

Fig. 68: Histogram of step spacing of the 96 steps of the 2015b long-profile survey.

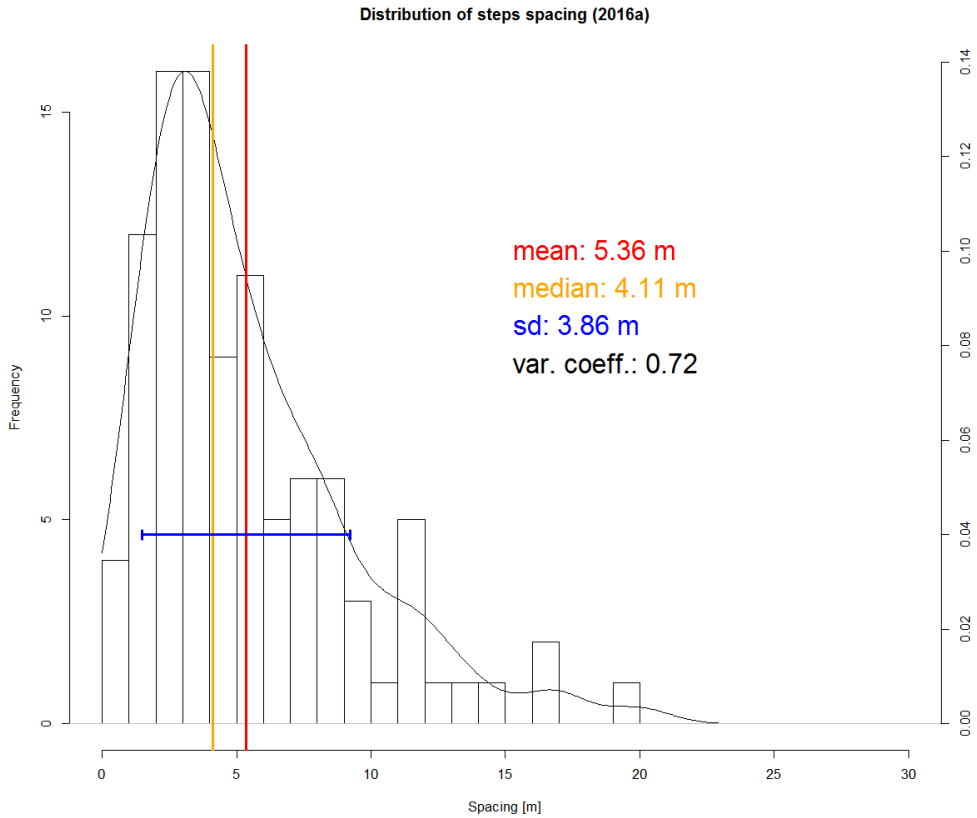

Fig. 69: Histogram of step spacing of the 100 steps of the 2016a long-profile survey.

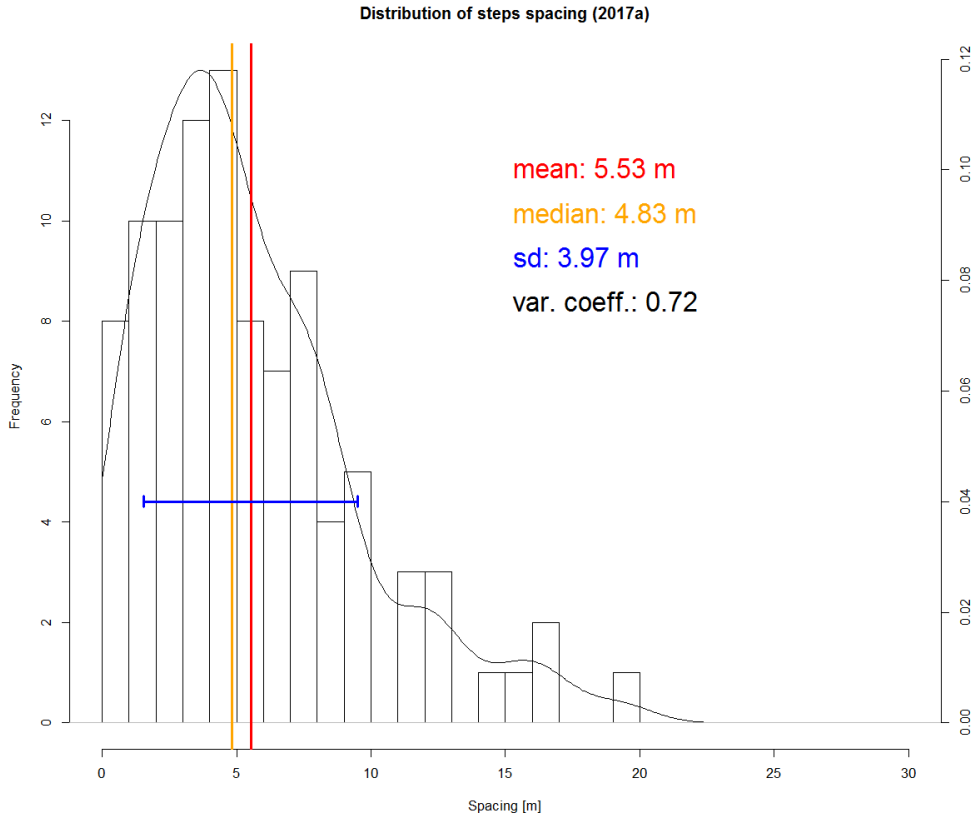

Fig. 70: Histogram of step spacing of the 97 steps of the 2017a long-profile survey.

References

Abbe, T. B. and Montgomery, D. R. (2003) 'Patterns and processes of wood debris accumulation in the Queets river basin, Washington', *Geomorphology*, 51(1–3), pp. 81–107. , https://doi.org/10.1016/S0169-555X(02)00326-4.

Abrahams, A. D. and Li, G. (1995) 'Step-pool streams: Adjustments to maximum flow resistance', *Water Resources Research*, 31(10), pp. 2593–2602. , https://doi.org/10.1029/95WR01957.

Ackerman, P. E. C. T. (2011) 'HEC-GeoRAS GIS Tools for Support of HEC-RAS using ArcGIS User's Manual', (February), p. 244.

Agisoft (2017) 'Agisoft PhotoScan user manual'. St. Petersburg. Available at: http://www.agisoft.com/pdf/photoscan-pro_1_3_en.pdf.

Almedeij, J. H. and Diplas, P. (2003) 'Bedload transport in gravel-bed streams with unimodal sediment', *Journal of Hydraulic Engineering*, 129(11), pp. 896–904. , https://doi.org/10.1061/(ASCE)0733-9429(2003)129:11(896).

Amit (2015) *Estimating river Channel Width using Python/ArcGIS/MATLAB/R?*, *Sep 24, 2015*. Available at: http://gis.stackexchange.com/questions/164169/estimating-river-channel-width-using-python-arcgis-matlab-r (Accessed: 14 March 2017).

Van Asch, T. W. J., Buma, J. and Van Beek, L. P. H. (1999) 'A view on some hydrological triggering systems in landslides', *Geomorphology*, 30(1–2), pp. 25–32. , https://doi.org/10.1016/S0169-555X(99)00042-2.

Asterics, S. (2013) 'Software-Handbuch ASTERICS, Version 4.1', pp. 1–120. Available at: http://www.fliessgewaesserbewertung.de/downloads/ASTERICS_Softwarehandbuch_Version4.pdf.

Azanon, J. *et al.* (2005) 'Late Quaternary large-scale rotational slides induced by river incision: The Arroyo de Gor area (Guadix basin, SE Spain)', *Geomorphology*, 69(1–4), pp. 152–168. , https://doi.org/10.1016/j.geomorph.2004.12.007.

Badoux, A. *et al.* (2016) 'Natural hazard fatalities in Switzerland from 1946 to 2015', *Natural Hazards and Earth System Sciences*, 16(12), pp. 2747–2768. , https://doi.org/10.5194/nhess-16-2747-2016.

Badoux, A., Andres, N. and Turowski, J. M. (2014) 'Damage costs due to bedload transport

processes in Switzerland', *Natural Hazards and Earth System Sciences*, 14(2), pp. 279–294. , https://doi.org/10.5194/nhess-14-279-2014.

Bänziger, R. and Burch, H. (1990) 'Acoustic sensors (hydrophones) as indicators for bedload transport in a mountain torrent', *Hydrology in Mountainous Regions I*. IAHS Publ, 193(193), pp. 207–214. Available at: http://hydrologie.org/redbooks/a193/iahs_193_0207.pdf (Accessed: 23 October 2017).

Barry, J. J., Buffington, J. M. and King, J. G. (2004) 'A general power equation for predicting bed load transport rates in gravel bed rivers', *Water Resources Research*, 40(10). , https://doi.org/10.1029/2004WR003190.

Bartnik, W., Madeyski, M. and Michalik, A. (1992) 'Suspended load and bed load transport in mountain streams determined by different methods', in *Erosion and sediment transport monitoring programmes in river basins.*, pp. 3–9. , https://doi.org/-.

Bathurst, J. (2002) 'At-a-site variation and minimum flow resistance for mountain rivers', *Journal of Hydrology*, 269, pp. 11–26. Available at: http://www.sciencedirect.com/science/article/pii/S0022169402001919 (Accessed: 27 January 2014).

Bathurst, J. C. (1985) 'Flow Resistance Estimation in Mountain Rivers', *Journal of Hydraulic Engineering*, 111(4), pp. 625–643. , https://doi.org/10.1061/(ASCE)0733-9429(1985)111:4(625).

Beer, A. R. *et al.* (2015) 'Field instrumentation for high-resolution parallel monitoring of bedrock erosion and bedload transport', *Earth Surface Processes and Landforms*, 40(4), pp. 530–541. , https://doi.org/10.1002/esp.3652.

Beer, A. R. and Turowski, J. M. (2015) 'Bedload transport controls bedrock erosion under sediment-starved conditions', *Earth Surface Dynamics*, 3(3), pp. 291–309. , https://doi.org/10.5194/esurf-3-291-2015.

Bennett, G. L. *et al.* (2016) 'Landslides, threshold slopes, and the survival of relict terrain in the wake of the Mendocino Triple Junction', *Geology*, 44(5), pp. 363–366. , https://doi.org/10.1130/G37530.1.

Beverloo, W. A., Leniger, H. A. and van de Velde, J. (1961) 'The flow of granular solids through orifices', *Chemical Engineering Science*. Pergamon, 15(3–4), pp. 260–269. , https://doi.org/10.1016/0009-2509(61)85030-6.

Bezzola, G. R. and Hegg, C. (2007) 'Ereignisanalyse Hochwasser 2005, Teil 1 - Prozessse, Schäden und erste Einordnung', *Umwelt Wissen*, 707, p. 215. , https://doi.org/Umwelt-Wissen Nr. 0707.

Bezzola, G. R. and Hegg, C. (2008) 'Ereignisanalyse Hochwasser 2005, Teil 2 - Analyse von Prozessen, Massnahmen und Gefahrengrundlagen', *Umwelt Wissen*, 825, p. 429. , https://doi.org/PNR61.

Bigi, A. *et al.* (2006) 'Knickpoints and hillslope failures: Interactions in a steady-state experimental landscape', *Geological Society of America Special Papers*, 398(March), pp. 295–307. , https://doi.org/10.1130/2006.2398(18).

Birnbaum, Z. W. and Tingey, F. H. (1951) 'One-Sided Confidence Contours for Probability Distribution Functions', *The Annals of Mathematical Statistics*. Institute of Mathematical Statistics, 22(4), pp. 592–596. , https://doi.org/10.1214/aoms/1177729550.

Buffington, J. M. and Montgomery, D. R. (2013) 'Geomorphic Classification of Rivers', in *Treatise on Geomorphology*, pp. 730–767. , https://doi.org/10.1016/B978-0-12-374739-6.00263-3.

Bunte, K. (2010) 'Measurements of gravel transport using the magnetic tracer technique : temporal variability over a highflow season and field-calibration', *Methods*, (March), pp. 85–106.

Burch, H. (1994) 'Ein Rckblick auf die hydrologische Forschung der WSL im Alptal(A Retrospective on the hydrological research at WSL in Alptal)', *Beiträge zur Hydrologie der Schweiz*, 35, pp. 18–33. , https://doi.org/-.

Burt, T. P. and Allison, R. J. (2009) 'Sediment Cascades in the Environment: An Integrated Approach', in *Sediment Cascades: An Integrated Approach*. Chichester, UK: John Wiley & Sons, Ltd, pp. 1–15. , https://doi.org/10.1002/9780470682876.ch1.

Cates, M. E. *et al.* (1998) 'Jamming, Force Chains and Fragile Matter', *Physical Review Letters*, 2(9), pp. 1841–1844. , https://doi.org/10.1103/PhysRevLett.81.1841.

Chartrand, S. M. and Whiting, P. J. (2000) 'Alluvial architecture in headwater streams with special emphasis on step-pool topography', *Earth Surface Processes and Landforms*, 25(6), pp. 583–600. , https://doi.org/10.1002/1096-9837(200006)25:6<583::AID-ESP92>3.0.CO;2-3.

Chin, A. (1989) 'Step pools in stream channels', *Progress in Physical Geography*, pp. 391–407. , https://doi.org/10.1177/030913338901300304.

Chin, A. (1999a) 'On the origin of step-pool sequences in mountain streams', *Geophysical Research Letters*, 26(2), pp. 231–234. , https://doi.org/10.1029/1998GL900270.

Chin, A. (1999b) 'The morphologic structure of step-pools in mountain streams', *Geomorphology*, 27(3–4), pp. 191–204. , https://doi.org/10.1016/S0169-555X(98)00083-X.

Chin, A. (2002) 'The periodic nature of step-pool mountain streams', *American Journal of Science*, 302, pp. 144–167.

Chin, A. (2003) 'The geomorphic significance of step-pools in mountain streams', *Geomorphology*, 55(1–4), pp. 125–137. , https://doi.org/10.1016/S0169-555X(03)00136-3.

Chin, A. and Phillips, J. D. (2007) 'The self-organization of step-pools in mountain streams', *Geomorphology*, 83(3–4), pp. 346–358. , https://doi.org/10.1016/j.geomorph.2006.02.021.

Chin, A. and Wohl, E. E. (2005) 'Toward a theory for step pools in stream channels', *Progress in Physical Geography*, 3(3), pp. 275–296. , https://doi.org/10.1191/0309133305pp449ra.

Church, M. and Zimmermann, A. (2007) 'Form and stability of step-pool channels: Research progress', *Water Resources Research*, 43(3), p. n/a-n/a. , https://doi.org/10.1029/2006WR005037.

Cook, K. L. (2017) 'An evaluation of the effectiveness of low-cost UAVs and structure from motion for geomorphic change detection', *Geomorphology*. Elsevier B.V., 278, pp. 195–208. , https://doi.org/10.1016/j.geomorph.2016.11.009.

Cook, K. L., Turowski, J. M. and Hovius, N. (2014) 'River gorge eradication by downstream sweep erosion', *Nature Geoscience*, 7(9), pp. 682–686. , https://doi.org/10.1038/ngeo2224.

Crosby, C. (2016) *Structure from Motion (SfM) Agisoft PhotoScan processing guide*. Available at: http://kb.unavco.org/kb/article/structure-from-motion-sfm-agisoft-photoscan-processing-guide-848.html (Accessed: 5 November 2017).

Curran, J. C. (2007) 'Step–pool formation models and associated step spacing', *Earth Surface Processes and Landforms*, 32(11), pp. 1611–1627. , https://doi.org/10.1002/esp.1589.

Curran, J. C. and Wilcock, P. (2005a) 'Effect of sand supply on transport rates in a gravel-bed channel', *Journal of Hydraulic Engineering*, (November), pp. 961–967. Available at: http://ascelibrary.org/doi/abs/10.1061/(ASCE)0733-9429(2005)131:11(961) (Accessed: 6 January 2014).

Curran, J. C. and Wilcock, P. R. (2005b) 'Characteristic dimensions of the step-pool bed

configuration: An experimental study', *Water Resources Research*, 41(2), pp. 1–11. , https://doi.org/10.1029/2004WR003568.

Curran, J. H. and Wohl, E. E. (2003) 'Large woody debris and flow resistance in step-pool channels, Cascade Range, Washington', *Geomorphology*, 51(1–3), pp. 141–157. , https://doi.org/10.1016/S0169-555X(02)00333-1.

Dietrich, J. T. (2014) 'Application of Structure-from-Motion photogrammetry to fluvial geomorphology', *PhD Thesis*, (December), p. 109.

Dilts, T. E. (2015) *Polygon to Centerline Tool for ArcGIS*, *University of Nevada Reno*. Available at: http://www.arcgis.com/home/item.html?id=bc642731870740aabf48134f90aa6165 (Accessed: 15 March 2017).

Egholm, D. L., Knudsen, M. F. and Sandiford, M. (2013) 'Lifespan of mountain ranges scaled by feedbacks between landsliding and erosion by rivers.', *Nature*, 498(7455), pp. 475–8. , https://doi.org/10.1038/nature12218.

Eltner, A. *et al.* (2017) 'Time lapse structure-from-motion photogrammetry for continuous geomorphic monitoring', *Earth Surface Processes and Landforms*, 2253(July), pp. 2240–2253. , https://doi.org/10.1002/esp.4178.

Ergenzinger, P. and De Jong, C. (2003) 'Perspectives on bed load measurement', *Erosion and sediment transport measurement in rivers: Technological and Methological advances*, (June 2002), pp. 113–125.

ESRI (2017) 'ESRI ArcMap Desktop'. Environmental Systems Research Institute: Redlands, CA: Environmental Systems Research Institute. Available at: http://desktop.arcgis.com/de/.

Ferreira, M. (2014) *Perpendicular Transects*. Available at: http://gis4geomorphology.com/stream-transects-partial/ (Accessed: 15 March 2017).

Ferrer-Boix, C. *et al.* (2016) 'On how spatial variations of channel width influence river profile curvature', *Geophysical Research Letters*, 43(12), pp. 6313–6323. , https://doi.org/10.1002/2016GL069824.

Gallen, S. F. *et al.* (2011) 'Hillslope response to knickpoint migration in the Southern Appalachians: Implications for the evolution of post-orogenic landscapes', *Earth Surface Processes and Landforms*, 36(9), pp. 1254–1267. , https://doi.org/10.1002/esp.2150.

Golly, A. *et al.* (2017a) 'Controls and feedbacks in the coupling of mountain channels and

hillslopes', *Geology*, 45(4), pp. 307–310. , https://doi.org/10.1130/G38831.1.

Golly, A. *et al.* (2017b) 'Testing models of step formation against observations of channel steps in a steep mountain stream', *Earth Surf. Process. Landforms*, under revi.

Golly, A. and Turowski, J. M. (2017) 'Deriving principal channel metrics from bank and long-profile geometry with the R-package cmgo', *Earth Surface Dynamics Discussions*, pp. 1–19. , https://doi.org/10.5194/esurf-2017-32.

Gómez-Gutiérrez, Á. *et al.* (2014) 'Using 3D photo-reconstruction methods to estimate gully headcut erosion', *Catena*. Elsevier B.V., 120(September 2014), pp. 91–101. , https://doi.org/10.1016/j.catena.2014.04.004.

Gray, H. J. *et al.* (2017) 'On extracting sediment transport information from measurements of luminescence in river sediment', *Journal of Geophysical Research: Earth Surface*, 122(3), pp. 654–677. , https://doi.org/10.1002/2016JF003858.

Gray, J. R., Laronne, J. . B. and Marr, J. D. G. (2010) 'Bedload-surrogate monitoring technologies', *U.S. Geological Survey Scientific Investigations Report*, 5091, pp. 1–37. Available at: https://pubs.usgs.gov/sir/2010/5091/pdf/sir2010-5091.pdf (Accessed: 7 November 2017).

Grimaud, J. L., Paola, C. and Voller, V. (2016) 'Experimental migration of knickpoints: Influence of style of base-level fall and bed lithology', *Earth Surface Dynamics*, 4(1), pp. 11–23. , https://doi.org/10.5194/esurf-4-11-2016.

Habersack, H. M. (2001) 'Radio-tracking gravel particles in a large braided river in New Zealand: A field test of the stochastic theory of bed load transport proposed by Einstein', *Hydrological Processes*, 15(3), pp. 377–391. , https://doi.org/10.1002/hyp.147.

Harvey, A. M. (2002) 'Effective timescales of coupling within fluvial systems', *Geomorphology*, 44, pp. 175–201. , https://doi.org/10.1016/S0169-555X(01)00174-X.

Heede, B. (1981) 'Dynamics of Selected Mountain Streams in the Western United States of America', *Zeitschrift fur geomorphology N.F.*, 25(1), pp. 17–32.

Heede, B. H. (1972) 'INFLUENCES OF A FOREST ON THE HYDRAULIC GEOMETRY OF TWO MOUNTAIN STREAMS', *JAWRA Journal of the American Water Resources Association*. Blackwell Publishing Ltd, 8(3), pp. 523–530. , https://doi.org/10.1111/j.1752-1688.1972.tb05174.x.

Hegg, C., McArdell, B. W. and Badoux, A. (2006) 'One hundred years of mountain hydrology in Switzerland by the WSL', *Hydrological Processes*, 20(2), pp. 371–376. , https://doi.org/10.1002/hyp.6055.

Hegg, C. and Rickenmann, D. (1998) 'Short-time Relations between runoff and bed load transport in a steep mountain torrent', in *Modelling Soil Erosin, Sediment Transport and Closely Related Hydrological Processes*. 1AHS Publ. Available at: http://hydrologie.org/redbooks/a249/iahs_249_0317.pdf (Accessed: 1 November 2017).

Hilker, N., Badoux, A. and Hegg, C. (2009) 'The Swiss flood and landslide damage database 1972–2007', *Natural Hazards and Earth System Science*, 9(3), pp. 913–925. , https://doi.org/10.5194/nhess-9-913-2009.

Hoey, T. B. (1992) 'Temporal variations in bedload transport in rates and sediment storage', *Progress in Physical Geography*, 16(3), pp. 319–338.

Hornby, D. (2017) *RivEX*. Available at: http://www.rivex.co.uk/Online-Manual/RivEX-Online-Manual.html?Extractchannelwidths.html (Accessed: 15 March 2017).

Horton, E. . R. (1945) 'Erosional development of streams and their drainage basins; hydrophysical approach to quantitative morphology', *Geological Society of America Bulletin*, 56.3(3), pp. 275–370.

Hovius, N. *et al.* (2000) 'Supply and Removal of Sediment in a Landslide-Dominated Mountain Belt: Central Range, Taiwan', *The Journal of Geology*, 108(1), pp. 73–89. , https://doi.org/10.1086/314387.

Hovius, N. and Stark, C. P. (2006) 'Landslide-driven erosion and topographic evoution of active mountain belts', *Landslides from massive Rock Slope Failure*, pp. 573–590. , https://doi.org/10.1007/978-1-4020-4037-5.

Howard, A. D. (1994) 'A detachment-limited model of drainage basin evolution', *Water Resources Research*, 30(7), pp. 2261–2285. , https://doi.org/10.1029/94WR00757.

von Humboldt, A. (1852) *A sketch of a physical description of the universe*. translated. New York.

Ives, J. D. and Messerli, B. (1989) *The Himalayan dilemma*. Abingdon, UK: Taylor & Francis. , https://doi.org/10.4324/9780203169193.

Ives, J. D., Messerli, B. and Spiess, E. (1997) *Mountains of the world: a global priority*. London:

Parthenon publishing group.

Jackson, C. W. (2009) *The Ambur project: Analyzing Moving Boundaries Using R*, *Department of Geology & Geography Georgia Southern University*. Available at: http://ambur.r-forge.r-project.org/ (Accessed: 27 March 2017).

Jäggi, M., Nigg, U. and Teysseire, P. (2004) 'Die Sedimentkatastrophe von Baltschieder', *In: Kongresspublikation des Internationalen Symposions Interpraevent 2004, Riva del Garda*, 3(7), pp. 165–180.

Jeník, J. (1997) *The diversity of mountain life (in Mountains of the world: a global priority)*. London: Parthenon publishing group.

Jochner, M. (2013) *Transport and Deposition of Woody Debris in a Mountain Stream*.

Jochner, M. *et al.* (2015) 'The role of log jams and exceptional flood events in mobilizing coarse particulate organic matter in a steep headwater stream', *Earth Surface Dynamics Discussions*, 3(3), pp. 173–196. , https://doi.org/10.5194/esurfd-3-173-2015.

Jochner, M., Badoux, A. and Turowski, J. M. (2013) 'Untersuchung des Schwemmholztransports in einem Wildbach', *FAN-Agenda*, 2/13, pp. 8–10.

Katul, G. *et al.* (2002) 'A mixing layer theory for flow resistance in shallow streams', *Water Resources Research*, 38(11), pp. 32-1-32–8. , https://doi.org/10.1029/2001WR000817.

Komar, P. D. and Li, Z. (1988) 'Applications of grain-pivoting and sliding analyses to selective entrapment of gravel and to flow-competence evaluations', *Sedimentology*, 35(4), pp. 681–695. , https://doi.org/10.1111/j.1365-3091.1988.tb01244.x.

Korup, O., Densmore, A. L. and Schlunegger, F. (2010) 'The role of landslides in mountain range evolution', *Geomorphology*. Elsevier B.V., 120(1–2), pp. 77–90. , https://doi.org/10.1016/j.geomorph.2009.09.017.

Lamb, M. P., Dietrich, W. E. and Venditti, J. G. (2008) 'Is the critical shields stress for incipient sediment motion dependent on channel-bed slope?', *Journal of Geophysical Research: Earth Surface*, 113(2), pp. 1–20. , https://doi.org/10.1029/2007JF000831.

Landolt, E. (1869) 'Die Wasserverheerungen in der Schweiz im September und Oktober 1886', *Schweizerische Zeitschrift für Forstwesen*, 10(1), pp. 1–9.

Legg, N. *et al.* (2014) 'The Channel Migration Toolbox: ArcGIS Tools for Measuring Stream Channel Migration', (Publication no. 14-no. 06-no. 032). Available at:

https://fortress.wa.gov/ecy/publications/SummaryPages/1406032.html.

Lenzi, M. A. *et al.* (1999) 'Bedload transport in the instrumented catchment of the Rio Cordon. Part 1: Analysis of Bedload Records, Conditions and Threshold of Bedload Entrainment', *Catena*, 36, pp. 171–190.

Lenzi, M. A. (2001) 'Step-pool evolution in the Rio Cordon, Northeastern Italy', *Earth Surface Processes and Landforms*, 26(9), pp. 991–1008. , https://doi.org/10.1002/esp.239.

Lenzi, M. A. *et al.* (2004) 'Impact of sediment supply on bed load transport in a high-altitude alpine torrent', *Int. Symposion Interpraevent*, p. Bd, 1, III/171-182.

Lévy, S. *et al.* (2012) 'Erosion and channel change as factors of landslides and valley formation in Champlain Sea Clays: The Chacoura River, Quebec, Canada', *Geomorphology*. Elsevier B.V., 145–146, pp. 12–18. , https://doi.org/10.1016/j.geomorph.2011.09.014.

Liechti, K. (2008) 'Starke Gewitter im Juni 2007: Einordnung und Hydrologische Modellierung für die Regionen Huttwil (BE) une Einsiedeln (SZ)', *Master Thesis*, pp. 1–117.

Lopez, S. *et al.* (2009) 'Process-Based Stochastic Modelling: Meandering Channelized Reservoirs', in *Analogue and Numerical Modelling of Sedimentary Systems: From Understanding to Prediction*. Oxford, UK: Wiley-Blackwell, pp. 139–144. , https://doi.org/10.1002/9781444303131.ch5.

MacFarlane, W. A. and Wohl, E. E. (2003) 'Influence of step composition on step geometry and flow resistance in step-pool streams of the Washington Cascades', *Water Resources Research*, 39(2), pp. 1–13. , https://doi.org/10.1029/2001WR001238.

Mackey, B. H. *et al.* (2014) 'Knickpoint formation, rapid propagation, and landscape response following coastal cliff retreat at the last interglacial sea-level highstand: Kaua'i, Hawai'i', *Bulletin of the Geological Society of America*, 126(7–8), pp. 925–942. , https://doi.org/10.1130/B30930.1.

Mandelbrot, B. (1967) 'How Long Is the Coast of Britain? Statistical Self-Similarity and Fractional Dimension', *Science*, 156(3775), pp. 636–638. , https://doi.org/10.1126/science.156.3775.636.

Mao, L. *et al.* (2006) 'Long-term monitoring of bedload and debris flows in two small catchments of the Eastern Italian Alps', *WIT Transactions on Ecology and the Environment*. Southampton, UK: WIT Press (WIT Transactions on Ecology and the Environment, Vol 90), 90, pp. 147–157. , https://doi.org/10.2495/DEB060151.

Mao, L. *et al.* (2014) 'Bedload hysteresis in a glacier-fed mountain river', *Earth Surface Processes and Landforms*, 39(7), pp. 964–976. , https://doi.org/10.1002/esp.3563.

Marston, R. A. (1982) 'The Geomorphic Significance of Log steps in Forest Streams', *Annals of the Association of American Geographers*. Taylor & Francis, Ltd.Association of American Geographers, pp. 99–108. , https://doi.org/10.2307/2563228.

Marston, R. A. (2008) 'Land, Life, and Environmental Change in Mountains', *Annals of the Association of American Geographers*, 98(3), pp. 507–520. , https://doi.org/10.1080/00045600802118491.

Masteller, C. and Finnegan, N. J. (2016) 'How rivers remember: The impacts of prior stress history on grain scale topography and bedload transport', in *AGU Abstract*.

Micheletti, N., Chandler, J. H. and Lane, S. N. (2015) 'Structure from Motion (SfM) Photogrammetry', *British Society for Geomorphology Geomorphological Techniques*, 2(2), pp. 1–12. , https://doi.org/10.5194/isprsarchives-XL-5-W4-37-2015.

Millar, R. G. (1999) 'Grain and form resistance in gravel-bed rivers', *Journal of Hydraulic Research*. Taylor & Francis Group, 37(3), pp. 303–312. , https://doi.org/10.1080/00221686.1999.9628249.

Milzow, C. *et al.* (2006) 'Spatial organization in the step-pool structure of a steep mountain stream (Vogelbach, Switzerland)', *Water Resources Research*, 42(4), pp. 1–11. , https://doi.org/10.1029/2004WR003870.

Mir, K., Tariq, A. and Atif, S. (2013) 'River Width Calculator'. Available at: http://www.arcgis.com/home/item.html?id=4e7c9370e3e8455e8ff57d6b23baf760.

Molnar, P. *et al.* (2010) 'Analysis of changes in the step-pool morphology and channel profile of a steep mountain stream following a large flood', *Geomorphology*. Elsevier B.V., 124(1–2), pp. 85–94. , https://doi.org/10.1016/j.geomorph.2010.08.014.

Montgomery, D. R. and Buffington, J. M. (1997) 'Channel-reach morphology in mountain drainage basins', *Bulletin of the Geological Society of America*, 109(5), pp. 596–611. , https://doi.org/10.1130/0016-7606(1997)109<0596:CRMIMD>2.3.CO.

Moog, D. B. and Whiting, P. J. (1998) 'Annual hysteresis in bed load rating curves', *Water Resources Research*, 34(9), pp. 2393–2399. , https://doi.org/10.1029/98WR01658.

Mosbrucker, A. R. *et al.* (2017) 'Camera system considerations for geomorphic applications of

SfM photogrammetry', *Earth Surface Processes and Landforms*, 42(6), pp. 969–986. , https://doi.org/10.1002/esp.4066.

Munich Re (2012) 'Natural Catastrophes 2011: Earthquake, flood, nuclear accident', *TOPICS GEO*. Available at: www.munichre.com (Accessed: 19 October 2017).

Muthuswamy, M. and Tordesillas, A. (2006) 'How do interparticle contact friction, packing density and degree of polydispersity affect force propagation in particulate assemblies?', *Journal of Statistical Mechanics: Theory and Experiment*, 2006(9), pp. P09003–P09003. , https://doi.org/10.1088/1742-5468/2006/09/P09003.

Nichols, M. H. *et al.* (2016) 'Monitoring channel head erosion processes in response to an artificially induced abrupt base level change using time-lapse photography', *Geomorphology*. Elsevier B.V., 265, pp. 107–116. , https://doi.org/10.1016/j.geomorph.2016.05.001.

Nitsche, M. *et al.* (2011) 'Evaluation of bedload transport predictions using flow resistance equations to account for macro-roughness in steep mountain streams', *Water Resources Research*, 47(8). , https://doi.org/10.1029/2011WR010645.

Nitsche, M. *et al.* (2012a) 'Macroroughness and variations in reach-averaged flow resistance in steep mountain streams', *Water Resources Research*, 48(12), p. n/a-n/a. , https://doi.org/10.1029/2012WR012091.

Nitsche, M. *et al.* (2012b) 'Verbesserung von Geschiebevorhersagen in Wildbächen und Gebirgsflüssen durch Berücksichtigung von Makrorauigkeit', *Wasser Energie Luft*, 104(2), pp. 129–139.

Pavelsky, T. M. and Smith, L. C. (2008) 'RivWidth: A Software Tool for the Calculation of River Widths From Remotely Sensed Imagery', *IEEE Geoscience and Remote Sensing Letters*, 5(1), pp. 70–73. , https://doi.org/10.1109/LGRS.2007.908305.

Pizzuto, J. E. (2008) 'Streambank Erosion and River Width Adjustment', in *Sedimentation Engineering*. Reston, VA: American Society of Civil Engineers, pp. 387–438. , https://doi.org/10.1061/9780784408148.ch07.

R Development Core Team (2008) *Computational Many-Particle Physics*, *R Foundation for Statistical Computing*. R Foundation for Statistical Computing, Vienna, Austria. , https://doi.org/10.1007/978-3-540-74686-7.

Rapp, A. (1960) 'Recent development of mountain slopes in Kärkevagge and surroundings, northern Scandinavia', *Geografiska Annaler*, 42.2/3, pp. 65–200.

Raymond Pralong, M. *et al.* (2015) 'Climate change impacts on bedload transport in alpine drainage basins with hydropower exploitation', *Earth Surface Processes and Landforms*, 40(12), pp. 1587–1599. , https://doi.org/10.1002/esp.3737.

Recking, A. (2012) 'Influence of sediment supply on mountain streams bedload transport', *Geomorphology*. Elsevier B.V., 175–176, pp. 139–150. , https://doi.org/10.1016/j.geomorph.2012.07.005.

Reid, I., Frostick, L. E. and Layman, J. T. (1985) 'The incidence and nature of bedload transport during flood flows in coarse-grained alluvial channels', *Earth Surface Processes and Landforms*. John Wiley & Sons, Ltd, 10(1), pp. 33–44. , https://doi.org/10.1002/esp.3290100107.

Rickenmann, D. (1997) 'Sediment transport in Swiss torrents', *Earth Surface Processes and Landforms*, 22(10), pp. 937–951. , https://doi.org/10.1002/(SICI)1096-9837(199710)22:10<937::AID-ESP786>3.0.CO;2-R.

Rickenmann, D. (2001) 'Comparison of bed load transport in torrents and gravel bed streams', *Water Resources Research*, 37(12), pp. 3295–3305. , https://doi.org/10.1029/2001WR000319.

Rickenmann, D. *et al.* (2012) 'Bedload transport measurements at the Erlenbach stream with geophones and automated basket samplers', *Earth Surface Processes and Landforms*, 37(9), pp. 1000–1011. , https://doi.org/10.1002/esp.3225.

Rickenmann, D. *et al.* (2014) 'Bedload transport measurements with impact plate geophones: Comparison of sensor calibration in different gravel-bed streams', *Earth Surface Processes and Landforms*, 39(7), pp. 928–942. , https://doi.org/10.1002/esp.3499.

Rickenmann, D. and Jakob, M. (2015) 'Erosion and sediment flux in mountain watersheds', *The High Mountain Cryosphere: Environmental Changes and Human Risks*, pp. 166–183. , https://doi.org/10.1017/CBO9781107588653.010.

Rickenmann, D. and McArdell, B. (2007) 'Continuous measurement of sediment transport in the Erlenbach stream using piezoelectric bedload impact sensors', *Earth Surface Processes and …*, 1378(January), pp. 1362–1378. , https://doi.org/10.1002/esp.

Rickenmann, D. and Recking, A. (2011) 'Evaluation of flow resistance in gravel-bed rivers through a large field data set', *Water Resources Research*, 47(7), p. n/a-n/a. , https://doi.org/10.1029/2010WR009793.

Roering, J. J. *et al.* (2015) 'Beyond the angle of repose: A review and synthesis of landslide processes in response to rapid uplift, Eel River, Northern California', *Geomorphology*. Elsevier B.V., 236, pp. 109–131. , https://doi.org/10.1016/j.geomorph.2015.02.013.

Roth, D. L. *et al.* (2016) 'Bed load sediment transport inferred from seismic signals near a river', *Journal of Geophysical Research: Earth Surface*, 121(4), pp. 725–747. , https://doi.org/10.1002/2015JF003782.

Roth, D. L. *et al.* (2017) 'Bed load transport and boundary roughness changes as competing causes of hysteresis in the relationship between river discharge and seismic amplitude recorded near a steep mountain stream', *Journal of Geophysical Research: Earth Surface*, 122(5), pp. 1182–1200. , https://doi.org/10.1002/2016JF004062.

Saletti, M. *et al.* (2016) 'A reduced-complexity model for sediment transport and step-pool morphology', *Earth Surface Dynamics*, 4(3), pp. 549–566. , https://doi.org/10.5194/esurf-4-549-2016.

Schneider, J. (2014) 'Scaling relationships between bed load volumes, transport distances, and stream power in steep mountain channels', *Journal of …*, pp. 533–549. , https://doi.org/10.1002/2013JF002874.Received.

Schneider, J. M. *et al.* (2014) 'Scaling relationships between bed load volumes, transport distances, and stream power in steep mountain channels', *Journal of Geophysical Research: Earth Surface*, 119(3), pp. 533–549. , https://doi.org/10.1002/2013JF002874.

Schneider, J. M. *et al.* (2015) 'Applicability of bed load transport models for mixed-size sediments in steep streams considering macro-roughness', *Water Resources Research*, 51(7), pp. 5260–5283. , https://doi.org/10.1002/2014WR016417.

Schuerch, P. *et al.* (2006) 'The influence of landsliding on sediment supply and channel change in a steep mountain catchment', *Geomorphology*, 78(3–4), pp. 222–235. , https://doi.org/10.1016/j.geomorph.2006.01.025.

Schumm, S. A. (1977) *The Fluvial System*. Chichester and New York: John Wiley and Sons. , https://doi.org/10.1002/gj.3350130112.

Schumm, S. A. (1993) 'River Response to Baselevel Change: Implications for Sequence Stratigraphy', *Source: The Journal of Geology*, 101(2), pp. 279–294. , https://doi.org/10.1086/648221.

Schwenk, J. *et al.* (2017) 'High spatiotemporal resolution of river planform dynamics from

Landsat: The RivMAP toolbox and results from the Ucayali River', *Earth and Space Science*, 4(2), pp. 46–75. , https://doi.org/10.1002/2016EA000196.

Sear, D. A. *et al.* (2001) 'Coarse Sediment Transport Measurement in Rivers and on Coasts Using Advanced Particle Tracing Technologies.', *EPSRC Review Report*. Engineering and Physical Sciences Research Council, GR/L94987/, pp. 1–13. Available at: https://eprints.soton.ac.uk/15193/ (Accessed: 23 October 2017).

Shobe, C. M., Tucker, G. E. and Anderson, R. S. (2016) 'Hillslope-derived blocks retard river incision', *Geophysical Research Letters*, 43(10), pp. 5070–5078. , https://doi.org/10.1002/2016GL069262.

Sklar, L. S. and Dietrich, W. E. (2006) 'The role of sediment in controlling steady-state bedrock channel slope: Implications of the saltation-abrasion incision model', *Geomorphology*, 82(1–2), pp. 58–83. , https://doi.org/10.1016/j.geomorph.2005.08.019.

Smith, J. C. *et al.* (2013) 'Runoff-driven export of particulate organic carbon from soil in temperate forested uplands', *Earth and Planetary Science Letters*. Elsevier, 365, pp. 198–208. , https://doi.org/10.1016/j.epsl.2013.01.027.

Stark, C. P. and Stark, G. J. (2001) 'A channelization model of landscape evolution', *American Journal of Science*. American Journal of Science, 301(4–5), pp. 486–512. , https://doi.org/10.2475/ajs.301.4-5.486.

Taniguchi, S. and Itakura, Y. (1992) 'A new acoustic sensor for sediment discharge measurement', *IAHS PUBLICATION*. IAHS Publ, (210), pp. 135–142. Available at: http://hydrologie.org/redbooks/a210/iahs_210_0135.pdf (Accessed: 23 October 2017).

Thieler, E. R. *et al.* (2009) 'Digital Shoreline Analysis System (DSAS) version 4.0— An ArcGIS extension for calculating shoreline change', *U.S. Geological Survey Open-File Report 2008*, p. 1278. Available at: http://woodshole.er.usgs.gov/project-pages/DSAS/.

To, K. (2002) 'Effect of hopper angles on jamming probability in 2-dimensional hoppers', *Chinese Journal of Physics*, 40(4), pp. 379–386.

To, K., Lai, P. Y. and Pak, H. K. (2001) 'Jamming of granular flow in a two-dimensional hopper', *Physical Review Letters*, 86(1), pp. 71–74. , https://doi.org/10.1103/PhysRevLett.86.71.

Totschnig, R., Sedlacek, W. and Fuchs, S. (2011) 'A quantitative vulnerability function for fluvial sediment transport', *Natural Hazards*. Springer Netherlands, 58(2), pp. 681–703. , https://doi.org/10.1007/s11069-010-9623-5.

Trimble, S. W. (1997) 'Contribution of Stream Channel Erosion to Sediment Yield from an Urbanizing Watershed', *Science*, 278(5342), pp. 1442–1444. , https://doi.org/10.1126/science.278.5342.1442.

Turowski *et al.* (2013a) 'Large floods, alluvial overprint, and bedrock erosion', *Earth Surface Processes and Landforms*, 38(9), pp. 947–958. , https://doi.org/10.1002/esp.3341.

Turowski, J. M. *et al.* (2008) 'Erfassung des Sedimenttransportes in Wildbächen und Gebirgsflüssen – Anwendungsmöglichkeiten von Geophonmessanlagen', *Wasser Energie Luft*, 100(1), pp. 69–74.

Turowski, J. M. *et al.* (2009) 'The impact of exceptional events on erosion, bedload transport and channel stability in a step-pool channel', *Earth Surface Processes and Landforms*, 1673, pp. 1661–1673. , https://doi.org/10.1002/esp.

Turowski, J. M. (2010) 'Probability distributions of bed load transport rates: A new derivation and comparison with field data', *Water Resources Research*, 46(8), p. W08501. , https://doi.org/10.1029/2009WR008488.

Turowski, J. M. *et al.* (2013b) 'Field measurements of the energy delivered to the channel bed by moving bed load and links to bedrock erosion', *Journal of Geophysical Research: Earth Surface*, 118(4), pp. 2438–2450. , https://doi.org/10.1002/2013JF002765.

Turowski, J. M. *et al.* (2013c) 'The mass distribution of coarse particulate organic matter exported from an Alpine headwater stream', *Earth Surface Dynamics*, 1(1), pp. 1–11. , https://doi.org/10.5194/esurf-1-1-2013.

Turowski, J. M., Badoux, A. and Rickenmann, D. (2011) 'Start and end of bedload transport in gravel-bed streams', *Geophysical Research Letters*, 38(4), pp. 1–5. , https://doi.org/10.1029/2010GL046558.

Turowski, J. M., Hilton, R. G. and Sparkes, R. (2016) 'Decadal carbon discharge by a mountain stream is dominated by coarse organic matter', *Geology*, 44(1), pp. 27–30. , https://doi.org/10.1130/G37192.1.

Turowski, J. M., Rickenmann, D. and Dadson, S. J. (2010) 'The partitioning of the total sediment load of a river into suspended load and bedload: a review of empirical data', *Sedimentology*, 57(4), pp. 1126–1146. , https://doi.org/10.1111/j.1365-3091.2009.01140.x.

Turowski, J. M., Wyss, C. R. and Beer, A. R. (2015) 'Grain size effects on energy delivery to the streambed and links to bedrock erosion', *Geophysical Research Letters*, 42(6), pp. 1775–1780.

, https://doi.org/10.1002/2015GL063159.

Waters, K. a. and Curran, J. C. (2012) 'Investigating step-pool sequence stability', *Water Resources Research*, 48(7), p. n/a-n/a. , https://doi.org/10.1029/2011WR011436.

Westoby, M. J. *et al.* (2012) '"Structure-from-Motion" photogrammetry: A low-cost, effective tool for geoscience applications', *Geomorphology*. Elsevier B.V., 179, pp. 300–314. , https://doi.org/10.1016/j.geomorph.2012.08.021.

Whipple, K. X. (2004) 'BEDROCK RIVERS AND THE GEOMORPHOLOGY OF ACTIVE OROGENS', *Annual Review of Earth and Planetary Sciences*. Annual Reviews, 32(1), pp. 151–185. , https://doi.org/10.1146/annurev.earth.32.101802.120356.

Whipple, K. X. and Tucker, G. E. (1999) 'Dynamics of the stream-power river incision model: Implications for height limits of mountain ranges, landscape response timescales, and research needs', *Journal of Geophysical Research: Solid Earth*, 104(B8), pp. 17661–17674. , https://doi.org/10.1029/1999JB900120.

Whittaker, J. and Jaeggi, M. (1982) 'Origin of Step-Pool Systems in Mountain Streams', *Journal of the Hydraulics Division*, 108(6), pp. 758–773. Available at: http://cedb.asce.org/cgi/WWWdisplay.cgi?34288.

Willett, S. D. and Brandon, M. T. (2002) 'On steady state in mountain belts', *Geology*, 30(2), pp. 175–178. , https://doi.org/10.1130/0091-7613(2002)030<0175.

Winkler, W. *et al.* (1985) 'Wägital-Flysch et autres flyschs penniques en Suisse Centrale - Stratigraphie, sédimentologie et comparaisons', *Eclogae geologicae Helvetiae*, 78(1), pp. 1–22. , https://doi.org/http://dx.doi.org/10.5169/seals-165641.

Wistuba, M. *et al.* (2015) 'Coupling between landslides and eroding stream channels reconstructed from spruce tree rings (examples from the Carpathians and Sudetes - Central Europe)', *Earth Surface Processes and Landforms*, 40(3), pp. 293–312. , https://doi.org/10.1002/esp.3632.

Wobus, C. *et al.* (2006) 'Tectonics from topography: procedurses, promise, and pitfalls', *Geological Society of America Special Paper*, 398(4), pp. 55–74. , https://doi.org/10.1130/2006.2398(04).

Wohl, E. E. (2000) *Mountain rivers*. Water Reso. American Geophysical Union.

Wohl, E. E. and Grodek, T. (1994) 'Channel bed-steps along Nahal Yael, Negev desert, Israel',

Geomorphology, 9(2), pp. 117–126. , https://doi.org/10.1016/0169-555X(94)90070-1.

Wohl, E. E. and Ikeda, H. (1997) 'Experimental simulation of channel incision into a cohesive substrate at varying gradients', *Geology*, 25(4), pp. 295–298. , https://doi.org/10.1130/0091-7613(1997)025<0295:ESOCII>2.3.CO.

Wohl, E. E., Madsen, S. and MacDonald, L. (1997) 'Characteristics of log and clast bed-steps in step-pool streams of northwestern Montana, USA', *Geomorphology*. Elsevier, 20(1–2), pp. 1–10. , https://doi.org/10.1016/S0169-555X(97)00021-4.

Wyss, C. R. *et al.* (2016a) 'Laboratory flume experiments with the Swiss plate geophone bed load monitoring system: 1. Impulse counts and particle size identification', *Water Resources Research*, 52(10), pp. 7744–7759. , https://doi.org/10.1002/2015WR018555.

Wyss, C. R. *et al.* (2016b) 'Laboratory flume experiments with the Swiss plate geophone bed load monitoring system: 2. Application to field sites with direct bed load samples', *Water Resources Research*, 52(10), pp. 7760–7778. , https://doi.org/10.1002/2016WR019283.

Wyss, C. R. *et al.* (2016c) 'Measuring Bed Load Transport Rates by Grain-Size Fraction Using the Swiss Plate Geophone Signal at the Erlenbach', *Journal of Hydraulic Engineering*, 142(5), pp. 040160031–0401600311. , https://doi.org/10.1061/(ASCE)HY.1943-7900.0001090.

Yager, E. M. *et al.* (2012a) 'Patch dynamics and stability in steep, rough streams', *Journal of Geophysical Research*, 117(F2), p. F02010. , https://doi.org/10.1029/2011JF002253.

Yager, E. M. *et al.* (2012b) 'Prediction of sediment transport in step-pool channels', *Water Resources Research*, 48(1), p. W01541. , https://doi.org/10.1029/2011WR010829.

Yager, E. M. *et al.* (2012c) 'Sediment supply, grain protrusion, and bedload transport in mountain streams', *Geophysical Research Letters*, 39(10), p. n/a-n/a. , https://doi.org/10.1029/2012GL051654.

Young, R. . and Twidale, C. . (1993) 'Geomorphology in Australia', in Grabau, H. J. and W.E., W. and (eds) *in The evolution of geomorphology*. New York: John Wiley and Sons, pp. 29–43.

Zimmermann, A. and Church, M. (2001) 'Channel morphology, gradient profiles and bed stresses during flood in a step–pool channel', *Geomorphology*, 40(3–4), pp. 311–327. , https://doi.org/10.1016/S0169-555X(01)00057-5.

Zimmermann, A., Church, M. and Hassan, M. a. (2008) 'Identification of steps and pools from stream longitudinal profile data', *Geomorphology*, 102(3–4), pp. 395–406. ,

https://doi.org/10.1016/j.geomorph.2008.04.009.

Zimmermann, A., Church, M. and Hassan, M. a. (2010) 'Step-pool stability: Testing the jammed state hypothesis', *Journal of Geophysical Research*, 115(F2), p. F02008. , https://doi.org/10.1029/2009JF001365.